Experimental and Analytical Studies of Semi-Active and Passive Structural Control of Buildings

Kerry Mulligan

A thesis presented for the degree of
Doctor of Philosophy
in
Mechanical Engineering
at the
University of Canterbury,
Christchurch, New Zealand.

26 April 2007

This thesis is dedicated in memory of,
my Grandfather
Derek Reginal Nelson 1920 to 2006

Abstract

This thesis explores semi-active structural control methods for mitigating damage during seismic events. Semi-active devices offer the adaptability of active devices in conjunction with low power requirements and thus the reliability of passive devices. A number of structural applications utilising semi-active resetable devices in structural control are described and analysed. A distinguishing feature of this research is the novel design of a large-scale resetable device developed, manufactured and extensively tested. This design dramatically extends the capabilities of resetable devices by readily manipulating the device response to the structural demands and specific structural control requirements. In particular, the unique ability to use these devices to reshape or sculpt structural hysteretic behaviour offers significant new opportunities in semi-active structural control.

The results indicate improvements in structural performance during seismic events is gained by approaches to structural control and enhanced damping methods that challenge conventional methods. Using an array of performance metrics the overall structural performance is examined without the typically narrow focus found in other studies. Suites of earthquake ground motion records are utilised to avoid bias to any particular type of motion and statistical analysis of the performance over these suites indicates the overall efficacy of the resetable devices in each case considered.

A model that accurately captures all the device dynamics is developed, which can be used for a variety of device types and designs. In addition, the testing capabilities of structural control methods is enhanced by the development of a high speed, real-time hybrid test procedure providing a link between pure simulation and full-scale testing to increase confidence before investing in large experiments. Finally, the resetable devices are extended to improve the response force to size ratio, which additionally increases the force-displacement manipulation ability.

Large-scale shake table experiments validate the findings of the analytical results. Very close correlation between analytical and experimental results including overall trends and numerical values verifies the analytical methods used and increases confidence in continuing research in this area. Furthermore, these large-scale experiments confirm the efficacy and accuracy of the the device model developed, leading to highly accurate quantitative prediction of the overall structural system response.

Overall, this research presents a methodology for designing, testing and applying resetable devices in structural control. The devices developed in this research and the extensive modelling and testing dramatically extend the understanding and scope of these devices. Guidelines developed for these large-scale resetable device designs including a validated dynamic model brings the application of resetable devices closer to real structural control applications.

Acknowledgements

I would like to begin this thesis by acknowledging all the people that helped make it possible. Without this continuing support, contribution and funding I would not have reached this point.

I wish to thank and acknowledge in particular my principal supervisor, Professor J. Geoffrey Chase, who encouraged me to pursue post graduate studies, worked through the difficult problems with me and understood that mountainbiking was a necessary activity at times. My co-supervisor, Professor John Mander tried his best to transform me into a Civil Engineer. Other academic staff from the Mechanical and Civil Engineering Departments, particularly Professor Athol Carr and Leicester Steven EQC Lecturer Bruce Deam, assisted me in their respective areas of expertise.

The Earthquake Commission who provided the funding for this research and travel to present the research findings at conferences.

The technical staff from the Mechanical and Civil Engineering Departments assisted and supported me during the laboratory testing procedures for this research project. Particular thanks to Rodney Elliot in this regard who provided me with extensive technical assistance in the laboratory. Lance Cleeve, and Douglas Heaton from C&M technologies contributed excellent practical advice and manufactured the prototype devices. Colleagues, and in particular Geoffrey Rodgers, Roberto Franco Anaya and Min Ho Chey collaborated with me in this research area and were always useful in discussion and debate to clarify problems and difficulties encountered. I found the librarians from the Engineering Library were always patient and helpful in assisting to find elusive references.

During the time of my studies, I had opportunity to interact with a number

of students from France on exchange in New Zealand to gain their certificate of proficiency. These students were always enthusiastic about the research in their New Zealand working environment and were equally enthusiastic about everything New Zealand had to offer. Then my thanks to all my office mates for your support, including the interesting conversations we had, particularly the ones that got so off topic we could no longer recall where they began!

There are a number of people to whom I owe acknowledgement, not for direct assistance in my project (or studies) but who enabled me to muster mental strength and tenacity. The people I met at the community garden on campus introduced me to such a peaceful and tranquil place and gave me the realisation I was not alone in my aspirations for a better world.

My family and Ryan who were always there for me and provided unquestioning love and understanding throughout what were sometimes tough times.

Lastly, thank you to all the people I have been mountain biking, rock climbing, snowboarding, and tramping with over the last few years. Without you I would have never experienced those delightful mornings when it hurts to move. I hope to share many more good times and adventures with all of you.

Contents

List of Figures

List of Tables

Nomenclature

I.M	intensity measure
PGA	peak ground acceleration
R.F	reduction factor
S.D	spectral displacement
A	area
B	width of rocking panel
B	devisive reduction factor
C, c	damping coefficient
Cc	shear capacity
D	device diameter
F	force
F_B	base shear (total structural force)
F_s	structural force
H	height of rocking panel
I	mass moment of inertia of rocking panel
K, k	stiffness
L_0	initial chamber length
M, m	mass
R	multiplicative reduction factor
S	slope
T	period
V	volume
Y, y	displacement
$\dot{Y}$, $\dot{y}$	velocity
$\ddot{Y}$, $\ddot{y}$	acceleration
Z	non-linear hysteretic component
g	acceleration due to gravity
p	air pressure
t	time
$\hat{x}$	log-normal geometric mean

β log-normal standard deviation

$\delta,\,x$ displacement

Δ change in a value

γ ratio of specific heats

σ multiplicative variance

θ rotation

$\ddot{\theta}$ rotational acceleration

ξ damping

ξ_{eq} equivalent viscous damping

Chapter 1

Introduction

During the time you are reading this sentence there is a 3% probability that there is a magnitude 5.0 or above earthquake occurring somewhere in the world. Most of these events pass unnoticed except by sophisticated sensory equipment. However, when a large earthquake strikes a populated area the results can be catastrophic with widespread damage to buildings, transportation networks and essential services.

Communities suffer devastating effects from these earthquakes, not only for the duration of the seismic event, but for years after. The cost to a community is measured in more than the direct physical consequences of the event. Areas where widespread damage occurred may take a number of years to return to the pre-event social and economic state. In the interim, people will lose jobs as businesses close and many residents may move to other 'greener pastures', which for New Zealand is often overseas. The results thus include lost human capacity along with the direct physical and economic consequences, a further destablising effect that extends recovery time.

Even for communities well prepared for large seismic events, the effects can still be devastating. The Great Hanshin or Kobe earthquake in Japan on the 17th of January 1995 was one of the worst catastrophic earthquake events in recent years. Japan is one of the most pro-active countries in terms of earthquake studies and preparation. However, the Kobe earthquake is considered as the costliest natural disaster to affect any one country. The earthquake caused an estimated 10 trillion yen in damage, or 2.5% of Japan's GDP at the time (Horwich [2000]). In addition, the effects of a major seismic event are not localised to one area. For example, the damage to the Kobe port disrupted shipping worldwide, as well

as circulating through Japan's economy due to Kobe's significant manufacturing and technology economies.

Figure 1.1   Severly damaged building in Kobe.

A lot of the physical destruction and loss of life during large seismic events is due to structures being severely damaged or collapsing. These significant failures occur when the demand placed upon them exceeds the design loads. If a structure survives a large earthquake, it is often rendered unusable without retrofit or significant rebuilding. Most of this damage occurs because structures are designed to dissipate large input energies through sacrificial partial yielding of structural members and connections. Critical service buildings, such as hospitals, are required directly after a large earthquake, so it is essential these buildings sustain minimal damage and can be occupied safely during and immediately after the event (Myrtle et al. [2005]).

Following each major seismic event, structural designs and codes are modified to reflect lessons learnt. For example, after the earthquake in Napier, New Zealand on the 3rd of February 1931 almost the entire city was rebuilt on new guidelines that restricted the buildings to two storeys, among other notable changes. Buildings constructed on street corners were required to have bevelled corners giving people exiting the building a quick, clear view down both streets. This requirement was intended to help people choose the best escape route and avoid the falling debris which was a major cause of injuries in the 1931 earthquake.

Modern building designs and codes are much more sophisticated than just limiting building height. However, severe damage to structures still occurs resulting in costly repair or demolition and rebuilding. For example, several hospitals suffered severe damage during the Northridge earthquake in California on the 17th of January 1994. These buildings did not collapse but were unusable after the event thus increasing the demand on other, already overburdened, hospitals in the area (Pickett [1995]). In addition, these hospitals were not fully functional for over a year, creating a long term loss of service capacity for the area along with lost health care jobs. This is an example of how short term structural damage from an earthquake can flow through an entire service system or economy with immediate and long term loss of capacity.

Reducing devastating social and economic impacts from a large earthquake event relies on resilient structural systems and communities. Essential structures and services need to be easily and safely accessible to the public and rescue teams directly after the event. Housing and businesses need to be able to be used rapidly or jobs and human capacity will be lost, delaying recovery and increasing impact. Furthermore, these requirements for resilient communities need to be simple, effective, reliable, and provided at a low cost.

Modern buildings are designed to fail sacrificially to dissipate the structural response energy from large ground motion events, similar to the way car panels are designed to crumple during an accident. The damage that occurs can be broken into two primary categories: damage to the structural elements, and damage to the occupants and building contents. Structural damage is the result of hysteretic energy dissipation by the structural joints, permanent residual deformation and weakened materials due to yielding. Occupant and content damage occurs from high structural accelerations resulting in relative motion between the structural elements and contents. Thus, people are injured from unsecured items and internal falling debris, and function or capacity is lost when equipment is damaged. Damage reduction can focus on either or both of these damage indicators depending primarily on the structure's foremost function.

Reducing the dynamic response of structures can be achieved by structural strengthening, increased ductility or additional damping. It is impractical in both cost and structural element size to build all structures with sufficient strength to withstand large seismic events. In contrast, high ductility results in severe

damage during larger earthquakes. Hence, any solutions have significant cost or damage outcomes and thus any seismic upgrade or solution implementation is a compromise.

An alternative concept to conventional methods of improving dynamic structural response was introduced by Yao [1972] who suggested active control to break these tradeoffs and directly alter the structure dynamics. Active control, in this sense, provides supplemental reaction forces, thereby reducing the structure's dynamic response (Spencer and Sain [1997]). Because the forces are active and feedback controlled, they effectively enable dynamic redesign of the structure during an event by modulating resistive and restoring forces, thus optimising the response outcome.

Hence, dissipating structural energy by means of structural control offers a potentially more cost effective solution of reducing or eliminating structural and foundation damage. Active structural control can present a cheaper alternative to strengthening or structure replacement (Housner et al. [1997]), providing there is power available to provide the necessary forces. In addition, actively modulated energy dissipation can reduce accelerations as well as displacements and thereby reduce occupant damage.

In broad terms, the control system diverts energy from the structural elements to the dissipation system. The amount of energy dissipated can be illustrated by the hysteretic force-displacement response of the structure, where the area enclosed by a hysteretic loop indicates the amount of energy dissipated for each motion cycle. Control systems alter the hysteretic response of the structure and *generally* the larger the area, the better the control system is at reducing structural damage, within constrains on peak forces and allowable displacements.

Structural control mechanisms can be divided into three main categories; passive, active and semi-active contollers:

1. **Passive control** is the most commonly used system. These systems are purely reactionary and redistribute the energy either spatially or in time. Although these systems provide supplemental damping to a structure, they are tuned to specific structural responses or frequencies, making them unable to respond to structural changes over time or any modelling and imple-

mentation error. Accurate and reliable structural response is difficult and time consuming to obtain. Hence, passive systems are not guaranteed to be correctly tuned to the actual structural response, potentially resulting in inefficient implementation of the passive control system.

2. **Active control** has the ability to add and/or dissipate energy through actuator control forces. Using sensor feedback they are able to actively control the structure for a desired dynamic response and for a variety of seismic excitations. The necessity of a large energy supply can make these systems expensive and complex to install compared to other control system types. In addition, the addition of energy to the structural system can result in structure response instability, if any unexpected behaviour or non-linearity occurs that was not accounted for in the system design (Chase et al. [2005b]). Hence, active systems offer high levels of control, but with potential, hidden problems.

3. **Semi-active control** combines the advantages of both passive and active systems, while reducing many of the disadvantages. Using sensor feedback they are able to change their strictly dissipative damping behaviour to the response of the structure. Thus, they are able to respond to structural non-linearity and changes over time. Being strictly dissipative they also attempt to assure stability of the system. Only, a small power supply is required to be directly coupled to each actuator allowing decentralising of the damper system, an important consideration during large seismic events where power is unreliable. Hence, semi-active systems offer most of the control flexibility of active systems, without the large power requirements.

Structural control has been well covered with semi-active devices being emphasised as a good option for structural control because they have the reliability of passive systems with the adaptability of active systems. Numerous summaries of structural control outline passive, active and semi-active or hybrid devices, their uses and full-scale applications (Spencer and Soong [1999], Soong and Spencer [2000]). State of the art reviews of structural control by Housner et al. [1997], Symans and Constantinous [1999], Soong and Spencer [2002], Datta [2003], Spencer and Nagarajaiah [2003] give an overview of the current state-of-the-practice in this field. Interestingly, Soong and Spencer [2000] discuss that one of the original aims of structural control that still requires attention is to provide systems that are economic and flexible in design and application.

Semi-active devices typically alter the reaction forces provided by the damping system, using a variety of techniques (Symans and Constantinous [1999]). The main point is that they use minimal power to modulate large, resistive forces, such as via changing a valve orifice size in a viscous damper to regulate flows and forces. As a result, semi-active devices can offer a range of control forces with little power input, but can be limited by specific device materials or physics.

Semi-active control system technologies that have been extensively studied include magnetorheological (MR) and electrorheological (ER) fluid dampers. (Dyke et al. [1996], Dyke et al. [1998], Jansen and Dyke [2000], Yi et al. [2001], Yang et al. [2002], Yoshida and Dyke [2004]). In these devices, an electric or magnetic field applied to the fluid significantly changes the properties, resulting in a large change in resisting force from the damping device. Altering the stiffness allows the damping forces to be applied only when required by the structure, resulting in efficient damping systems. Other semi-active devices include variable dampers, where a viscous fluid flows through a variable orifice, thereby altering the damping forces (Kawashima and Unjoh [1994]). Variable friction dampers have also been studied (Nishitana et al. [1999]). A recent review of semi-active and active control covers many of these methods and devices (Spencer and Nagarajaiah [2003]).

An alternative or simpler method for altering the stiffness of a damping device is for a liquid or gas to be compressed during relative structure motion. The fluid pressure is held or released depending on the desired response. These devices are termed resetable devices due to their ability to behave as spring with a resetable un-stressed length (Bobrow et al. [1995]). Resetable devices have significant promise in structural applications due to their simplicity and robustness in operation. Their operation is also highly flexible, offering a wide variety of customised responses. However, resetable devices have not yet been extensively examined to the level of other semi-active systems, such as MR and ER dampers.

The focus of prior semi-active resetable device studies has been analytical examination of building response and actuator architecture using *theoretical* device models (Barroso et al. [2003b], Hunt [2002]). These extensive studies examined structural response with little regard for the realistic dynamic, physical behaviour of large resetable devices. However, these studies show encouraging results and motivation for using semi-active resetable devices in structural control. While re-

alistic non-linear structural models were used, the knowledge of resetable device dynamics was insufficient at the time to use anything more than a simple device model. More specifically, the device model has a linear stiffness with a reaction force saturation point.

Only one resetable device had been manufactured prior to the start of this research. This device was small-scale, having a maximum force capacity of $\sim$100N (Bobrow and Jabbari [2002]). These studies assumed the results from the small scale test were directly scalable to large devices, an assumption that is challenged in this work. Recently, larger scale devices have been studied and, as expected, had limited results compared to ideal simulation or very small scale studies (Yang et al. [2007]).

During the time of this research there have been some experimental studies on resetable devices in Japan, U.S.A and Taiwan. However, these studies focus on the original resetable device configuration without progression to innovative configurations as described herein. Kajima corporation has produced a limited number of 1MN devices. These devices are used primarily in a support rather than a decisive control role (Kurino et al. [2006]). Recently, Yang et al. [2007] have experimentally examined resetable actuators using pressurised nitrogen as the working fluid for three disparate ground motions. These experiments show similar device response results to those in this investigation. However, the devices are significantly more complex in fluid routing, and are limited in applications with only one hysteretic response examined.

Furthermore, theoretical and experimental investigations of resetable devices have been singular in control method configurations. Thus, *large* scale resetable devices in an experimental setting is still an area requiring extensive examination. In particular, there needs to be an emphasis on device capabilities, limitations and bounds of manipulation in device response. This last point is particularly important, as resetable devices offer a great deal of potential to customise behaviour, which has not yet been examined.

The simulations for this study use ground motion records from the three ground motion suites of the SAC project (Sommerville et al. [1997]). These three suites represent ground motions having probability of exceedance of 50% in 50 years, 10% in 50 years, and 2% in 50 years for the Los Angeles region. In addition,

they encompass a wide range of ground motions, from near to far field, are well
accepted, and the collective response to these three suites of ground motions gives
an accurate account of structural control system performance and reliability, all
without bias to one particular ground motion record or type.

1.1   Structural Control Problem

Traditional structural design has advanced to the stage where large improve-
ments in structural performance for earthquake loading is difficult. The same
applies if the designer is also trying to minimise sacrifical energy and absorbing
damage. Currently, measurable improvement requires large effort and often yield
only small additional benefits. In addition, major design and building codes are
demanding greater levels of performance and damage avoidance, particularly for
critical infrastructure such as hospitals and civil defence centres. The overall
situation has created a significant potential design opportunity for innovative
methods.

During strong motion events, structures built to seismic design codes are
most likely to remain standing and avoid collapse or catastrophic failure. This
positive outcome is largely due to the energy absorbtion from sacrificial damage
to structural connections and cladding. However, the significant cost to repair
or rebuild severely damaged structures puts a heavy strain on communities and
resources. Thus, reduction in damage to structural members, cladding and equip-
ment housed in the structure, as well as improved safety for the occupants will
increase serviceability and reduce the social and economic cost to communities.

Older structures or structures not built to seismic design codes may not have
sufficient strength and robustness to withstand a large earthquake event (Smith
[1985]). Thus, these structure may sustain major structural damage or complete
and unpredictable, rapid collapse. Improving the performance of these structures
to meet current design standards (The New Zealand Building Act [2004]) with
retrofit methods will reduce the cost of repair or rebuilding after a damaging
seismic event, but also have a significant investment cost. Providing a low cost
approach to meet current standards would thus encourage retrofit and preserva-
tion of important structural heritage (Forum [2005]), as well as minimising the

required investment.

Structural control offers a means of improving structural performance without the invasive addition of large amounts of structural material, a potential advantage for all structures, new and old. It may also offer the opportunity to break out of the paradigm of sacrificial structural elements being used to absorb energy and mitigate response via the use of sensors, actuators/devices and feedback control. The addition of control via non-structural active or semi-active elements to a structural system can be designed to specifically reduce or alter the most damaging portions of the dynamic response.

Each structural system is unique depending on several factors:

- **Size and slenderness ratio**, which determines the natural frequency and the potential or likely vulnerability to environmental loads such as earthquake and wind loading.

- **Site**, which determines the specific local and geographic vulnerability to environmental loads and dictates the foundation design.

- **Age**, which determines the strength and ductility of the structure based on how it was designed and built, as well as degradation over time.

- **Use**, which determines the acceptable level of damage and serviceability required during and following an extreme event.

Similarly, existing structures that require improved performance to meet design codes have retrofit options that are based on many of these parameters.

This research examines structural response from a hysteretic force-displacement perspective. The larger the area enclosed by the hysteresis loop of the overall structural system the more energy dissipated per cycle of motion. Hence, there is a drive to create structures that dissipate greater energy, but (in contrast) with less damage.

This result has led to the initial concepts of using control, both passive and active, to increase energy absorption. However, many initial efforts sought to dissipate maximum structural energy without regard for any adverse effects that

can be introduced to the rest of the structure and foundation. Therefore, a broad view of structural response with a control system is required to break away from conventional thinking and methods.

When designing a structural control system it is important to tailor the system for the demands of each structural application to obtain maximum benefits. Of particular importance is to thoroughly understand the consequences of the control system on the dynamics of the structural system. This consideration must include both the potential improvements *and* the potential increases in demand on some structural elements. To date, most reports have focused only on the former aspect.

Figure 1.2 illustrates, a single-degree-of-freedom (SDOF) structure hysteretic force-displacement response to a viscous damper and two potential configurations of semi-active resetable devices. While Figure 1.2 presents a simplified situation the observations are equally valid for real structures with more complex and/or active control systems. The left column shows the force-displacement hysteresis of a linear, SDOF structure with no damping for clarity. The middle column shows the hysteretic response of the applied control device. A viscous damper is presented in the first row, while two configurations of resetable dampers are presented in the middle and bottom row. The right column shows the resulting overall structural system hysteretic force-displacement response.

The viscous damper in Figure 1.2 has a fixed response shape where the only variable is the magnitude of the reaction forces, as might be determined by the orifice size (Teixeira [2006]). The addition of the viscous damper to the SDOF structure results in an area enclosed in the overall structural hysteresis loop. Thus, energy dissipation occurs for each motion cycle reducing the structural response and mitigating some damage. The first configuration of the resetable damper, presented in the second row, shows a similar result to the viscous damper. However, these two cases both *increase* the demand on the foundations of the structural system,F_B, compared to the structure alone, regardless of the internal damping the structure might posses. As a result, the foundation could be damaged, eliminating any savings from reduced structural damage.

Forces produced in a structural system in response to motion are transferred through the beams and columns and are reacted by the structural foundations.
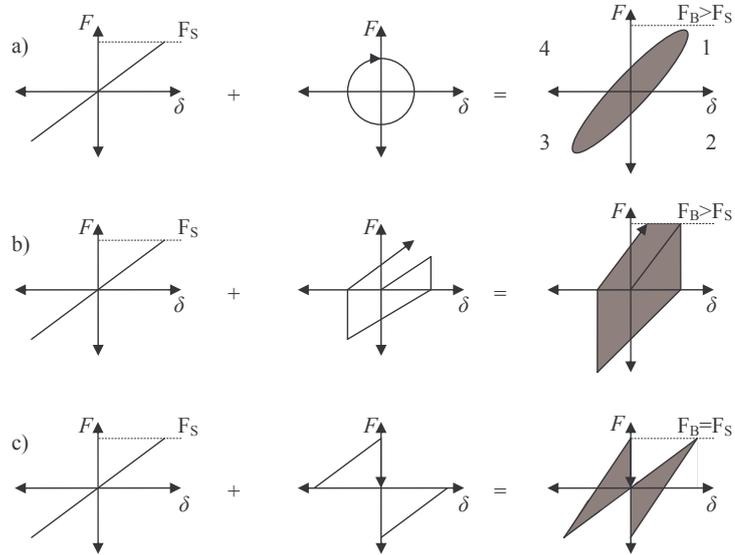
Figure 1.2   Change in hysteretic response of a linear single-degree-of-freedom structure with the addition of a viscous and resetable device. The first row shows the viscous damper. Rows two and three show two configurations of resetable devices. The shaded area indicates the amount of energy dissipated per structural motion cycle. F_S is the maximum structural force, F_B is the maximum total base shear of the structure and damping device combination.

Additional reaction forces produced by an attached damping system are *also* reacted by the foundations. Hence, an increase in base shear demand results when the damping forces coincide with the maximum structural forces, the maximum base shear (F_B) is greater than the maximum structural force (F_S), or $F_B > F_S$.

In contrast the third row in Figure 1.2 presents a different, and novel to this research, configuration of a resetable device. For this case, the overall structural hysteresis loop still encloses some area. However, the maximum base shear of the combined system is *equal* to the structure alone, or $F_B = F_S$. This result is significant because it illustrates the ability to achieve one objective, increasing structural energy dissipation, without creating other potential problems that eliminate the benefit.

Overall, Figure 1.2 illustrates the capability of the novel device design developed in this research to manipulate the hysteretic response. The most important

point is the ability of the device design developed to achieve a response specifi-
cally fitted for each structural application. Thus, rather than accept the tradeoffs
(such as reducing displacements with a corresponding increase in overall struc-
tural forces) that exist in response metrics, designers can specify a structural
control system that gives improvements in a number of metrics and/or reduces
the required strengthening of structural elements for a retrofit application.

Resetable device control systems offer this ability to manipulate the hysteretic
response of the overall structural system and potentially, at lower complexity and
cost than fully active systems. This research examines the broad scope potential
of increasing structural control system robustness and their application arena
by tailoring the control system to the demands and realistic constraints of each
specific structural application. The aim is to broaden the scope of semi-active
structural control and emphasise systems that improve structural performance
over a spectrum of performance metrics to avoid solutions that benefit some
metrics, but degrade others.

1.2   Objective and Scope

The objective of this study is to investigate the efficacy of semi-active resetable
devices in structural control. Analytical and experimental studies are pursued to
validate the full potential and limitations of this technology, as well as examining
the range of possible implementations. The study concentrates on the seismic
response of structures and the scope encompasses five main areas:

1. The design and manufacture of large, near full-scale resetable devices ca-
   pable of modifying or re-shaping structural hysteresis loops in novel ways.

2. The creation of design tradeoffs and guidelines for these devices via:

   - Experimental characterisation of these devices to a full range of input
     motions, including hybrid hardware-in-the-loop testing (HILT).

   - Experimental design and analysis of a wide range of semi-active con-
     trol laws for customising device and structural energy absorption be-
     haviour.

3. Experimental application of resetable devices to large-scale structures.

4. Analytical model development that accurately captures the resetable device dynamics for use in theoretical studies and design.

5. Analysis and simulation study of semi-active implementations using different customised control approaches, and development of performance trade-off curves for design. A particular focus is paid to creating generic design guidelines suitable for use in structural codes or the methodology to create them.

The overall approach is to take semi-active structural control and specifically resetable devices, from the laboratory to realistic implementation and design.

1.3   Overview

Chapter 2 introduces resetable device design with the focus on a new novel design that allows greater flexibility in device response, control, and structural applications. The design method is outlined and possible device configurations are discussed. In addition, an ideal device model is derived, which is used for initial analytical studies. Chapter 3 describes the spectral analysis procedure that investigates the efficacy of resetable actuator control methods introduced in Chapter 2. Chapter 3 provides the motivation for continuing the investigation to realistic devices and structures, as well as creating a methodology to derive design guidelines suitable for use in structural design codes.

Chapter 4 gives device design specifics and the results of extensive experimental device characterisation testing. Chapter 5 details a progression of improvements to the idealised device model to capture all of the realistic and observed device dynamics. The result of an accurate device model is a thorough understanding of the complex device dynamics and how to alter these dynamics via device control to obtain the required response. Hence, the outcome of Chapter 5 is a full set of non-linear models and methods enabling ready design of realistic large-scale resetable devices. In summary, Chapters 2 to 5 present the design, validation and modelling of large-scale semi-active resetable devices which are utilised in a number of applications in Chapters 6 to 9.

Chapter 6 presents an analytical qualitative analysis of a tuned mass damper structural control method utilising semi-active resetable devices. In addition, this chapter presents a novel structural configuration where part of the structural mass is utilised as the damping mechanism. Chapter 7 presents the development of a testing procedure intended as an intermediary step between analytical and full-scale testing. Chapter 8 presents the response of a semi-active rocking wall panel structural system to a suite of earthquake ground motions utilising the testing method developed in Chapter 7. In addition, the semi-active rocking wall response is examined analytically using the validated semi-active resetable device model derived in Chapter 5. Chapter 9 presents the shake table test results for a $\frac{1}{5}^{th}$ scale structure using a resetable damping system and a variety of device control configurations. The results show the efficacy of semi-active resetable damping systems at improving structural performance and highlight the impacts of the different control methods.

Chapter 10 presents the next generation of semi-active resetable devices. The development of these devices recognises some of the improvements that can be made to further increase resetable device capability in structural control. The advantages of the novel resetable device configuration developed in this research are further enhanced in these next generation devices. Finally, Chapters 11 and 12 complete the thesis and present a series of overall conclusions along with some recommendations for future work.

1.4   Summary

This research explores the design, manufacturing and experimental testing of large scale resetable devices, particularly to examine and quantify the device dynamics to motions simulating those during an earthquake. If resetable devices, of a scale suitable for structural implementation, provide significantly improved performance of structures during a seismic event, with minimal cost, the potential to reduce fatalities and structural damage, thereby improving the resilience of communities, is significant.

This chapter has introduced the motivation for this research, in the context of structural control as a means of reducing structural damage. A discussion on

previous and current resetable device research emphasises the need for large scale experimentation, as well as the need for better understanding of these devices to deliver their full potential. The distinguishing feature of this research is the advancement of control methods to widen the application scope of resetable and other semi-active devices, and a thorough understanding of large scale device dynamics and control to provide the knowledge that enables ready implementation.

Chapter 2

Device Design

2.1 Introduction

This chapter introduces the design of semi-active resetable devices and delineates the advantages they offer compared to other structural control devices and approaches. A generic semi-active resetable device design, significantly different to prior designs is developed and the main features and components of the device are discussed. In particular, this novel design offers a far wider range of control response behaviour than other resetable design implementations. A design space is derived that relates basic device dimensions and their force-displacement characteristics. In addition, an ideal model is developed from the governing equations, which is used to begin examining the capabilities of these devices for mitigating seismic response.

2.2 Why Semi-active

Semi-active devices have two major benefits over passive or active control devices. First, they do not require a large energy source to operate, as active devices do. This characteristic is the result of modulating the device physics or mechanics via changes to the physical space or material properties they use to operate. Hence, they can only provide and modulate resistive forces. Therefore, the addition of energy to the system is effectively prohibited, as with passive devices, making the system inherently stable.

Second, the smart control of the devices makes them suited to more applications and better able to respond to structural changes over time, than passive devices. More specifically, unlike a passive device, the active modulation of the resistive forces provides a far greater ability to minimise a range of structural responses.

2.3   What is a Resetable Device

Resetable devices are essentially non-linear spring elements that are able to actively reset their rest length, releasing stored energy before it is returned to the structure. Therefore, instead of altering the damping of the system directly, resetable devices non-linearly alter the stiffness, with the stored energy being released rather than returned to the structure as the compressed fluid is allowed to revert to its initial pressure.

2.3.1   Traditional and Prior Devices

The originally proposed resetable device (Bobrow and Jabbari [2002]) has both chambers connected via a valve that can be internal or external to the device as depicted in Figure 2.1. This valve controls the hysteretic response of the device by holding or releasing the pressure between the chambers. The valve is activated, equilibrating the pressure in each chamber, on the peak displacement in each cycle resulting in the force-displacement hysteretic loop shown in Figure 2.2.

This original design configuration limits the hysteretic response shape that can be obtained and, in larger devices, its full force potential. More specifically, the chambers are directly linked so the pressure in each chamber is a function of the pressure in the other chamber. This interdependency affects the energy release time, as large devices with high pressure and larger chamber volumes require more time for the active chamber to revert or return to equilibrium pressure on resetting. This time period can be significant compared to structural response periods (Chase et al. [2006]). For this single valve design, pressure equalisation of the active chamber relies on venting to the other chamber. Therefore, during the time required to equalise and reset, the structural motion is not being resisted.
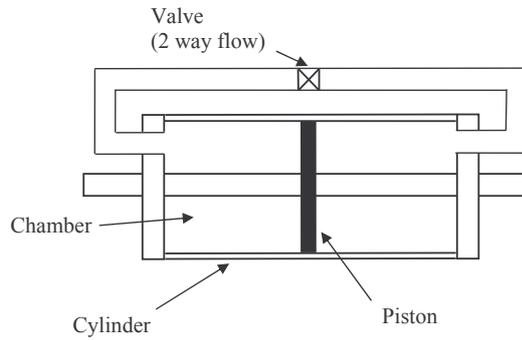
Figure 2.1   Schematic of original proposal of a resetable device with a single valve connecting the chambers.

This delay limits the peak forces the device may obtain on subsequent cycles and thus its overall ability to reduce response. In fact, the more the device resists motion and the more energy it stores on a given cycle, the greater this effect on the subsequent cycle.
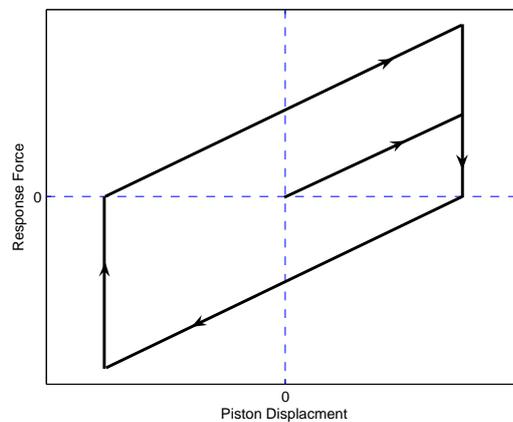
Figure 2.2   Ideal hysteretic response of originally proposed resetable device utilising a single valve connecting the device chambers. The active chamber valve is opened releasing the stored energy at the peak piston displacement for each cycle.

2.3.2   Independent Chamber Design

To overcome the limitations in energy release time and hysteretic response of the single valve design, a device with a valve on *each* chamber was designed,
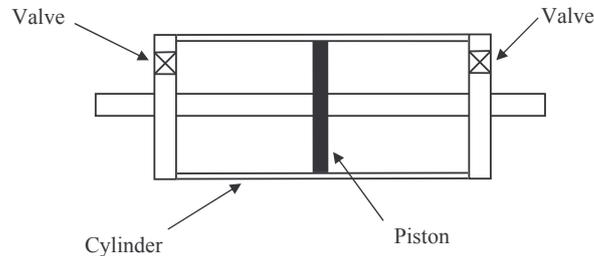
Figure 2.3   Schematic of independent chamber design, one valve per chamber.

as illustrated in Figure 2.3. Using this novel independent chamber design, the pressure in each chamber is no longer a function of the pressure in the other chamber. In addition, the resetting of each chamber does not require the other chamber to be reset or effectively out of use at the same time. Thus, hysteretic behaviours that are not possible with the single valve design becomes apparent.

More importantly, by independently controlling each chamber, the energy reset time is able to be much longer, as motion can be resisted by the other chamber during this time. Hence, this design controls the pressure-volume state of each chamber independently. As a result, the active chamber can be utilised to resist motion effectively instantly without waiting for the energy release to be completed for the other chamber. Equally importantly, independent control of each chamber allows a far wider range of device force-displacement behaviour. This ability to semi-actively sculpt the hysteretic behaviour and allow for long reset times leads to the potential use of resetable devices in a wider range of applications, as well as enhanced energy dissipation properties.

The devices in this research use air as the working fluid, which eliminates the need for complex external plumbing systems. More specifically, to release the stored energy the pressurised air is vented to atmosphere. Device response forces can feasibly be altered by using a different working fluid or pre-pressurising the device as discussed in Chapter 10. However, regardless of any additional working fluids or plumbing used, the overall independent chamber approach presented can be generalised with all its potential advantages.

2.4   Device Design

This section details the design procedure of two prototype devices used in this research. The design space is first defined in a general way using ideal equations, which lead to a series of trade off curves. From these curves basic device dimensions for these prototypes can be determined based on the desired application requirements. The final device dimensions are determined from required force and stiffness parameters and practical limits on the size and weight. In addition, the hardware required to complete the devices and for control is specified to fully define these prototype devices.

The largest resetable device built prior to the start of this research had a peak force in the order of 100N (0.1kN) (Bobrow and Jabbari [2002]). In the interim Kajima Corporation has produced limited numbers of 1-2MN devices using the traditional device control of Section 2.3.1, using hydraulic servo-mechanisms to generate these very large forces. These devices are used primarily in a support rather than a full control role (Yang et al. [2007]) and have not yet been tested in a large seismic event.

2.4.1   Device Design Space and Dimensions

The main design considerations are the nominal stiffness required from the device and the device size. The stiffness determines the typical force response values obtained from the device and installation size restrictions may exist in the structural application. In addition, specified forces need to be produced at specified piston displacements, which therefore relates the stiffness and size parameters. A design space constructed from a series of trade off curves gives possible dimensions for these types of devices for a series of different stiffness values.

The fundamental force-displacement response of a resetable device is determined by the following parameters:

- the initial chamber length, L_0.

- the maximum piston displacement, δ where $\delta \leq L_0$.

- the piston diameter, D

- any additional chamber volume, as discussed in Section 4.4.2.1.

These parameters are shown schematically in Figure 2.4.
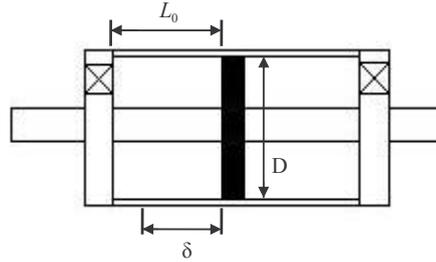
Figure 2.4   Basic device dimensions.

Assuming air is an ideal gas which undergoes isentropic compression (no heat transfer) then the ideal gas law may be used.

$$pV^{\gamma} = c \tag{2.1}$$

where:

- p is the air pressure

- V is the air volume

- γ is the ratio of specific heats ($\gamma = 1.4$ for air)

- and c is a constant.

Let the pressures in each chamber be p_{c1} and p_{c2}, respectively. The ideal or theoretical response force (F) produced by the device is the pressure difference between the two chambers multiplied by the cross-sectional area (A) of the piston, or $F = (p_{c2} - p_{c1})A$. Assuming that the piston starts initially from the center position so that the initial chamber volumes (V_0) and pressures (p_0) are equal, then $p_0 V_0^{\gamma} = c$. Therefore, $F = (p_{c2} - p_{c1})A = [(V_0 + Ax)^{-\gamma} - (V_0 - Ax)^{-\gamma}]Ac$, where $V_0 \pm Ax$ is the change in volume of the chambers as the piston moves.

Given that $(1 + \frac{Ax}{V_0})^{-\gamma} = 1 - \frac{\gamma Ax}{V_0} + O(x)^2$, by a first order approximation from a Taylor series expansion, the force produced for a piston displacement x is

$$F = \frac{2A^2\gamma P_0}{V_0}x \qquad (2.2)$$

Therefore, the device stiffness can be first order approximated:

$$K = \frac{2A^2\gamma P_0}{V_0} \qquad (2.3)$$

Equations 2.2 and 2.3 create an approximate stiffness for design purposes and a simple model. They are taken directly from the initial work of Bobrow and Jabbari [2002].

The initial chamber volume is related to the initial chamber length by $V_0 = L_0 A = L_0 \pi \frac{D^2}{4}$. Substitution of this term into Equation 2.3 and rearranging for the chamber diameter D creates a design equation:

$$D = \sqrt{\frac{2L_0 K}{\pi \gamma P_0}} \qquad (2.4)$$

Equation 2.4 relates the device diameter (D) to the required device stiffness (K). The initial chamber pressure (P_0) is typically atmospheric pressure. Similarly, the length (L_0) is typically constrained by the application and is determined by the stroke required during large structural response. Overall, this equation relates the three basic design parameters, device diameter and length as a function of required stiffness.

To investigate the full range of capabilities of the devices, trade off curves for a number of different stiffness values are created using Equation 2.4, and plotted in Figure 2.5. The nominal stiffness values give a range of maximum forces of 0.25kN to 2.5kN for a 10mm piston displacement. The 10mm displacement is based on the $\frac{1}{5}^{th}$ scale application to be studied in Chapter 9, and thus specifies L_0.

The design space is shown boxed and is limited by minimum diameters and practical limitations on the size of the device. More specifically, the practical limitations include ensuring the chamber length is greater than the maximum expected displacement, limiting the internal pressure to 250kPa, keeping the mass under 20kg (for ease of transport), and limiting the maximum diameter to 0.2m and maximum length to 0.6m. The size constraints relate to practical packaging constraints for the $\frac{1}{5}^{th}$ scale structure. The pressure limit is related to using basic lower cost seals, valve pressure limits, as well as for safety.
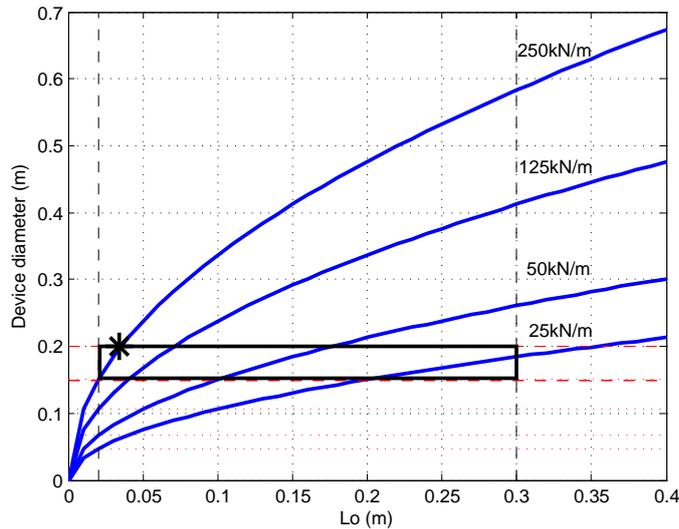
Figure 2.5   Trade off curves relating initial chamber length L_0 to diameter d for different device nominal stiffness values. The possible design space is shown boxed and the first prototype dimensions and stiffness are marked with an $*$.

The design space curves determined from the basic, ideal analytical equations presented give an *indication* of the device response. The curves could be reproduced using more realistic device dynamics once a number of devices have been manufactured and experimentally characterised. Such advanced models would create a better design tool to obtain realistic and accurate values for incorporating these types of devices into real structures. However, these ideal equations allow basic tradeoffs to be examined and initial design dimensions to be selected.

Specific device parameters can readily be determined from the design space. The characteristics of the first prototype were based on the demands of a $\frac{1}{5}^{th}$ scale,

two bay, four storey moment resisting steel frame building with a total mass of approximately 3 tonnes (Kao [1998]). Previous studies (Hunt [2002]) have shown that a practically realisable and effective peak force for effective structural control is around 10-15% of the total structural weight. Therefore, with 2 devices, one on each side of the structure, a maximum force of 2.5kN per device is required for this $\frac{1}{5}^{th}$ scale case. More specifically, the device was required to develop this maximum force around a displacement of 10mm based on studies of the structural response under earthquake loading. This requirement yields a nominal stiffness of 250kN/m (Mulligan et al. [2005], Chase et al. [2005a]). Thus, the expected response of the first prototype is located in the upper left corner of the design space, as shown in Figure 2.5.

These specific design parameters are by no means the only point that could be selected. However, the highest possible stiffness was preferred, as it gave the maximum force and greatest energy dissipation for the smallest displacement. In addition, maximising forces from an idealised tradeoff curve allows for any underestimation achieved due to valve or seal leakage, or any other specific design and manufacturing flaw. Hence, it is also a safer, more conservative design choice.

The second prototype was designed to produce a force of 10kN at 17mm displacement, giving a nominal stiffness of 590kN/m (Anaya et al. [2007]). This second prototype was also designed for the $\frac{1}{5}^{th}$ scale structure. However, the force and stiffness requirements are higher than the first prototype due to re-evaluation of the $\frac{1}{5}^{th}$ scale structure dynamics. More specifically, modelling of this structure incorporating resetable devices for structural control resulted in significantly reduced structural displacements. Hence, the second prototype was designed with a shorter piston stroke and the peak forces increased to further improve the structural performance over the modelled result using the first prototype response.

Figure 2.6 depicts an exploded view of the initial prototype resetable device design, including some more specific details. The main components are the cylinder, piston, piston shafts, end caps, valve holes and seals. The seals are an important aspect of the design as they are required to prevent air from moving between the two chambers and escaping from the device. O-rings are used at the end caps and cylinder join, and a teflon seal with piston rings is used around the piston. Teflon seals are used where the piston passes through the end cap.
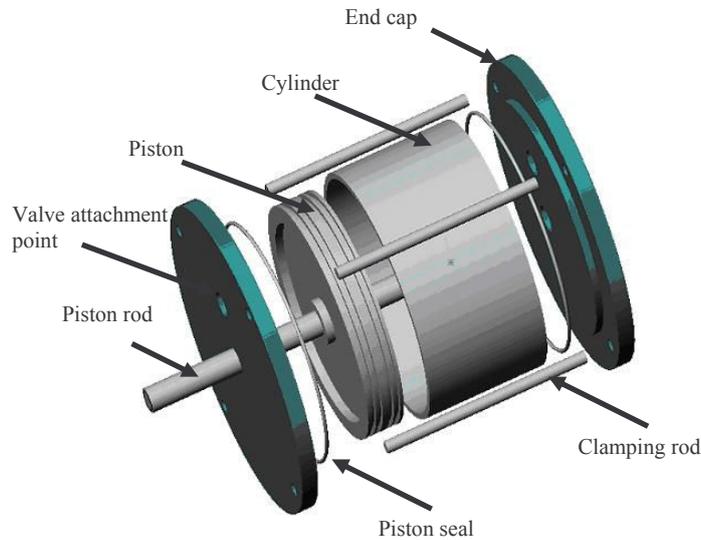
Figure 2.6   Exploded view of device with the cylinder, piston, end caps, piston rod, piston seal, and clamping rod labelled.

2.4.2   Control System and Integration

The hysteretic response of the device is determined by the control system managing each chamber's valve. A robust control system relies on systematically and accurately detecting specific points or events, over a general (sinusoidal) motion cycle. The important aspect to note here is *generalised* motion. It is easy to assume that the piston motion is known in advance when testing. Hence, the control law for a simple sinusoidal or other tests could be based on specific displacements, rather than specific characteristics of an unknown displacement. For generic motion, there is no way of determining the motion amplitude prior to each cycle. Therefore, for a completely generic control law the only systematically detectable points are the maximum displacements as they occur in each cycle before reversal, and the zero crossing points. These two generalised points can be found in any response input motion using displacement sensors on the device, or inferred via other sensors.

Using an intermediary point between the maximum displacement and zero crossing point may limit the energy dissipation. In particular, during fast piston motion there may be insufficient time to release the energy if the valve is commanded to close again too soon after opening. However, these issues may be addressed by selecting large valves that allow faster equilibration. In other cases a specific displacement, for a valve state change, may be stipulated as part of the

control logic where this displacement is determined from the structural dynamics.

The maximum cycle displacement of the device piston coincides with a change in sign of the velocity. The piston velocity is readily calculated from the displacement signal. However, due to noise associated with the displacement signal, filtering is required to avoid repeated valve actuation. A zero crossing is detected when the sign of the displacement changes. Thus, a typical sinusoidal motion cycle can be divided into quadrants, as shown in Figure 2.7. Control laws based on these quadrants can readily be implemented and tested to compare performance with sinusoidal input motion and then tested with more general input motion.
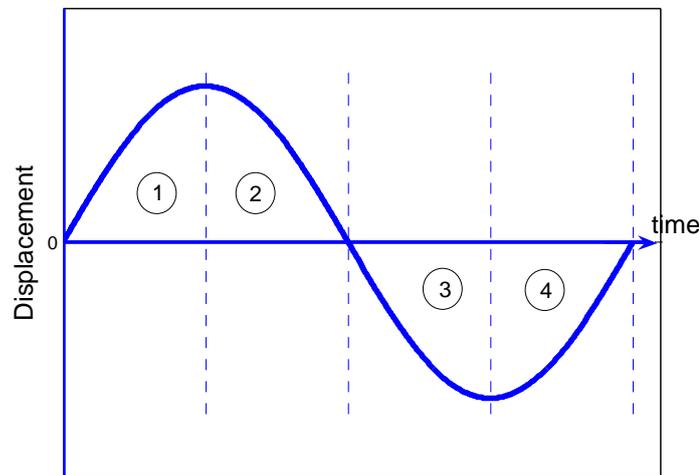
Figure 2.7   General, sinusoidal motion divided into quadrants, numbered 1 to 4.

The active chamber is the chamber where the pressure differs from the pressure of the fluid reservoir, which occurs when the valve is closed. Normally the active chamber is reducing in volume, so the active chamber is on the side of the device that the piston is moving towards. Hence, the active chamber pressure generally increases, storing energy to be dissipated.

The quadrant numbers shown in Figure 2.7 are similarly shown on force-displacement axes in Figure 2.8. This depiction gives each control law in this research its name. Original proposals for resetable devices (Bobrow and Jabbari [2002]) describe the control law as resisting all the motion of the piston out to the maximum displacement and releasing the energy at the maximum piston displacement, when the piston velocity is zero. This results in the force-displacement response shown in Figure 2.2 and in detail in Figure 2.9. Because it is active in all

four quadrants of Figures 2.7 and 2.8, it has been termed the 'one through four' (1-4) control law, as there are resistive/reaction forces in all of the quadrants.
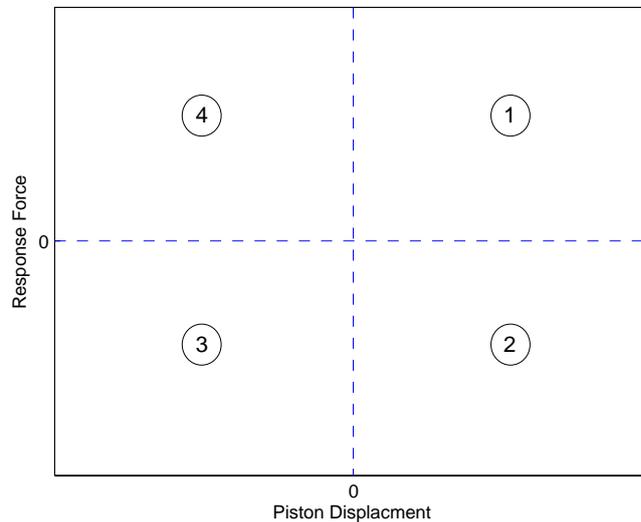
Figure 2.8   Quadrants 1 to 4 shown on force-displacement axes.

Figure 2.10 shows the force-displacement response if only motion *away* from zero is resisted. This law closes the valve on the active chamber from the zero position to the maximum piston displacement, while holding the opposite valve open. Once again at the peak piston displacement, or zero velocity point, the valve on the active chamber is opened releasing the stored energy. Once the piston has passed the zero position, moving in the opposite direction, the opposite valve is closed and that specific motion is resisted. This behaviour is detailed in Figure 2.10.

This law results in some parts of the motion having zero resistive forces. Thus, the law is termed the one-three (1-3) law as resistive forces are provided in only the first and third quadrants. Typical peak forces produced by the device under the 1-3 law are less than the peak forces for the 1-4 law, with the same piston displacement. This reduction in peak force values is expected as only half the amount of motion input to the device is resisted.

If only motion *towards* zero from peak the displacement is resisted, the resulting force-displacement response is that of Figure 2.11. Following the convention of the other control law names, this law is denoted the two-four (2-4) control law, as it provides reactive/resistive forces only in the second and fourth quadrants. In this case, the active chamber valve is closed at the peak piston displacement
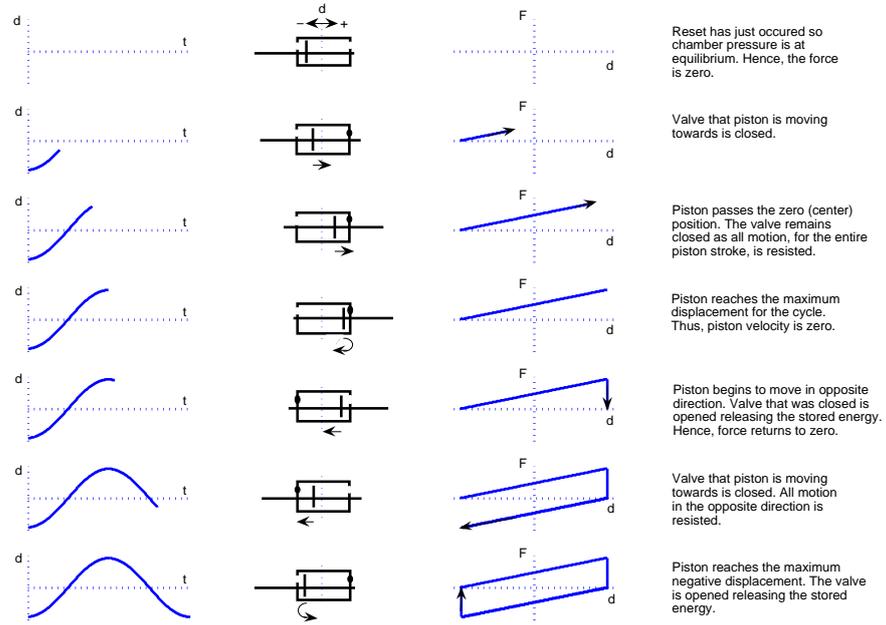
Figure 2.9 Schematic showing one cycle of device under the 1-4 control law. The first column shows the piston displacement with respect to time. The second column shows a diagram of the device indicating the piston motion direction and the valve states. The third column shows the ideal force-displacement response.
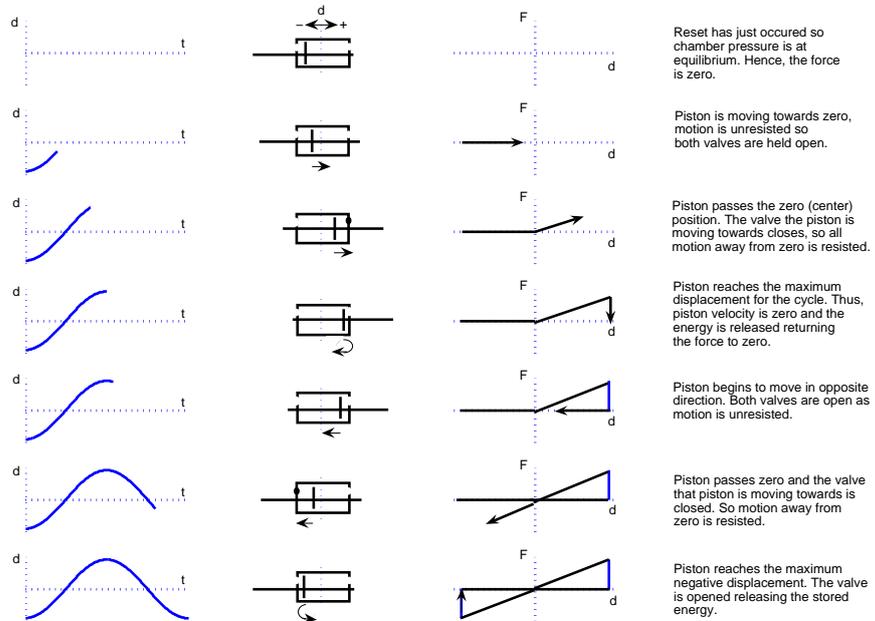
Figure 2.10 Schematic showing one cycle of device under the 1-3 control law. The first column shows the piston displacement with respect to time. The second column shows a diagram of the device indicating the piston motion direction and the valve states. The third column shows the ideal force-displacement response.

and the energy is released when the piston crosses the zero position. This approach leaves the motion from the zero position to the peak position un-resisted. Peak forces produced by the device under this control law are again less than the peak forces of the device under the 1-4 control law, for the same total piston displacement. In addition, the peak forces can be slightly lower again than those for the 1-3 response due to the active chamber volume being relatively large.
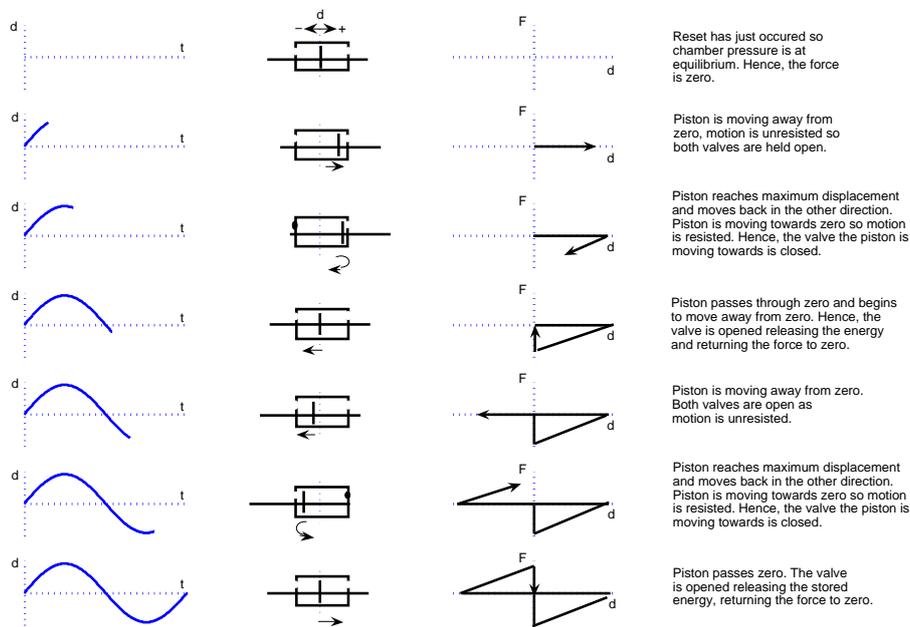
Figure 2.11 Schematic showing one cycle of device under the 2-4 control law. The first column shows the piston displacement with respect to time. The second column shows a diagram of the device indicating the piston motion direction and the valve states. The third column shows the ideal force-displacement response.

It should be noted that valve switching commands are determined by a change in the piston direction and zero crossing. Thus, the device force-displacement behaviour is not dependent on the motion amplitude. The behaviour of the device is (or valves) is exactly the same given any piston displacement amplitude. To clarify further, the valve control system detects changes in motion rather than the numerical value of the piston displacement.

2.5   Ideal Device Model

An ideal device model derived from the ideal gas equations was developed to investigate the expected device response to these different control laws. More specifically, the device force response (dependent on the active chamber pressure) for a change in chamber volume, which in turn is dependent on piston displacement, can be defined:

$$p_2 = p_1 (\frac{V_1}{V_2})^{\gamma} \tag{2.5}$$

where p_1 and p_2 are the pressures before and after piston displacement, V_1 and V_2 are the volumes of the active chamber before and after piston displacement.

$$F = (p_{c1} - p_{c2})A \tag{2.6}$$

where F is the force produced by the device, p_{c1} and p_{c2} are the pressures in each chamber, and A is the piston area.

The ideal model assumes ideal behaviour in all aspects of the device response. Ideal behaviour includes assuming an instantaneous energy (pressure) release reset time. It also assumes zero force is developed when the chambers are open to the fluid reservoir, as well as exactly symmetrical behaviour. More specifically, instantaneous energy release dictates that the response force return to zero immediately after a valve is opened. Symmetrical behaviour requires the central piston position to be perfectly assigned.

2.6   Summary

This chapter has introduced the design for resetable devices with air as the working fluid. More importantly, it has introduced a novel design that disassociates the chamber pressures resulting in control law applications not possible for the originally proposed design. This novel device design allows manipulation or sculpting of the hysteretic response depending on the structural demands. In addition, the sculpting of the response alleviates some of the response metric tradeoffs that can

occur with structural control.

The parameters that define the response are introduced and a design space is created. Detailed device design is discussed in Chapter 4. Three control laws are outlined that give markedly different hysteretic response from the device. Last, equations and assumptions for an ideal model of the device are defined. This model is used in a spectral analysis detailed in Chapter 3.

Chapter 3

Spectral Analysis

3.1 Introduction

The study discussed in this chapter investigates the effectiveness of the addition of a resetable actuator to a structural system. More specifically, the efficacy of these devices is examined by comparing the response of a linear single-degree-of-freedom (SDOF) structure with an energy dissipation system comprising of resetable actuators using the three control laws introduced in Chapter 2. The results are normalised to the uncontrolled structural case to remove any structural stiffness dependency.

The method utilises three earthquake suites from the SAC project. Each suite is comprised of 10 different time histories with two orthogonal directions for each history (Sommerville et al. [1997]). The three suites represent ground motions having probabilities of exceedance of 50%, 10% and 2% in 50 years in the Los Angeles region. The suites are termed the low, medium and high suites respectively. Using suites of ground motions rather than a single individual event eliminates the probability of reaching erroneous conclusions about the efficacy of a particular control method, or percentage of additional stiffness.

This analysis provides an extensive insight into the capabilities of resetable devices to improve structural performance. The relative performances of the three control laws, introduced in Figures 2.9 to 2.11, at improving the structure performance in terms of reducing structural damage is highlighted (Rodgers et al. [2007b]). In addition, the results indicate which control law is suitable to particular structural applications.

3.2   Analysis Procedure

Response spectra are generated for each suite with the structural displacement, structural force, total base shear and area under the response spectra in the seismically important range of $T = 0.5 - 2.5s$ being the metrics of interest. The structural force and total base shear both indicate strength requirements. However, they are distinct, as the structural force is defined as the base shear for a linear, undamped structure, whereas the total base shear is the *sum* of the structure force and resistive forces from the resetable device. Thus, the structural force indicates the required column strength and the total base shear indicates the required foundation capacity.

Reduction factors illustrate the improvement in structure performance with the addition of a resetable device damping system compared to the uncontrolled structure. These reduction factors are normalised to the uncontrolled case to allow easy comparison of the improvements gained via each control design. The response spectra are created for structure periods from 0.1 to 5.0s in 0.1s increments.

The SDOF structure model includes structural damping of 5%. This value is commonly adopted by design codes and standards and represents the inherent structure damping. The stiffness of the structure is determined by the required natural frequency for the spectra point. An *additional* 50% or 100% of the structure stiffness is provided by the resetable devices.

The distributions of the results can be well modelled by a log-normal probability density function. Therefore, appropriate lognormal statistics are utilised to analyse the spectra results within the suites and for all ground motions. Thus, variables that define the spectra results are the log-normal geometric mean ($\hat{x}$), and standard deviation, or dispersion factor (β). The log-normal geometric mean is defined:

$$\hat{x} = \exp\left(\frac{1}{n}\sum_{i=1}^{n}\ln(x_i)\right) \tag{3.1}$$

Similarly, the dispersion factor is defined:

$$\beta = \sqrt{\frac{1}{n-1}\sum_{i=1}^{n}(\ln(\frac{x_i}{\hat{x}}))^2} \tag{3.2}$$

The statistical values defined in Equations 3.1 and 3.2 are used to indicate the change in structure response for the three control laws investigated. The geometric mean indicates the expected response value across the suite, while the dispersion factor indicates the relative spread of results. These two statistical parameters $(\hat{x}, \beta)$ are plotted against each natural period to investigate overall trends.

All results are normalised to the uncontrolled case. Hence, the results are insensitive to structure stiffness. More specifically, the results can be applied to any sized structure as they are only dependent on the control law type and relative ratio of structure stiffness to device stiffness. In addition, normalised metrics allow rapid and easy comparison between results, unlike absolute values where data collation is not intuitive and can be difficult.

3.3 Spectral Analysis Results

The maximum structure displacement, maximum structure force, and maximum total base shear at each period for all ground motion are recorded to generate response spectra. These values are normalised to the uncontrolled case to give reduction factors. Response spectra for 0%, 50% and 100% additional stiffness for the three control laws are thus created.

All results indicate the structure response for each control law is largely suite invariant. Therefore, along with the results for each suite, the results across *all* suites are presented. This comparison over all the suites clearly shows and highlights the effect of each control law on the metrics of interest.

The structural force reduction factor mean values for each suite are shown for the 1-4, 1-3 and 2-4 control laws in Figure 3.1. In addition, the structural force

reduction factors for all ground motions and all control types are shown in Figure 3.2. Figure 3.2 indicates that the 1-3 and 2-4 control laws have similar structural force reduction median values across all periods. However, the 1-4 control law case is approximately twice as effective at reducing the reduction factor for small periods and approximately 30% more effective at larger periods than the other two control laws. This result is expected as the device using the 1-4 control law resists the structure motion at all times, whereas devices under the 1-3 and 2-4 laws only operate for half of the motion cycle. Thus, the devices under the 1-4 control law are able to significantly reduce the structural forces by storing and dissipating more energy.

The total base shear reduction factors are similarly shown in Figures 3.3 and 3.4. The results show that the addition of a resetable device can for some control laws *increase* the total base shear. More specifically, the total base shear reduction factors are above 1.0 for most periods with the 1-4 and 1-3 control laws. In contrast, the 2-4 control law has a reduction in the total base shear reduction factor across all periods. This result is significant as it indicates a reduction in the foundation demands if the 2-4 control law is used.

The structure displacement reduction factors are shown in Figure 3.5 for 50% and 100% additional stiffness. Once again the results are largely suite invariant. All control laws result in a reduction of the structure displacement compared to the uncontrolled case. As expected, the 1-4 control law has the greatest reduction in structure displacement with the 1-3 and 2-4 control laws showing similar results.

The reduction factors for the structural displacements were observed to be largely suite invariant. Therefore, the area under the displacement response spectra over the seismic response is examined as an indication of response magnitude. More specifically, the response over the range of 0.5 to 2.5 seconds was numerically integrated for each earthquake record and presented as reductions factors by normalising to the uncontrolled case. The geometric mean for each suite was found and then averaged across all suites. Thus, reduction factors for additional stiffness values of 0, 20, 50, 80 and 100% for the three control laws were obtained, as shown in Figure 3.6.
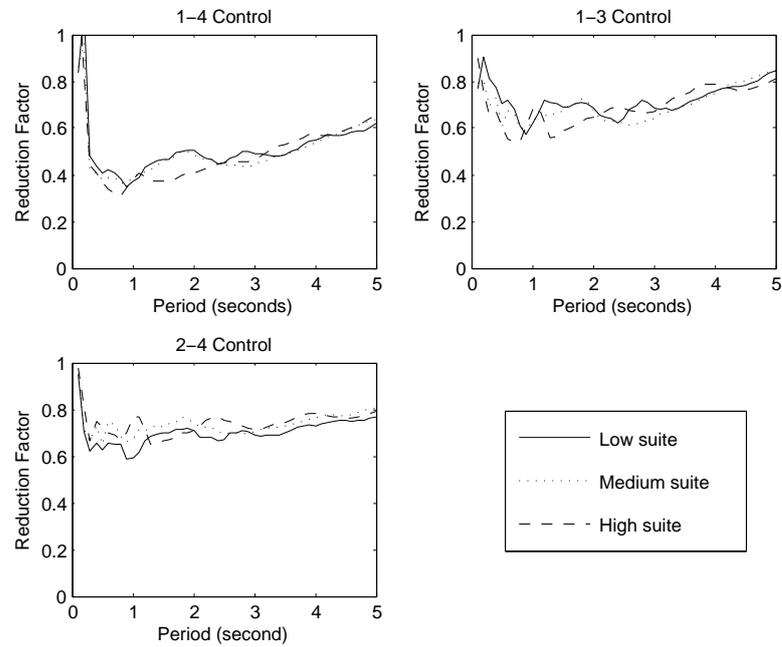
Figure 3.1 Structure force for additional device stiffness of 100% for the three ground motion suites and the three control laws.
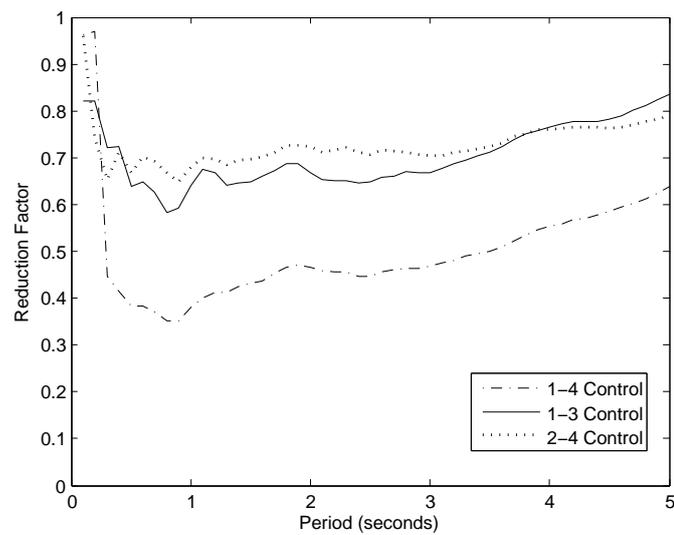
Figure 3.2 Structure force for additional device stiffness of 100% averaged over all suites.
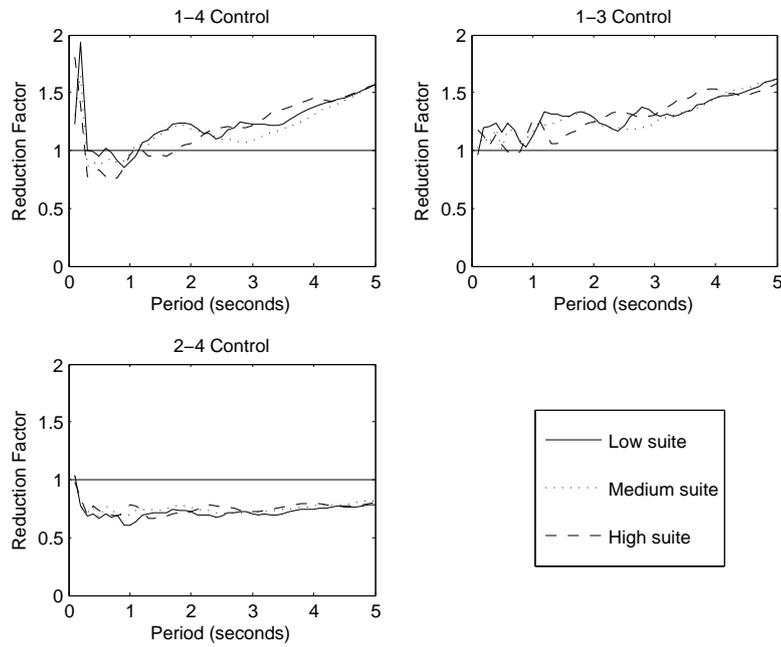
Figure 3.3   Total force (base shear) for additional device stiffness of 100% for the different control laws for each suite and the three control laws.
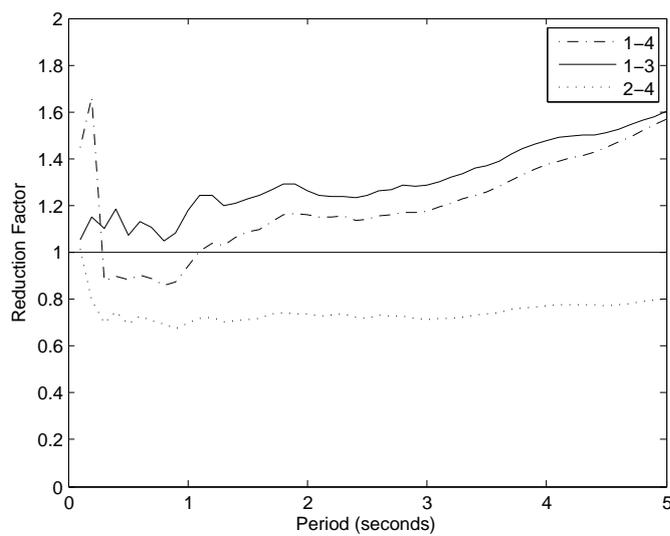
Figure 3.4   Total force (base shear) for additional device stiffness of 100% averaged over all suites.
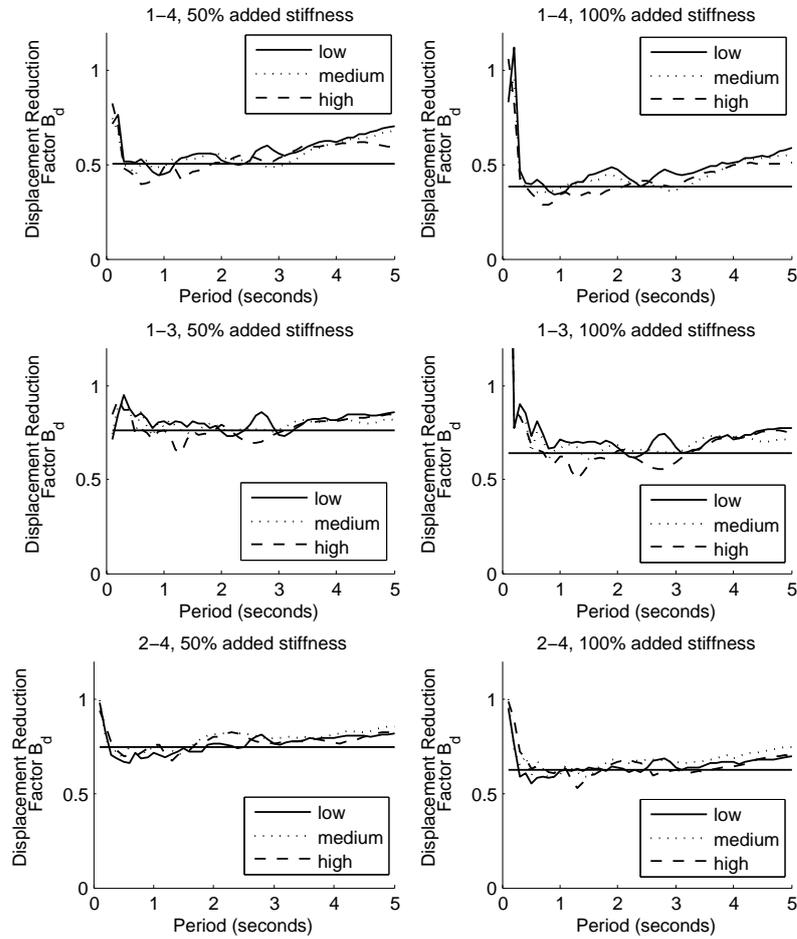
Figure 3.5   Reduction displacement factors for 50 and 100% additional stiffness. The value calculated from Equations 3.3 and 3.4 is also shown.

The area reduction factors across the range of seismically important natural periods, representing the majority of the constant velocity region of the spectra, can be interpreted as an average reduction factor. The reductions observed with the 1-3 and 2-4 control laws are similar with the 2-4 slightly outperforming the 1-3 case across the entire range of additional stiffness. Reduction factors for these laws range from 1.0 to ∼ 0.65. The 1-4 control law outperforms both the 1-3 and 2-4 laws in the reduction of the displacement spectral areas. A reduction factor value of ∼0.39 is achieved for 100% additional stiffness with the 1-4 control law.
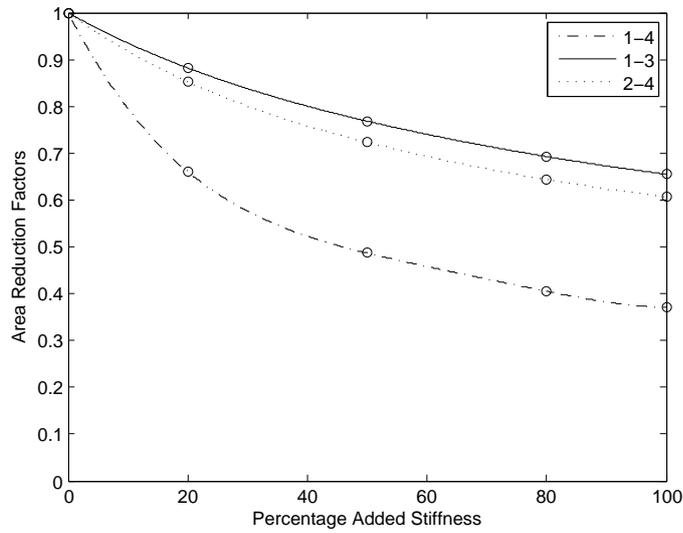
Figure 3.6   Reduction factors for the area under the displacement response spectra between 0.5 and 2.5 second periods normalised to the uncontrolled case and averaged across all suites. The data points show the results for 0, 20, 40, 60, 80, and 100% additional stiffness. The lines indicate the area reduction factors derived from the empirical equations.

3.3.1   Empirical Area Reduction Factors

To bring resetable devices into the design analysis realm, empirical equations are fitted over the range of additional percentage stiffness results to approximate the reduction factors. The empirically calculated area reduction factors are also plotted in Figure 3.6. The form of the empirical equation is:

$$R = 1/B \tag{3.3}$$

where R is the multiplicative reduction factor and B is the divisive reduction factor, defined as:

$$B = \sqrt{1 + C\frac{K_{resetable}}{K_{structural}}} \tag{3.4}$$

where $K_{resetable}$ is the additional stiffness provided by the resetable device, $K_{structural}$ is the structural stiffness, and C is a constant dependent on the control law. C has values of 5.75, 1.43, and 1.59 for the 1-4, 1-3 and 2-4 control laws, respectively.

In addition, the equivalent viscous damping can be quantified from the additional stiffness using the empirical reduction factors. Equivalent viscous damping allows comparison between reductions achieved with resetable devices to conventional viscous damping systems. Thus, the overall effective damping is comprised of the inherent structural damping and hysteretic damping component, defined as the equivalent viscous damping. The inherent structural damping is typically defined as 5% of critical for spectral investigations. The hysteretic component can be defined as:

$$\xi_{eq} = \frac{C}{10}\frac{K_{resetable}}{K_{structural}} \tag{3.5}$$

where ξ_{eq} is the equivalent viscous damping of the added resetable device. Thus, 100% additional stiffness from the resetable devices will produce 57.5, 14.3, and 15.9% equivalent viscous damping for the 1-4, 1-3, and 2-4 control laws, respectively.

Figure 3.5 shows the displacement reduction factors for the 50% and 100% additional stiffness with the three control laws. In addition, the reduction factors given by the empirical Equations 3.3 and 3.4 are shown. These empirically derived reduction factors accurately represent the actual displacement reduction factors. Some variation between the empirically derived and actual reduction factors is seen above $T = 3.0$ s. However, the empirical equations are appropriate between 0.4 and 3.0 s, the entire constant velocity region of the spectra.

Figure 3.7 shows the displacement reduction factor for each suite normalised

to the average value for all ground motions. For all control laws the deviations away from 1.0 are small, indicating the structure response for the control laws is motion type independent. More specifically, the frequency content of each earthquake record does not alter the efficacy of each control law. Thus, the structure response to any earthquake event is able to be predicted with high confidence.
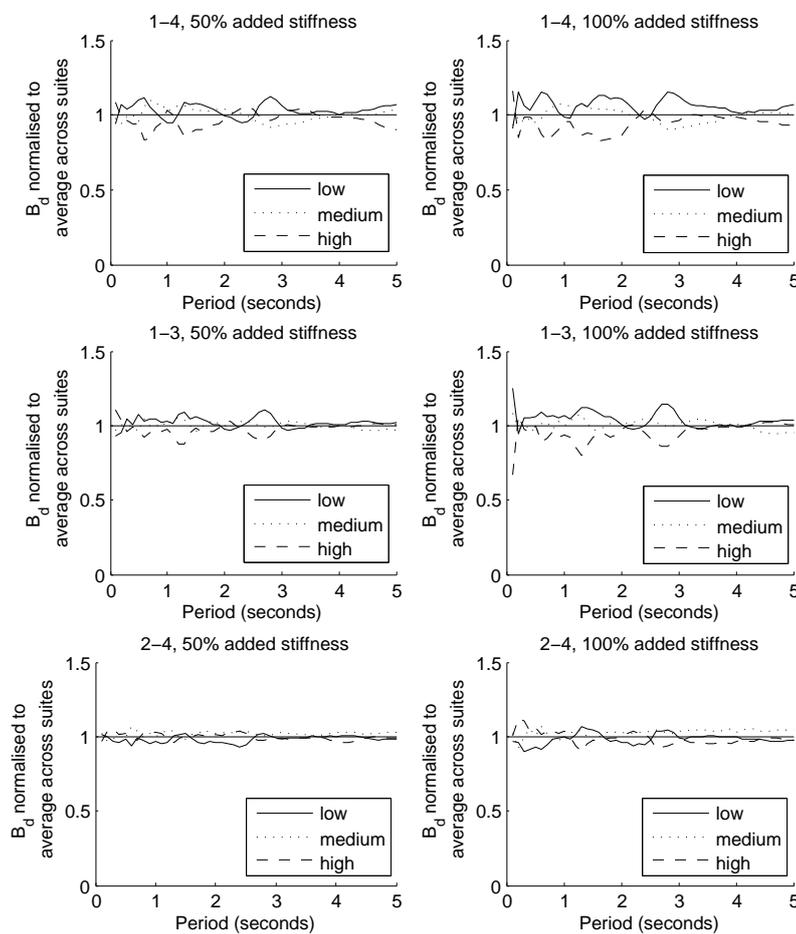
Figure 3.7   Reduction displacement factors for 50 and 100% additional stiffness for each suite normalised to the average across all ground motions.

3.4   Summary of Control Law Dependent Results

3.4.1   1-4 Control Law

The 1-4 control law shows excellent ability at reducing the structure displacement and structure forces. These results were expected, as the 1-4 control law device resists all the structure motion, allowing the device to store and dissipate a large amount of the structural energy, as shown in Figures 1.2 and 2.9. However, resisting all the structural motion increases the foundation demand, shown by an increase in the total base shear compared to the uncontrolled structure. Thus, the addition of a resetable damping system using the 1-4 control law is beneficial when the foundations have sufficient strength to withstand an increase in demand, which is most likely to occur for new structures where the damping system is designed simultaneously with the structure.

3.4.2   1-3 Control Law

The results using the 1-3 control law show similar results to the 1-4 control law. However, the benefits are not as considerable and the disadvantages are approximately equal. Thus, in general for conventional structural types it may not be desirable to resist only motion away from the center position. However, this control law may be useful in structural applications where it is desirable for the devices to work only in tension, such as rocking wall panels described in Chapter 8.

3.4.3   2-4 Control Law

The 2-4 control law does not show as great a reduction in structure displacement and force as the 1-4 control law. However, the main advantage of this control law is the ability to reduce the total structural forces, or foundation demands, while also significantly reducing the structure demands and displacements, as shown in Figures 3.1 to 3.7. Thus, this control law is of benefit to already constructed buildings where it is difficult to increase the foundation strength. In particular,

historical structures requiring structural performance improvement would benefit from the addition of a damping system using resetable devices under the 2-4 control law. In these cases foundation strengthening may be a prohibitively costly and significant damage could result if foundation strengthening was attempted.

3.5   Closure

This investigation has shown the efficacy of resetable devices at improving structural performance over the seismically important period range of $T = 0.5$ to $2.5s$. The three control laws investigated have different strengths and potential weaknesses. Specifically, the 1-4 control law greatly reduces the structural forces and structural displacements, while increasing the total structure forces. The 1-3 law has similar qualitative response to the 1-4 case but is significantly outperformed in terms of quantitative response. The 2-4 control law has similar displacement reduction factor values to the 1-3 case. The significantly different advantage achieved with the 2-4 control law that makes it stand apart from the other two laws is the ability to reduce the total structural forces.

Chapter 4

Design Specifics and Device Validation

4.1 Introduction

This chapter details the specific prototype device design and the experimental device characterisation prior to use in experimental structural applications. One outcome is a general device characterisation approach that provides the necessary information to fully define device dynamics and capabilities for any similar device or system. As part of this process, the ideal model predictions of Section 2.4.2 are compared to the experimental results to see how well this simple model captures the fundamental device dynamics. The overall result is a thorough understanding of *all* the device dynamics, including those that were not necessarily expected for these large scale devices prior to this investigation.

The prototypes designed and tested in this research are the first near to full-scale semi-active resetable devices utilising air as the working fluid. In addition, it is the first time any such devices have been fully characterised to determine the true dynamic response. The size and force capacity of these devices makes them suitable for large-scale structural experimental testing that produces results applicable to real structures. Hence, a full dynamic characterisation is required to ensure the results are fully understood and any limitations can be minimised or avoided in a practical implementation.

The test structure used for large scale device application testing has four storeys with a mass of one tonne per storey. Previous studies have shown that practical and achievable control forces of approximately 15% of structure weight (Hunt [2002]) can produce excellent response mitigation. Therefore, the response

forces for this test structure are required to be in excess of 2kN in total capacity at peak load.

Devices built prior to the start of this research had maximum response forces around 100N. This value is over an order of magnitude below that required for the control of this realistic test structure and further below that of a full-scale case. The prototype devices developed in this research have maximum force responses between 1 and 20kN, a significant increase compared to the previous devices, and in the desired range for these tests on realistic applications.

Bobrow et al. [1995] calculated that the time for the force to return to zero after a reset is negligible for their 100N prototype. They thus assumed that the reset time does not affect the device performance or resulting structural control. However, with these much larger devices, the reset time can be an important part of the overall behaviour. Thus, full scale resetable devices may exhibit important dynamics that were not considered in previous studies. Hence, the energy release rate and resulting reset times, along with other critical device dynamics are extensively examined in the device characterisation contained in this chapter.

4.2   Physical Device Design

The basic device dimensions are dependent on the device stiffness, the maximum stroke expected, and the peak force required. However, the dimensions of each part of the device are further defined by materials and hardware availability and the manufacturing processes. The device parts must also have adequate strength to avoid material failure.

Detailed design using SolidWorks$^{\circledR}$ was used to examine the proposed physical design, and iterate to a final solution, as shown in Figure 4.1. Some dimensions are defined by hardware selection (Chase et al. [2005a]). The manufacturer (C&M Technologies, Christchurch, New Zealand) of the prototype devices were consulted during the design process for practical advice stemming from extensive experience in manufacturing for the aerospace industry. Suggestions included advice on the endcap clamping design, seal selection, and materials readily and inexpensively available. These materials suggestions provided a fixed point for

the design from which the variable dimensions could be determined.
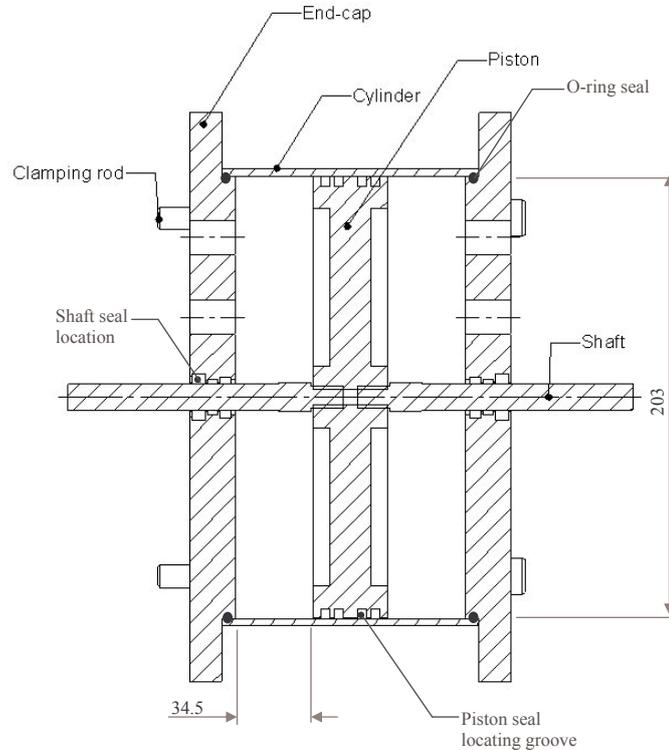
Figure 4.1   Cross-section of device showing the cylinder, piston, shaft, end-cap, and clamping rod. The clamping rods pass around the outside of the device cylinder.

4.2.1   Hardware Selection

Valve and seal selection are an important part of the design procedure for these large, high pressure devices, as leakage will degrade performance. Standard sized seals are much cheaper and easier to source than non-standard sizes. Therefore, the exact piston and cylinder sizes were determined by the size of commercially available seals. More specifically, a combination of 203.2mm (8 inch) diesel piston rings and a teflon seal are used around the piston thus defining the internal device diameter. A wiper, guiding and pressure seal are used where the piston rod passes through the end caps.

The cost of valves increases dramatically with higher working pressures, greater switching rates and valve type. Buschjost solenoid operated, 2-way, normally closed valves were selected for their high flow rate and direct control ca-

pabilities. Two valve attachment points per chamber allow for a maximum of four valves for each device. For most cases in this research, there is one valve per chamber (two valves per device), with the extra attachment point blocked. The extra attachment points can be used for internal sensor attachment if required or to add valves or plumbing to extend the device capabilities as discussed in Chapter 10.

4.2.2   Hardware and Software Integration

The total system is comprised of the physical device including the valves and the sensors. The software system controls the device operation. The seamless integration of these subsystems is critical for the system to operate to its full potential.

The dSpace$^{\circledR}$ rapid prototyping system is utilised as the software and real-time integration system for experimental work. In addition, dSpace is used for experimental data collection and processing. Utilising the dSpace system allows for rapid implementation of control methods and system testing. Thus, the time required for new control method implementation that, in the absence of the dSpace system would have required significant effort in electronic programming, can be accomplished rapidly without software integration errors. However, in the case of real structure applications, the device control systems would be coded onto a small DSP chip located with the device, where the effort of doing so is justified by the continued application of the device to a specific structure.

The control logic command for the device valves depends on the current and previous piston position, determined from displacement sensors attached to the device. In this case, a Sakae potentiometer is utilised to measures the piston position. The potentiometer is readily installed externally to the device for ease of use in this research. The resulting potentiometer signal is readily converted to a displacement signal with high resolution. Note that using a pressure sensor is not viable, as the pressure in a chamber is dependent on the piston displacement *and* valve state.

The control system is the "brain" of the whole device system. The raw sensor data is processed to determine the piston position and direction of motion. More

specifically, the potentiometer data is filtered to obtain a clean signal to eliminate erroneous or erratic valve commands. Valve commands are determined from this filtered feedback signal and the specific control law logic employed.

Any time delay between a specific valve activation point and the actual valve operation will reduce the efficacy of the device system. Therefore, minimising this time lag is an important aspect of the control system design. The total delay is comprised of the following potential elements relevant to the control system design:

- Time delays or lags due to data filtering.

- The number of time steps required to determine the sign change in velocity or displacement that is used in the device control laws.

- Valve operation itself which is independent of the control system.

The goal is to reduce the first two elements to a minimum value based on the central system design in dSpace and sensors used. The total resulting delay is measured in terms of the cumulative number of time-steps between the specific point occurring and the valves operating.

Filtering is necessary to remove the noise associated with the (input) data signals. A low or band pass filter, optimised for the observed noise, ensures a clean input signal with minimum lag. Without filtering, multiple or incorrect valve actuation can occur, which leads to unintended pressure release, reducing device efficiency. In addition, the valve solenoids overheat if rapidly activated for an extended period of time (on the order of 5 minutes) producing another reason to avoid spurious activation or commands.

A minimum of three time steps are required to determine a change in sign of the velocity or displacement of the piston. The quadrant determination (Figures 2.7 and 2.8) section of the control system compares the current velocity or displacement value to a small fixed percentage of the maximum value for each cycle. If the current value is out of the bounds of the percentage difference of the maximum, a peak has occurred and the valves are commanded accordingly.

Valve electro-mechanical operation lag is the time between the command

signal being received and air beginning to flow through the valves. This lag is largely dependent on the physical characteristics of the valves. More specifically, the valves utilised in this research have a flexible diaphragm held in place by a spring. When the solenoid is actuated to open the valves the diaphragm is free to move against the spring force. Thus, some differential air pressure across the valve is required to open the valves and the mechanical rate of opening is dependent on that pressure differential, as determined by the pressure in the chamber. Hence, very low internal chamber pressures will result in slightly slower operation, but low chamber pressures are a function of minimal stored energy. Therefore, the impact on device performance of specific pressure vs. electro-mechanical lag will be small.

The operation lag can be reduced with specialised valve and valve solenoid selection. However, the first two lags are functions of the noise environment, filtering and electronics in the specific implementation. Optimisation of the filtering and smart design of the control system can go someway to decreasing the adverse effects of delays in the control system dynamics.

4.3   Prototype Device Characterisation Metrics

Dynamic device characteristics depend on a number of parameters. The most influential parameters include: the device chamber diameter and length, maximum piston displacement, and the effective valve opening size. The first influence the forces generated, and the last the time required to equalise and reset after valve opening. The device system characteristics of particular interest and the area of performance they affect include:

1. Maximum forces generated - device capacity.

2. Response lags - inefficiency due to delays in responding to device control commands.

3. Energy release time - rate of equilibration after reset.

4. Effect of piston offset - results in asymmetry in the forces generated.

These characteristics are examined for each device prototype in the following sections. It is important to note that characteristics 2 to 4 have not been examined prior to this research. Hence, this research aims to bring *all* of these characteristics to the forefront of structural control with resetable devices design. In addition, these characteristics are quantified for the prototype devices used in this research as part of the full characterisation method presented.

Characterisation of prototype devices involves a number of steps. First, the device was tested to ensure it had been manufactured to specifications, and all the components, including seals and valves, behaved as expected. This investigation utilised quasi-static tests where the piston displacement is very slow, having a cycle frequency of less than 0.1Hz. Second, dynamic tests with the valves uncontrolled were used to examine the device characteristics, such as the peak force and device stiffness. Last, controlled tests where the valves were either controlled manually or by the control system, examine parameters such as the maximum force generated, friction, valve lag, the effect of initial piston offset, and the importance of energy release time. The controlled tests are also used to investigate the effect of different control laws on the hysteretic behaviour and energy dissipation capabilities of the device.

4.4   Prototype Device #1

The following sections describe the procedure used to characterise the first prototype. The outcome is a thorough understanding of the device dynamics and any deviations from ideal behaviour. In addition, knowledge on how device design characteristics affect performance is also obtained. As a result, some changes were made to the design to address the desired changes in device characteristics.

4.4.1   Initial Examination using Quasi-static Testing

Air is utilised as the device working fluid. Therefore, it is critical that the device is able to maintain sufficient air pressure while operating, without unintended air mass loss. The device was tested for 'air tightness' upon receipt from the manufacturers. Two points of potential air loss from the active chamber were

identified. These points are where the piston rod passes through the end cap and air flow between the two chambers around the piston.

Quasi-static piston displacement revealed a plateau at approximately 0.1kN in the force response. Further piston displacement did not result in an increase in force as expected with both valves closed. Applying soapy water to the area where the piston rods pass through the end caps revealed significant air flow out of the device at this point. On disassembly of the device it was discovered that only two, instead of three, components of the seal arrangement had been installed. The missing seal components were installed and no further air flow through this location occurred. This result indicates the need to ensure sufficient seals are utilised.

The device was quasi-statically tested again with a maximum force produced of 1kN, which is still well below the calculated design value of 2.5kN at 10mm displacement. It was hypothesised that air was flowing between the two chambers around the piston. To test this hypothesis the device was entirely submerged in water. One chamber was charged with compressed air, while the other was open to the surrounding water. Air was observed bubbling from the open chamber indicating that air was able to flow from the active pressurised chamber to the open chamber. However, the slow flow rate was deemed to be inconsequential to effective use in structural systems, where each motion cycle takes approximately 0.2 to 2.0s.

4.4.2   Dynamic Tests

Dynamic tests refer to cyclic piston motion inputs at frequencies above 0.1Hz. These tests are designed to examine the dynamic response of the devices to representative structural motions, frequencies, displacements and velocities. The dynamic tests are divided into two subsections, namely passive and controlled valve tests.

4.4.2.1   Passive Tests

Passive tests are defined as tests when the valves are not controlled. The valves
are shut by default so the chamber stays completely sealed. Thus, the mass of air
in the active chamber is constant for the duration of the test. As the volume of
an active chamber decreases the response force is expected to increase, followed
by a decrease in the response force as the active chamber volume increases when
the piston changes direction. Sinusoidal motion with amplitudes between 10mm
and 25mm and frequencies of 1.0 to 5.0Hz were used to form a collection of input
motions tests. Cyclic motion is used to examine the device response for both
directions of piston motion, away and towards the zero position. The overall
outcome is that the compressed air spring stiffness of the device can be measured
over a range of amplitudes and frequencies.

Results show the first prototype device behaves as expected, with nominal
linear stiffness values between 150kN/m and 230kN/m, depending on the rate of
piston displacement, as shown in Figure 4.2. These stiffness values are below the
design value of 250kN/m due to relatively small differences in chamber volume
between the nominal design value and the as built device.
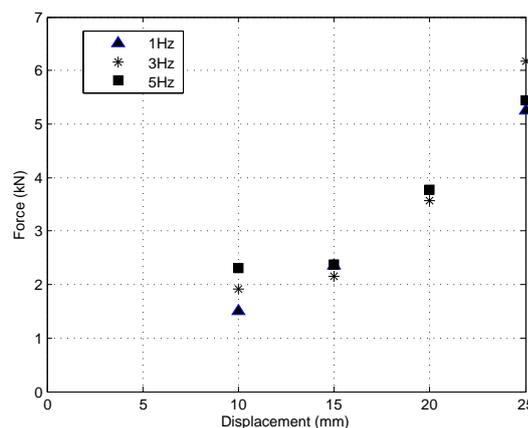
Figure 4.2   Prototype #1 average peak forces for 10 to 25mm sinusoidal displacements at 1,
3 and 5Hz. Nominal stiffness values are calculated from 10mm displacements.

The basic device dimensions during the design stage were calculated assuming
a chamber volume equal to the piston area multiplied by the chamber length.
However, the piston cross-section, for the first prototype, has two thicknesses.
Most of the piston is 18mm thick, with extra thickness around the circumference

to house the seals and in the center to accommodate the attachment of the piston rods, as shown in Figure 4.3. This piston design is referred to as a scalloped piston. The scalloped piston design ensures some air volume remains in the limit case, should the piston touch the end caps. Therefore, the effective volume in the as built device is slightly greater than the volume used in the design calculations due to the extra scalloped volume.
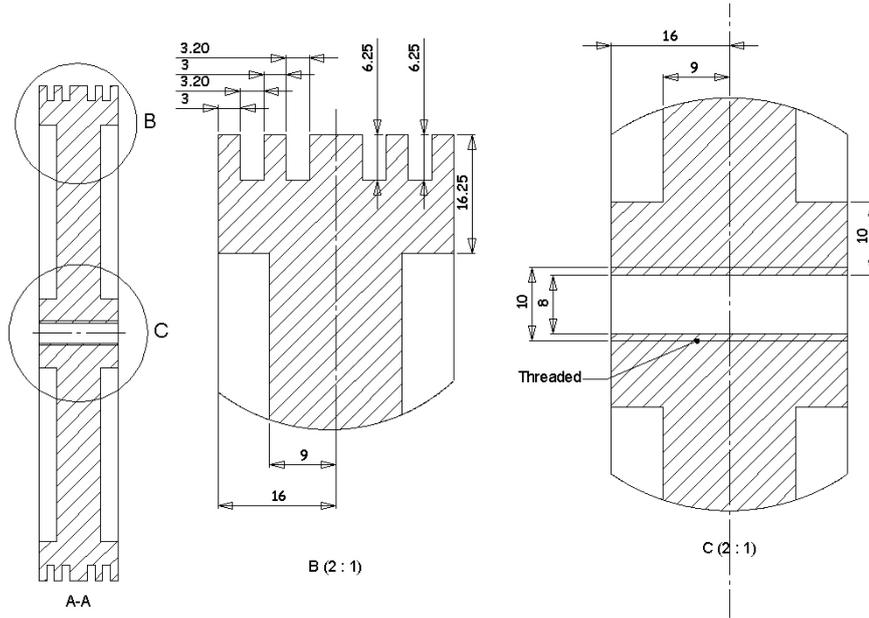
Figure 4.3   Cross-section of prototype #1 piston. Note the different thicknesses resulting in a scalloped piston.

The effect of a different volume is illustrated by comparing the force-displacement response of the device with and without the additional volume from the scalloped piston. These results are shown in Figure 4.4 using the ideal model of Equations 2.5 and 2.6. The chamber volume modelled as the basic volume results in a force of 2.45kN, for a 10mm displacement, whereas if the scalloped volume is included in the calculation the force produced is 0.93kN, a significant difference. Note that these values are lower than the experimental forces produced due to friction effects not incorporated in the ideal model.

The scalloping of the piston adds a relatively large amount of extra volume to each chamber of approximately $936mm^3$ (0.9L) in the case of this device. More specifically, this additional volume is constant and always present even at the limit of piston motion. Thus, the minimum volume in a chamber with a scalloped piston is the volume of air in the scalloped section, whereas a device with a flat piston has a minimum volume of zero. Hence, the effect of the scalloped
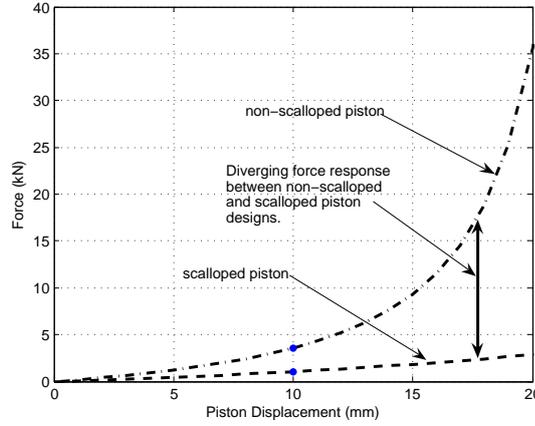
Figure 4.4 Theoretical force-displacement response for a device with a scalloped and non-scalloped piston.

volume grows as the chamber volume decreases with piston motion. As a result, the force is greatly reduced compared to the non-scalloped piston case at the extreme values of piston motion, as is evident in Figure 4.4.

In equation form, the change in volume in the first prototype device is:

$$V\text{total}_{scallop} \quad = \quad V_{nominal} - \Delta V_{chamber} + V_{scallop} \qquad (4.1)$$

$$V\text{total}_{no-scallop} \quad = \quad V_{nominal} - \Delta V_{chamber} \qquad (4.2)$$

The limit of Equation 4.2 is zero, whereas for Equation 4.1 as $\Delta V_{chamber} \longrightarrow V_{nominal}$ the effect or contribution of $V_{scallop}$ grows large. Hence, given the same chamber dimensions and an equal piston displacement, the total change in volume is less for the scalloped design than for the non-scalloped design. Since force is a function of chamber volume, the non-scalloped piston device design produces larger forces for comparative piston displacements. These alternative piston designs result in deviating stiffness profiles, as seen in Figure 4.4, where the force-displacement relationship are overlayed for the different piston designs using modelled results.

The most notable difference in the stiffness profile is the portion of the piston displacement that results in a linear stiffness profile. The profile of the original design is linear for a much larger piston displacement than for a device with a

flat, unscalloped piston design. However, a unique conclusion of this intial design study is that using this difference in characterisitics, (scalloped vs. no scallop) it is possible to tailor the stiffness of the device to be either linear over the length of device displacement or highly non-linear over the same displacement range.

Correct zero positioning of the piston is also important to avoid undesired piston offset and asymmetric results in sinusoidal testing. More specifically, piston offset is the difference between where the control system considers the zero position to be in relation to the physical center position. Piston offset may occur due to either incorrect centering during installation or a prior event not returning the piston to the exact centered position. In addition, a structure may have a permanent deflection after an event so the center position of the device would require adaptation to match the new zero position of the structure.

The impact of initial piston offset was investigated for offsets up to 3mm. The piston offset results in the chambers with differing nominal volumes. Hence, for the same displacement in each direction, with less initial volume, the resulting force response will be greater for one direction than the other. The difference in response is particulary marked if the piston nears the end of the chamber in the nominally short chamber direction. The largest offset examined, of 3mm, produced differences up to 17% in the maximum force obtained.

Allowances for initial piston offset need to be incorporated into any final system design or semi-active structural analysis. In particular, in normal working conditions, there is no guarantee the piston will be exactly at the center every time the device is utilised. More importantly, the zero position needs to be correctly defined in the control system. Finally, zero tracking should be utilised for structures where a permanent offset is possible to align the device response with the new deformed structure dynamics to avoid instabilities in control action (Hunt [2002], Chase et al. [2005b]). However, it should be noted that piston offset may be useful for some structural applications where asymmetric device response is desired.

4.4.2.2   Controlled Tests

The valves are either manually or control system commanded in these initial controlled tests for device dynamic characterisation. Manual control is used to reset the devices following a test, or to move the piston without producing large forces. In addition, the manual control can be used to override the logic control command when the device is tested with both valves open, or as a one sided device. Otherwise, dynamic or controlled tests are used to test different device laws.

Note that the normal and off state of the valves are closed. Therefore, if power is lost to the valve solenoids or control system, the device is still able to provide supplemental reaction forces by resisting the structural motion as an *air spring* with some additional friction damping. However, it should be noted that the magnitude and timing of these fail-safe or off mode reaction forces may not be optimised to the structural application.

Manual control tests

Figure 4.5 shows the device response to linear piston motion at 2mm/s, up to five different displacements. The active chamber valve is held closed for the duration of the ramp and for a ~2s once the maximum displacement for each test is reached. The valve is then opened releasing the pressurised air. Note, the initial response force of ~0.5kN is due to friction between the piston seals and internal surface of the device cylinder.

The initial portion of the curve appears almost linear with non-linear response observed for displacements above 15mm. The point at which the non-linear response becomes obvious is a function of the chamber length. This length dependency can be illustrated using an example of two chambers with the same nominal volume, a short, large diameter chamber and a long, small diameter chamber. For the *same* piston displacement, the short chamber volume changes more than the long chamber volume. Hence, the short chamber operates in the range where a small change in piston displacement results in a large change in volume, resulting in a non-linear force-displacement response.
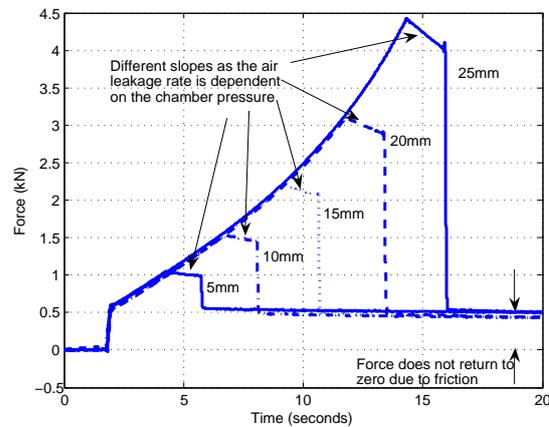
Figure 4.5 Device response to a linear piston displacement at 2mm/s. The valve is held closed during the ramp, then opened after a few seconds allowing the chamber pressure to equalise with the external fluid reservoir. The dependence of the air leakage rate is clearly dependent on the chamber pressure, with a greater rate at higher pressures shown by a steeper decrease in force. Note the non-linear force response during the ramp period and that the force does not return to zero on pressure equalisation.

The $\sim$2s hold period, when the piston is at the maximum displacement and the valve is still closed, shows the effect of the limited air leakage from the active chamber. This effect is quantified and illustrated by a decrease in the force during this period. This leakage is always present and is a function of the differential pressure between the two chambers, and the types of seals used around the piston. The diesel piston rings create a labyrinth seal which allows a moderate amount of flow between chambers. The teflon seal, which, in comparison is a complete connecting ring, reduces but does not eliminate the air flow between the chambers. A small rate of air leakage does not have a significant effect on the device response for earthquake motion where typical motion frequencies are 1 to 5Hz, and substantial periods of zero motion would not occur.

When the valve is opened air begins to flow out of the active chamber. The flow continues until the pressure inside the chamber equalises with the external fluid reservoir; the atmosphere for devices with air as the working fluid. Pressure equalisation is *not* an instantaneous event. Figure 4.6 shows a close up of the equalising period where non-instantaneous energy release is clearly observed. An elapsed time of $\sim$0.1s is required in both cases to release the stored energy and return the force to a constant, near zero value.

This result of a significant release period contrasts with prior work where the release period was considered negligible (Bobrow et al. [1995]). More specifically, for 2.0Hz structural motion, a reset time of 0.1s corresponds to a fifth of a motion cycle, which is highly significant for a total displacement based device. The device is required for most control laws to reset twice per motion cycle.

Therefore, the reset time is a dominating factor in the device response, particularly for device control laws that require equilibration of the active chamber before resisting further motion. More specifically, the 1-4 control law of Bobrow and Jabbari [2002] would suffer significant degradation of performance, in particular for high frequency structural response. Note that devices with the independent chamber design developed in this research reduce the potentially adverse affects on the device energy dissipation ability due to finite energy release times.
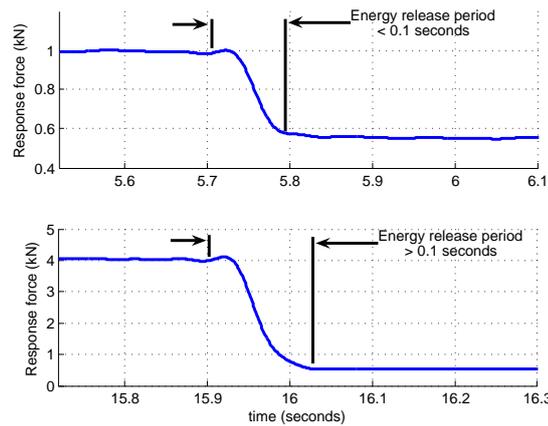
Figure 4.6   Close up of the energy release period of the device response for 5mm and 25mm piston displacement from the center position. The release time is finite and not insignificant.

The longer the release time the greater the effect on the performance of the device. When the frequency of the input motion signal is greater than 3.0Hz, all the energy may not be released from the device before the valves are closed. Therefore, at high frequency piston motion the device may not be operating as efficiently as theoretically possible. To mitigate this shortfall, extra valves or valves enabling greater exit flow rates could be utilised.

The independent chamber design employed in this work mitigates much of the impact of long release times. For the single valve device of Figure 2.1, the long release time prohibits the device from storing energy or resisting motion with the newly active chamber. In contrast, the novel two valve, independent

chamber design allows one chamber to store energy while the other is still releasing energy. This feature is a major advantage for specialised applications that might experience higher frequency structural responses than normally seen for full civil structures, such as are found in non-structural systems like refining plants or specialised sculptures.

The force response is expected to return to zero when the chamber pressure equalises with the external fluid reservoir. However, the force response observed experimentally returns to ~0.3 to 0.5kN, which has been equated to the static friction force. This friction force can readily be determined by a series of tests where the valves are manually held open. Thus, the only force response is from overcoming static friction, kinetic friction between the moving parts, and viscous damping from air being forced to flow through the restricted area of the valves.

Figure 4.7 shows the valves open, friction response for 10mm sinusoidal piston motions at 0.1, 1.0 and 3.0Hz. The static friction between the piston seals and cylinder wall is the force response value at the maximum piston displacement. The bulge in the response is due to insufficient air flow rate through the valves to maintain equilibrium air mass for the chamber volume and any kinetic friction. Given that the bulge grows significantly with frequency and thus velocity of motion, this latter effect can be almost fully attributed to viscous damping from air flowing through the valve orifice. Finally, note that this friction value (of ~0.3 to 0.4kN) corresponds to the initial step response seen in Figure 4.5.
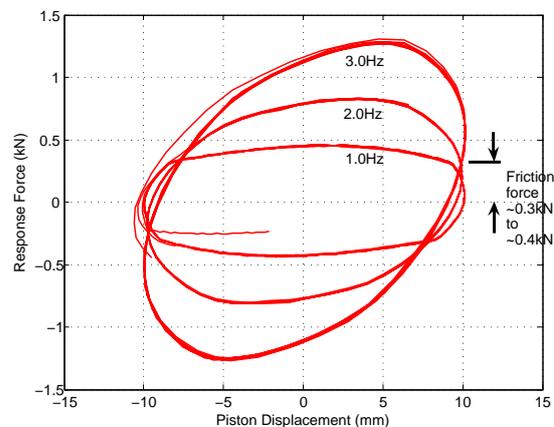
Figure 4.7   Open valve response of prototype #1. The friction value is ~0.3kN to 0.4kN for this device.

Control System Command Tests

The first control tests were done by manually commanding the valves to fixed states. The displacement response was observed and a switch manually activated to command the valves state. As expected, the piston motion rate at which this method can produce the correct valve response was very slow. Hence, this method of valve control was used to conceptualise the control system logic prior to developing the control law software, rather than to provide meaningful results.

4.4.2.3   Impact of Valves on Performance

The valves are two way operating, so air can flow both ways. This feature is required as the valves not only hold and release the pressure, they are also required to let the working fluid flow into the chamber from the fluid reservoir to recharge the inactive chamber of the device. The valves used in this research are rated to 10bar (1000kPa). Hence, at higher pressures they are unable to maintain their controlled state and are partially forced open. This feature, although marginally limiting the device performance, is a useful safety feature as it results in the valves being the weak point in the system. Hence, excessive pressure is released via the valves rather than with a potentially catastrophic failure at some other point.

Figure 4.8 indicates air loss from the active chamber due to the valves being partially forced open at high pressures. The rate of piston motion is also a determining function in air loss from the active chamber. At slow piston motion, sinusoidal motion at 1.0Hz or less, there is practically no loss of air mass from the active chamber. However, at relatively rapid piston motion, greater than 2.0Hz, the air mass in the active chamber is decreased until an equilibrium point is reached, as shown in Figure 4.8.

4.4.3   Prototype #1 Summary

Prototype #1 is the first large scale resetable device to be manufactured and dynamically characterised. The analysis process to determine the device characteristics is extensive by including quasi-static and dynamic input motion as well
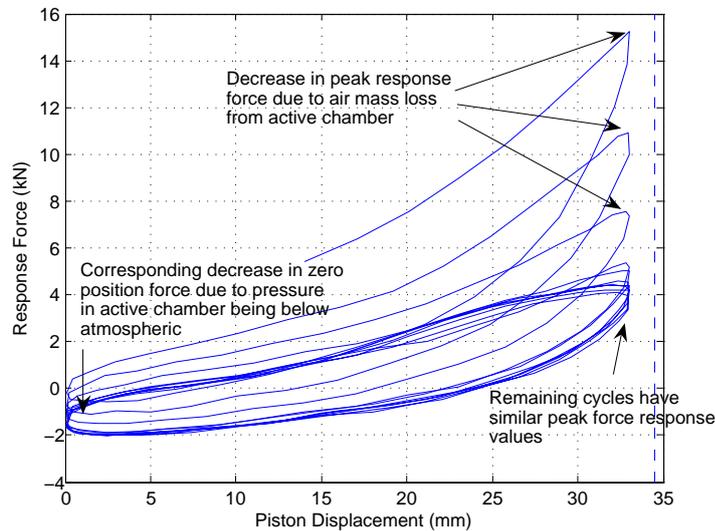
Figure 4.8 Reduction in peak force response due to air mass loss via unintentional valve opening. The peak force decreases until the rate of pressure change is below the threshold the valves are able to withstand. Piston motion is sinusoidal with an amplitude of 33mm and frequency 3Hz. The maximum allowable piston displacement is indicated by the dashed line.

as examining the uncontrolled and controlled device response. The force response and equivalent linear stiffness of this first device did not reach the design values mainly due to the scalloped piston design, which increased the nominal active chamber volume from the design value. The amount of scallop in the piston is an important design consideration and can be adjusted to provide the required device response and amount of linear and non-linear force-displacement response over the length of the device piston displacement. In addition, a number of experimentally determined response characteristics, which were not considered in prior studies, have been quantified. The two distinguishing characteristics are the energy release rate which is a function of the valve orifice size and the static and air damping friction forces. The static friction is a function of the piston seals, while the air damping is dependent on the valve orifice size.

4.5   Device Prototype #2 Design and Characterisation

The second prototype was designed based on the results from the first prototype and the required response for installation in a $\frac{1}{5}^{th}$ scale test structure representative of a reinforced concrete building (Kao [1998]). More specifically, this structure required a device with a nominal stiffness of 590kN/m, giving a response force of 10kN at a piston displacement of 17mm (Anaya et al. [2007]). Two devices were manufactured according to these specifications, as a device is required for each side of the building. These second prototype devices were characterised to examine if their dynamic response meet requirements, as well as to ensure the two, otherwise identical devices respond similarly.

4.5.1   Prototype #2 Design Changes

The major alteration to the design between the initial and second prototype devices is the piston design and cross-sectional dimensions. The original prototype piston was thin, with additional thickness for the piston rod attachment and to house the seals around the circumference. The second prototype device has a wide flat piston with a thickness of 32mm, the amount required for the circumference seals. In addition, due to material availability the piston rods have an enlarged diameter of 30mm as opposed to 10mm in the first prototype. The device chamber length (L_0) was almost halved for the second prototype, making $L_0 = 18.5$mm. The length was decreased to increase the peak forces generated at smaller piston displacements due to the limited motion expected from the test structure of 10-12mm. In addition, a shorter chamber in combination with a non-scalloped piston results in the non-linear force-displacement response encompassing more of the total device response and generating higher forces than the original scalloped piston design.

4.5.2   Dynamic Tests

4.5.2.1   Passive Tests

The friction response of the second prototype was expected to be similar to the first prototype. Figure 4.9 shows the second prototype device friction response. The friction contribution is the slightly higher value of ∼0.5kN, likely due to using two teflon seals around the piston. In addition, closer tolerances between the piston and device cylinder increases the static friction. The tradeoff between friction response values and better chamber sealing weighs towards reducing the air leakage. Reduction in air leakage from the active chamber by using two teflon seals results in a more consistent device force response over a range of frequencies that is worth a slight increase of ∼0.1kN in the friction response. The friction force constitutes the portion of the force response that cannot be dissipated by the device. However, it is still a reaction force that resists structural motion and dissipates energy. Hence, some friction force does not degrade the ability of the resetable device to dissipate structural energy.
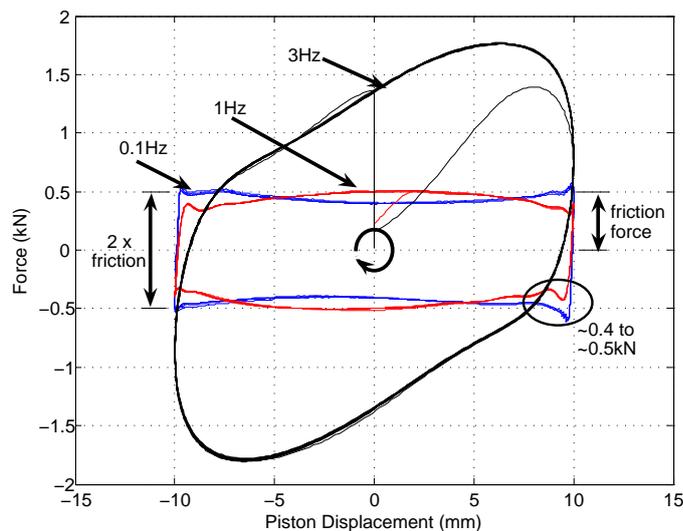
Figure 4.9   Static friction and air damping response of prototype #2. The static friction force is approximately 0.1kN greater than the value for prototype #1.

As designed and expected, the peak forces produced by prototype #2 are greater than those produced by prototype #1. Figure 4.10 shows the average peak forces for prototype #2 at different amplitude motions. The peak forces at 10mm piston displacement are approximately three times greater for the shorter chamber device, with 2kN reported for the long chamber and 6kN for the shorter chamber shown here.

The nominal stiffness value is calculated as a linear stiffness of the force value at 10mm displacement. The experimental value is ∼600kN/m, which is more than three times the nominal stiffness calculated at the same displacement for the first prototype. However, the nominal stiffness value does not give a full representation of the device response. The non-linear response of the device is clearly observable in Figure 4.11. Hence, to make accurate predictions of the device response for analytical studies of resetable devices, a more accurate non-linear model needs to be developed that captures this non-linearity and other important dynamics. This advanced model is discussed in more detail in Chapter 5.

The frequency dependency of the results are not as pronounced for prototype #2. This result is illustrated by the peak force results only diverging noticeably at 15mm piston displacement, which is very near the end cap and piston stroke limit, as shown in Figure 4.10. Conversely, the peak forces for prototype #1 were more divergent at all frequencies, as seen previously in Figure 4.2. This result is attributed to the teflon seals and closer tolerances in the second prototype. Hence, the air leakage from the active chamber is much reduced compared to the first prototype, resulting in less of a difference in the amount of air lost for different frequency input motions.

Figure 4.11 shows a typical first quarter cycle response to 15mm sinusoidal piston motion at 0.1, 0.5 and 1.0Hz. Once again, the frequency dependency of the response is not as pronounced as with the first prototype response, becoming apparent only above ∼7mm. The result of this greater frequency independence is to have much more predictable peak forces over wider displacement ranges. Hence, the response of the device is more reliable and thus easier to model with confidence. In addition, model results will be easier to match quantitatively, giving more assurance of accuracy in the overall results.
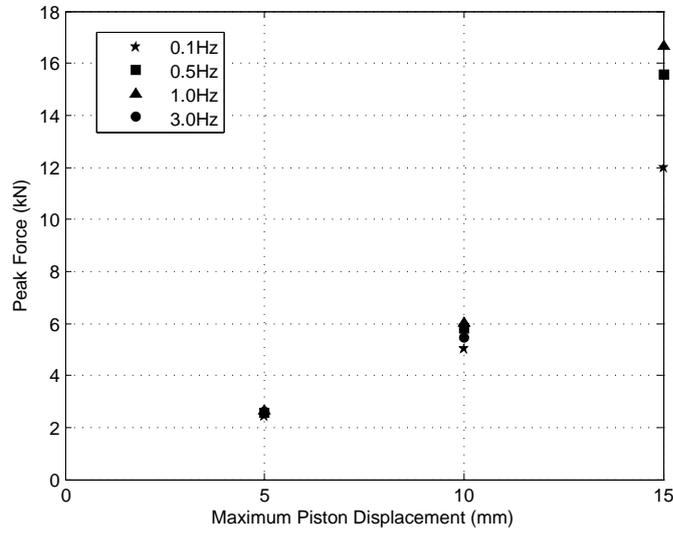
Figure 4.10   Peak force response for prototype #2. The frequency dependency of the response is more pronounced for large displacements.
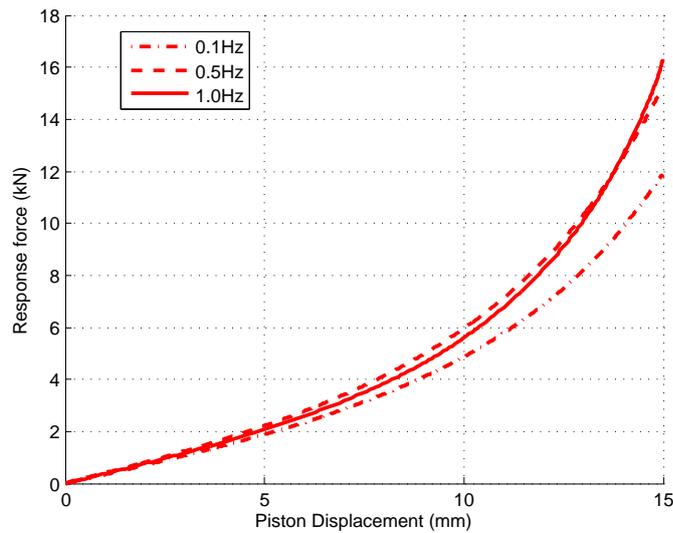
Figure 4.11   First quarter cycle response of prototype #2. The piston motions is sinusoidal with an amplitude of 15mm and frequencies of 0.1, 0.5 and 1.0Hz.

The difference in device stiffness between prototype #1 and prototype #2 is illustrated in Figure 4.12. Here, peak forces are shown as a percentage of maximum allowable piston stroke, normalising the comparison between prototype devices. It is clear in this comparison that the second prototype is generating greater forces for similar percentage changes in active chamber volume, indicating a stiffer device.
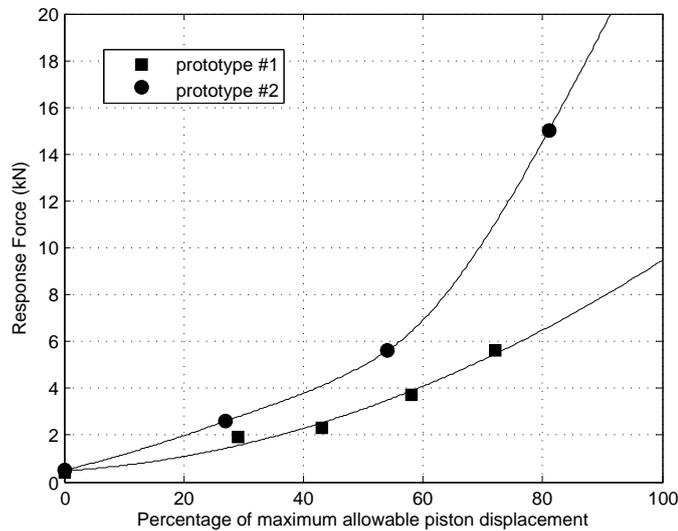
Figure 4.12 Peak forces as a function of the percentage of maximum allowable piston displacement for both prototypes. The second prototype clearly has a higher stiffness.

4.5.2.2 Controlled Tests

The controlled tests show prototype #2 broadly has the same qualitative behaviour the hysteresis shape introduced in Figure 2.9. Figure 4.13 shows prototype #2 response under the 1-4 control law. Most noticeable is the difference in response during the energy reset period at the various input motion frequencies, as circled in the figure. For input frequency motion of 0.1Hz the energy reset results in a vertical line on the force-displacement plot because the motion is slow enough that the reset essentially occurs when the piston is at the maximum displacement and the chamber pressure is fully equilibrated before it is required on the next cycle. However, for the 0.5 and 1.0Hz input motion frequencies the

reset occurs only after the piston has moved ∼1 and ∼2.5mm respectively, in the opposite direction. Hence, the reset time has a substantial influence in the resulting hysteresis loop produced by the device, as some of that stored energy is still returned to the structure, rather than being dissipated.

The independent chamber design helps to mitigate the resulting reduction in the enclosed area of the hysteresis loop due to the relatively long energy release times that result from finite air flow rate through these valves. While the resetting chamber is releasing the stored energy, the other chamber can be resisting the motion. Interestingly, other researchers (Yang et al. [2007]) who have investigated devices similar to the original proposal, with a schematic similar to Figure 2.1 do not mention the effects of the reset time on the hysteretic response.
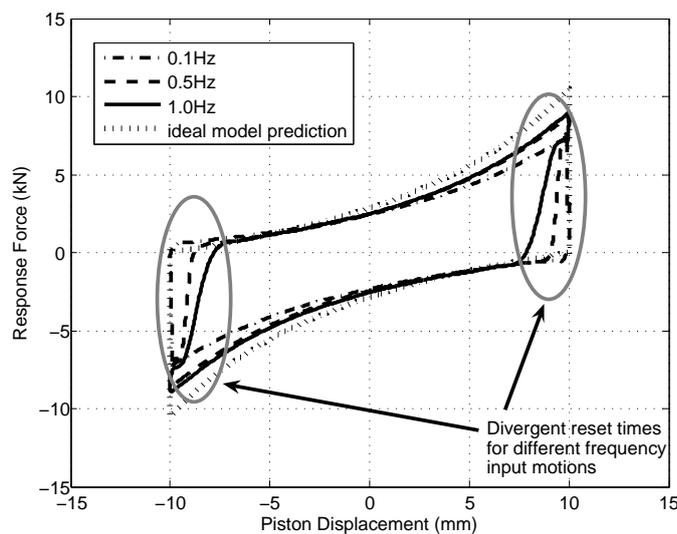
Figure 4.13 Prototype #2B response under 1-4 control to 10mm piston motion at 0.1, 0.5, 1.0Hz. The divergent reset times are clearly distinguishable.

The response of prototype #2 to the 1-3 control law at different input frequencies is shown in Figure 4.14. The hysteresis shape matches well to the ideal shape shown in Figure 2.10. In particular, the 'zero' force response, during motion towards the zero position, is apparent. The ideal model prediction, which is derived from ideal gas laws in Equations 2.5 and 2.6, illustrates where this model captures the response well and where definite differences exist. The most notable difference is the value of the 'zero' force. The model assumes that when the valve on the active chamber is open there is no contribution from this chamber to the overall force response. However, as seen in Figure 4.14 the force does not stay at zero. Instead, the force response during the valves open time is at a constant

value of approximately 0.5kN, which is the force contribution from friction that is obviously not accounted for in the ideal model.

The effect of energy reset time, while being apparent in Figure 4.14, is not as pronounced for the 1-3 case as it was in Figure 4.13 for the 1-4 control case. This result is due to the peak forces achieved in the two cases. For a 10mm piston motion, the peak force achieved for the 1-4 case is ∼8kN, whereas for the 1-3 case it is ∼5kN. The device under the 1-3 control law only resist motion for half of each cycle. Therefore, in the 1-3 case there is less energy stored and released reducing the required energy release time. Hence, the energy release time has less of an effect on the hysteretic response when the peak forces are lower, as expected.

Figure 4.15 shows the response of the two seperate devices built to prototype #2 specifications under 1-3 control. For clarity only the 10mm, 0.1Hz sinusoidal motion result is shown. Other amplitudes, frequencies and control laws show similar results. The two device responses are very similar indicating that multiple devices can be built with confidence that the behaviour will be, for practical purposes, identical. Thus, when the devices are required to be installed on either side of a test structure, there should be no adverse effects introduced by differential behaviour between devices. More specifically, if a device is installed on each side of a structure, torsional effects will not be introduced or amplified by any (small) differences in the devices.

Figure 4.16 shows the device response to 2-4 control. The hysteretic response is similar to that predicted in Figure 2.11, particularly for low frequency (0.1Hz) input motion. However, at higher frequencies the response differs increasingly significantly from the ideal behaviour. More specifically, the energy release effect is very prominent in the hysteretic response. It is the most marked for 2-4 control because the active chamber volume is still *decreasing* when the energy is released.

Hence, for the period directly after the active chamber valve is opened the pressure in this chamber is balanced between an increase due to the chamber volume decreasing and the pressure decreasing due to the air mass exiting via the open valve. The greater the rate of decreasing chamber volume, the longer the pressure balance takes before the reduction in air mass is the dominant factor in the chamber pressure. Therefore, at relatively high frequency piston motion
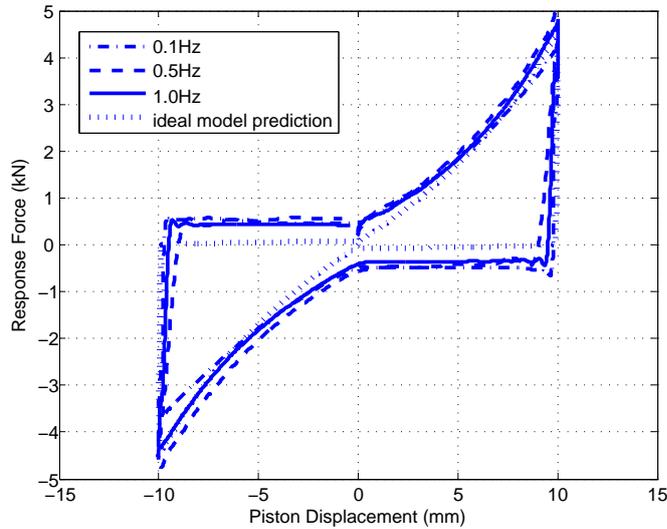
Figure 4.14   Prototype #2 response under 1-3 control for 10mm sinusoidal piston motion at 0.1, 0.5 and 1Hz. The ideal model prediction is also shown.

there are two contributing factors to a long energy reset time, the rate of air flow through the valves, and the decrease in chamber volume during the reset time. Note that larger diameter valves that allow more rapid release would ameliorate this effect if desired.

The deviation away from ideal behaviour shown by the device in the experimental tests using the 2-4 control law may not necessarily be detrimental to the overall behaviour of a structure system with these devices installed. For example, (Kurino et al. [2006]) have found that the optimum hysteretic shape for a base isolating damping system is very similar to the response of this 2-4 device with piston motion between 1.0 and 3.0Hz, which corresponds with the majority of the frequencies of interest for earthquake loading. In addition, the diamond shaped 2-4 control responses in Figure 4.16 are also optimal for maximising damping without increasing base shear in a linear system.

The motion frequency at which the optimum hysteretic shape is achieved is a function of the valve size compared to the energy required to be released. Therefore, with intelligent design, it is possible to achieve the optimum hysteretic shape for the dominant frequencies of interest for any specific structural case at the design stage. Similar results could also be achieved by controlling valve size and/or the number of valves available.
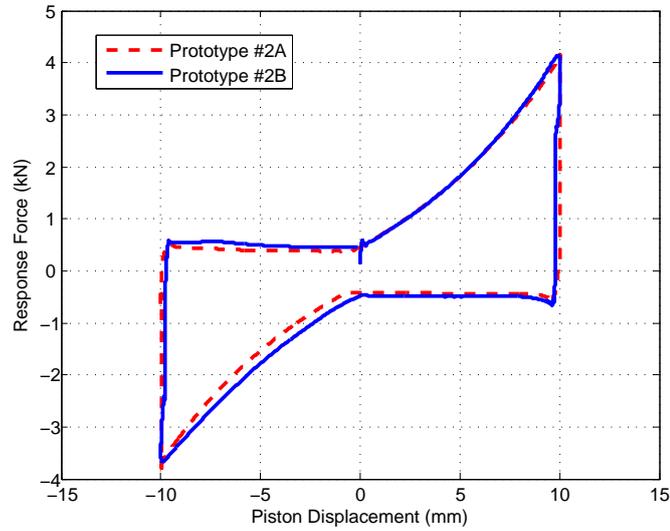
Figure 4.15   Comparison of response of two devices built to prototype #2 design. Piston motion is 10mm at 0.1Hz and control law is 1-3.

4.5.3   Prototype #2 Summary

Characterisation of the two devices built to the second prototype specifications show good comparison with the design peak force and device stiffness values. The uncontrolled peak response is approximately 6kN at a 10mm piston displacement, giving a nominal device stiffness of 600kN/m. The stiffness of the second prototype device is significantly greater than the first prototype due to a shorter chamber length and an unscalloped piston. The controlled peak force is dependent on the control law, which determines the motion resisted. The peak forces at 10mm are ∼8.0, ∼4.5, and ∼3.0kN for the 1-4, 1-3 and 2-4 control laws respectively. The force-displacement hysteretic response is highly influenced by the energy reset rate. This rate is a function of the valve orifice size and can be altered depending on the size and number of valves available. In addition, the two second prototype devices have, for practical purposes, identical dynamics responses.
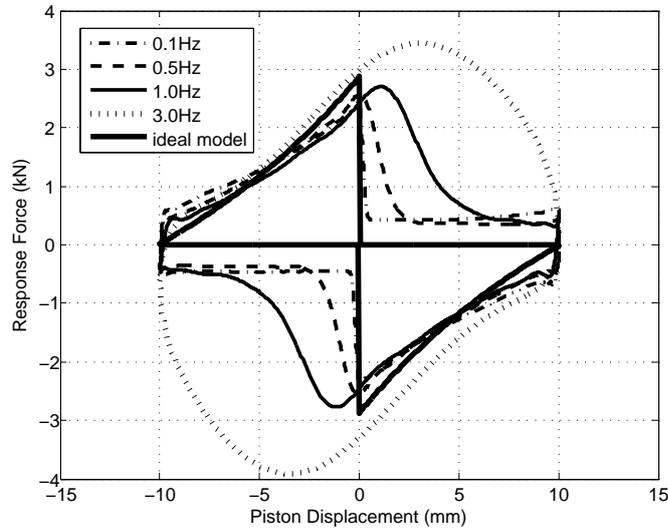
Figure 4.16   Prototype #2A response under 2-4 control to 10mm piston motion at 0.1, 0.5, 1.0 and 3.0Hz.

4.6   Summary

The main features of the device characterisation method and results are:

- The characterisation method captures and quantifies the dynamic response of these resetable devices. Uncontrolled and controlled valve experimentation give the peak forces, friction response, and energy release rate. These characteristics define the force-displacement hysteretic response of the devices.

- The piston design can be altered to achieve the desired amount of linear and non-linear force-displacement response over the length of the piston displacement. A scalloped piston increases the nominal active chamber volume thus reducing the rate at which the total volume decreases with piston displacement compared to an unscalloped piston design. Therefore, a scalloped piston design results in a linear force-displacement response over more of the piston displacement than a non-scalloped piston. In contrast, a non-scalloped piston design produces higher forces for comparable piston displacements.

- The valve orifice size and number of valves available affects the energy release rate. There is a maximum rate at which air can flow through the valve

orifice thus the energy release rate is finite and not negligible, particularly for large piston motion. The effect of the energy release rate on the force-displacement response is more obvious at relatively high frequency piston motion and large piston displacements. In these cases a large amount of stored energy is required to be released, resulting in a significant time period for complete energy release to occur. The energy release rate is most obvious for the 2-4 control law because the active chamber volume is still decreasing when the active chamber is opened to equalise the pressure.

- Friction between the piston seals and cylinder wall contributes to the force-displacement hysteretic response as static friction that is required to be overcome before the piston can be displaced. In addition, air damping results from air being forced out the valve orifice.

All of these device characteristics can be altered depending on the desired device response. Finally, the prototype devices show good correlation to the quantitative force-displacement response for the control laws introduced in Section 2.4.2, Figures 2.9 to 2.11. The deviations away from ideal behaviour are identified and discussed further in Chapter 5 where an enhanced non-linear model is developed.

Chapter 5

Enhanced Non-Linear Device Model and Validation

5.1   Introduction

This chapter details the extension of the ideal model to account for non-linear dynamics evident in experimental results. The model progresses from a very simplified ideal model to a more complex and representational model. The model is expanded to include the critical dynamics that affect device performance, such as friction forces, air flow rates, valve sizes and operating rates and valve command delays. The chapter details each effect addition individually and validates the final model with comparison to experimental data.

5.2   Friction

The most obvious difference between all experimental results and ideal model predictions is the discrepancy in the force obtained after pressure release. The ideal model assumes that a response force produced by the device is only due to the air being pressurised. Hence, when all the pressure is released the force is expected to return zero. However, experimentally, the device force returns to a non-zero value, as seen in Figure 5.1. This non-zero resetting force is due to friction between the moving parts, mainly the piston rings and the inside wall of the cylinder.
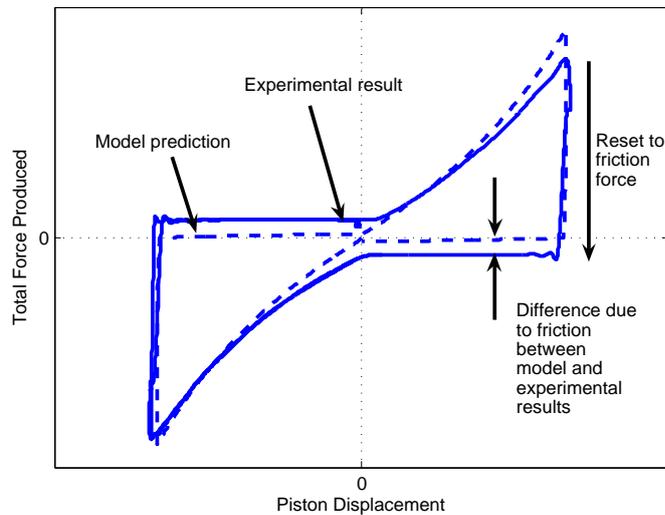
Figure 5.1   Experimental result and ideal model prediction showing the contribution of friction to the total force produced.

The amount of friction is readily determined by measuring the device response to piston displacements with both valves open. In this situation there is only a small increase in pressure in the chambers with piston motion. Figure 5.2, which is a repeat of Figure 4.9 shown here for clarity, shows the device response to sinusoidal motion with 10 mm displacement at 0.1, 1.0 and 3.0Hz. The friction is determined to be ∼0.4 to ∼0.5kN, from the force value at the peak displacements for the 0.1 and 1.0Hz motions.

The difference in the three responses in Figure 5.2 are due to the different frequencies of the sinusoidal motion. As the volume of each chamber changes, the mass of air in each chamber changes correspondingly because the valves are open during these tests. In particular, the air has to flow in and out through the valves. If the flow rate through the valve orifice is insufficient to balance the change in volume with a corresponding change in mass the pressure in the chamber will increase resulting in a reaction force. Thus, the faster the piston moves the more likely there is to be some increase in pressure for a fixed valve size. This effect is evident in the bulge in the force-displacement response of Figure 5.2. It is particularly evident when comparing the 1.0 and 3.0Hz motions, and effectively non-existent for the quasi-static 0.1Hz motion. Finally, note that all three motions clearly show the ∼0.5kN friction force, and for slower motions it is effectively the only force generated.

A simple analogy to better explain the physics of this situation is to consider pouring a large volume of water into a standard kitchen sink. If poured in rapidly, the water level continually rises, as it cannot flow out as fast as it cames in resulting in net positive mass flow. In contrast, poured slowly, the water level does not measurably rise in the sink resulting in effectively net zero mass gain or equilibrium. In this analogy, the water is the air volume, the pouring rate is the piston speed or input motion frequency and the valve orifice is the relatively narrow sink drain. Pressure rises based on the net mass flow rate out of the orifice, just like the water in the sink.
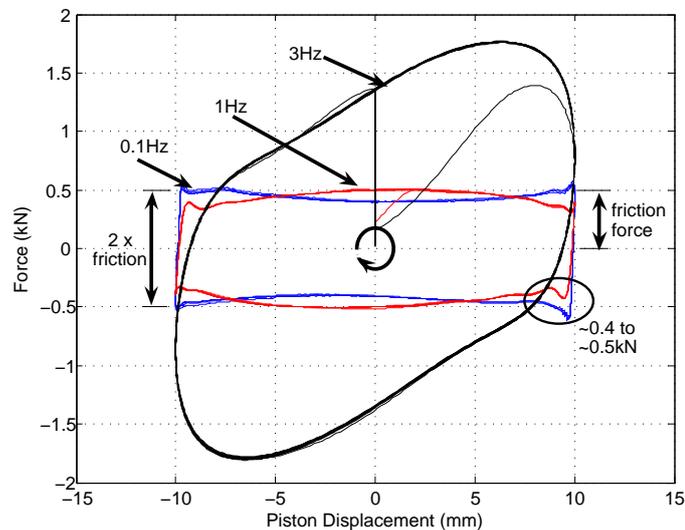
Figure 5.2 Experimental determination of the friction value. Note the bulge in the 3.0Hz motion result caused by air not able to flow through the valves at a high enough rate to maintain an equilibrium mass inside the chamber, resulting in a pressure rise with valves open.

The friction force was thus incorporated into the ideal model by resetting the device force to the friction level, rather than zero. The sign of the friction force is dependent on the direction of piston motion. Thus, when the piston changes direction the total change in force is twice the friction force value, as shown in Figure 5.2. A fixed value for the friction was used in the model as the additional force resulting from 'insufficient' air flow through the valves for the high frequency piston motion is accounted for in the energy release rate modelling.

5.3   Energy Release Rate

The other major difference between the ideal model results and the actual device response is the energy release rate, or air flow rate through the valves. The ideal model assumes that when the valves open the pressure instantly equalises with the pressure of the external fluid reservoir, which in most cases is the atmosphere. This assumption yields a perfectly vertical line on a force-displacement plot.

However, there is always a finite air flow rate through any valve. In this research, with the relatively larger volumes and pressures than the small devices of Bobrow and Jabbari [2002], the time required for sufficient flow to occur and for pressure to equalise is significant, compared to the device motion. Hence, there is some lapse in time between the valves opening and the pressure equalising with the fluid reservoir, resulting in a more diagonal line or gradient on the force-displacement plot, as shown in Figure 5.3.

The air flow rate through the valves is dependent on two parameters, namely the size of the valve opening and the pressure difference between the air inside the chamber and the external fluid reservoir. In general, the open valve can be assumed to be a circular orifice. The flow through the orifice is determined to be choked or non-choked depending on the pressure gradient across the orifice. Non-choked flow rate is dependent on the pressure gradient between the high pressure and low pressure zones on each side of an orifice. Choked flow is the limiting rate of flow depending on the size and type of an orifice. For a circular orifice, if Equation 5.1 is true the flow is choked (Hill and Peterson [1992]).

$$\frac{p_s}{p_a} \geq \left(\frac{\gamma+1}{2}\right)^{\frac{\gamma}{\gamma-1}} \tag{5.1}$$

where p_s is the upstream pressure, p_a is the down stream pressure, atmospheric for most cases and γ is the ratio of specific heats, γ=1.4 for air.
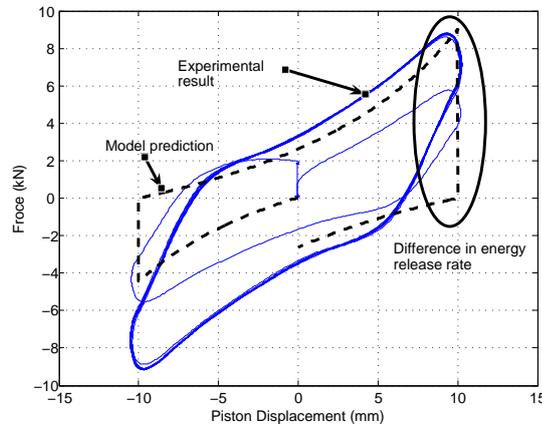
Figure 5.3 Experimental result and model model prediction to 10mm, 2Hz sinusoidal motion showing difference in energy release rates, model assumes instantaneous energy release.

The ideal model uses the air pressure inside each chamber as the basic parameters. However, with the added complexity of incorporating the air flow rate through the valves the air *mass* in each chamber is more representative and intuitive. Using the air mass as the base parameter readily accommodates using the air mass flow rate through the valves in the model.

The mass flow rate is calculated, using Equations 5.2 and 5.3. The mass flow rate, $\dot{m}$, is then multiplied by Δt to obtain the total mass change, due to flow through the valve, for each time step. Using the mass of air also ensures the model obeys the fundamental conservation laws of physics by not allowing the mass to increase beyond the equilibrium mass, which is defined by the chamber volume at atmospheric pressure with the valve open. Hence, the mass model accounts for the reduction in air mass with a decrease in volume, an effect that was not specifically accounted for in the ideal pressure model.

The finite air flow rate through the valves is particularly noticeable for high frequency piston motion, as seen in Figures 5.2 and 5.3. It is particularly evident in the device response to the 2-4 control law due to its device reset command at peak velocity when the piston crosses zero, as shown previously in Figure 4.16. For high frequency motion, the length of time required for the air mass to decrease to the equilibrium mass can become a significant percentage of the piston cycle time. Therefore, the mass reaches equilibrium after the piston has moved through a large amount of the cycle, resulting in a curved reset line on the force-displacement plot, as shown in Figure 5.4.

$$\dot{m} = CAp_s \sqrt{\frac{kM}{RT}} \left(\frac{2}{\gamma+1}\right)^{\frac{\gamma+1}{2\gamma-2}} \qquad \text{if flow is choked} \qquad (5.2)$$

$$\dot{m} = CAp_s \sqrt{\frac{2M}{RT}\left(\frac{\gamma}{\gamma-1}\right)\left[\left(\frac{p_a}{p_s}\right)^{\frac{2}{\gamma}} - \left(\frac{p_a}{p_s}\right)^{\frac{\gamma+1}{\gamma}}\right]} \qquad \text{if flow is un-choked} \quad (5.3)$$

where C is the orifice coefficient, A is the orifice area, M is the molecular weight, R is the universal gas law constant, and p_s, p_a and γ are as previously defined.

The 2-4 control law commands the valves to open and release the compressed air when the piston crosses the zero position. At this point the volume of the chamber is still decreasing, as shown schematically in Figure 2.11. Thus, the pressure in the chamber in this case becomes a balance between the reduction in pressure due to the reduction in the mass of air in the chamber, and an increase in pressure due to the chamber volume decreasing. The result of the pressure balance dynamics appears as a delay in the force reduction until a measurable displacement after the zero position in some cases. This behaviour is evident for the relatively high velocity piston motion with sinusoidal motion of 15mm amplitude at 1.0Hz, as shown in Figure 5.4.

Finally, the air flow rate into the device is modelled using the same mass flow rate equations. For low frequency piston motion, the air mass inside the open chamber will be the equilibrium mass as the rate of air flow in through the valves exceeds the required change air mass to maintain the equilibrium mass. However, for high frequency piston motion the mass flow rate through the valves may not be sufficient to maintain the equilibrium mass inside the open chamber. Hence, the pressure inside the chamber falls below the equilibrium pressure for the chamber volume, and at times below the external fluid reservoir, or atmospheric pressure. This lower pressure results in a greater pressure gradient between the chambers and thus a slightly greater overall force is produced by the device in these cases. Overall, by using mass flow equations all these effects can be included in the model.
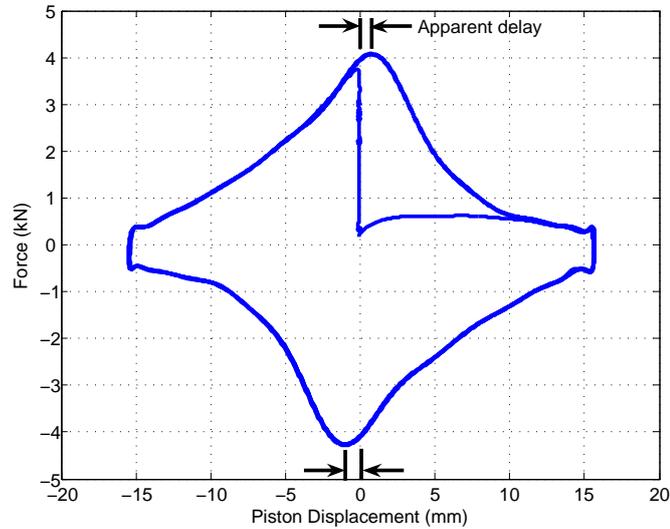
Figure 5.4 Experimental result to 15mm, 1Hz sinusoidal motion with the 2-4 control law. The chamber volume is still decreasing after the valve is opened resulting in an apparent delay between valve actuation and the force decreasing

5.4 Valve Delay

To complete the enhanced model, the delay between the valve solenoid being commanded to switch states and air beginning to flow through the opened valve is included. This delay is physically comprised of the delay between the command signal being sent to the valve and the solenoid receiving the signal, as well as the time taken for the valves to operate once the solenoid has received the command signal. The valve operation delay can, at times, be audibly detected by listening for the click of the solenoid operating and the subsequent sound of air being released. It can also be measured experimentally by comparing the difference in time between the valve command signal being sent and when the force begins to decrease on a time history plot.

The total solenoid command and valve delay is modelled as a fixed hold period on the state of the valve after the model has detected that a switching point has occurred. The delay, as measured from experiments, is not constant and the time taken for the valves to operate after receiving the signal to switch depends at least partially on the pressure inside the chamber at that time. More specifically, the valves have a flexible diaphragm that is held in place by a spring. Hence, a greater chamber air pressure results in a more rapid opening of the valves once the solenoid is released as that pressure helps open these valves.

An average value of 0.01 seconds was used in the model and is a good compromise between incorporating the delay effect in some way and adding undue complexity by determining the delay time on the chamber pressure. The delay value appears insignificant, however at high frequency, high velocity motion greater than 2Hz, the delay forms a noticeable part of the device response, as shown in Figure 5.5. Specifically, the 0.01s delay at peak velocity (zero displacement) can result in a 1.25 to 1.90mm delay for 10 to 15mm sinusoidal displacement motions at 2Hz.
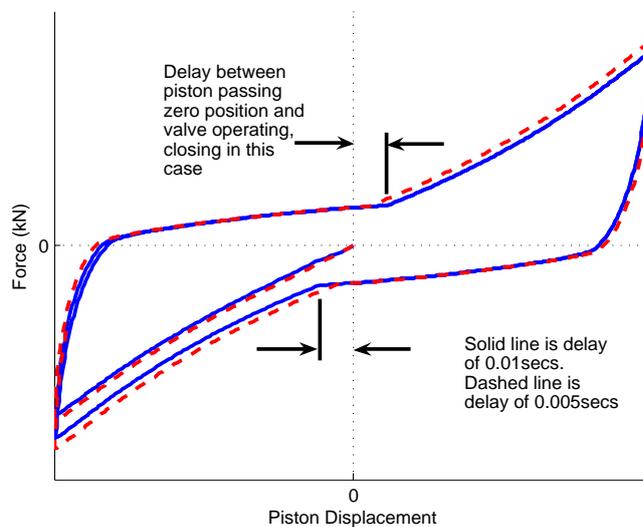
Figure 5.5   Modelled response to 2.0Hz sinusoidal motion. Note the delay between the piston passing the zero position and the change in slope of the response indicating where the valve closed.

5.5   Model Validation

A validated model is a very useful tool as it allows *rapid* examination of the device response to hardware and software alterations. For example, the valve orifice size and opening rate are fundamental metrics that determine the resulting device hysteretic response. Thus, an accurate model that has been vigorously validated by comparison with experimental data that captures all these metrics increases the understanding of how the device works and reasons for the dynamics and what changes result to the device behaviour when these metrics are altered.

Figure 5.6 shows how the experimental and modelled results compare for various input motions and control laws. The ability of the complex model developed

to capture the dynamics of the device is illustrated by a close correlation between the modelled prediction and experimental results. Further model development and correlation with experimental results is discussed in Chapter 10.
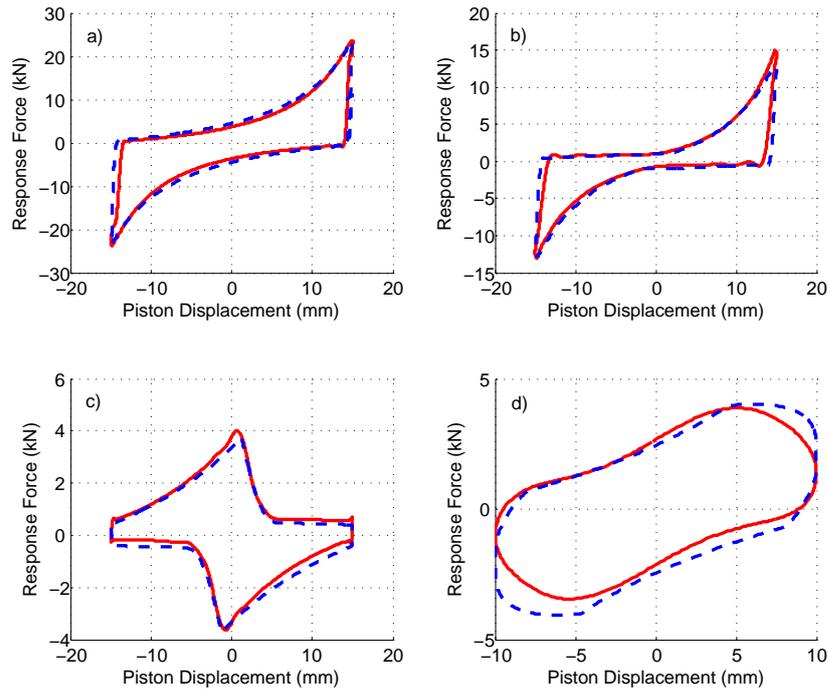
Figure 5.6   Experimental and modelled results showing the ability of the model to capture the dynamics of the device. All responses are to sinusoidal input piston motion. The amplitudes and frequencies of the input motion as well as the control laws are: a) 1-4 control, 15mm, 0.5Hz. b) 1-3 control, 15mm, 1.0Hz. c) 2-4 control, 15mm, 0.5Hz. d) 2-4 control, 10mm, 3.0Hz. Experimental results are shown with a solid line, while modelled results are indicated by a dashed line.

5.6   Closure

The device model now incorporates all the complex device dynamics observed experimentally. It has also been validated to accurately predict experimental results. Using the dimensions and design of a device, and some knowledge of the valve operation a realistic and accurate prediction of device response can be

obtained. Thus, the model can be used with confidence to predict the response of these and similar devices for design, analytical and experimental studies.

Chapter 6

Semi-active Tuned Mass Damper Systems

6.1 Introduction

A common method of passive structural control is achieved by the addition of a spring mass damper system. This system is specifically tuned to increase the attenuation of structure motion (Brock [1946], Den Hartog [1962], Warburton and Ayorinde [1980]) and are termed tuned mass damper (TMD) systems. TMD systems work by adding a mass and spring system tuned to a (typically) dominant frequency of the structure. As a result, TMD systems can be used to absorb structural vibration response and thus reduce the overall structural response.

Tuning of TMD systems to match specific structural modes is therefore critical for effective application (Sadek et al. [1997]). If the TMD system is not tuned correctly it is possible for the structure motion to be amplified for some earthquake ground motions, and/or to achieve significant degradation in performance. This lack of tuning may also occur if structural frequencies change over time due to degradation, retrofit or structural modification.

Typically, a TMD system requires an additional mass attached to the structure. However, this mass serves no purpose except for dynamic motion attenuation. Thus, it is redundant for a large percentage of the structure life, although some approaches use large HVAC or water storage units to avoid adding excessive mass. However, the added mass size is a limitation as bigger masses may absorb more energy, but cannot be justified only for damping purposes.

As an alternative approach, it is proposed to segregate the top section of a

structure to act as the 'tuned' mass. More specifically, the top 10 to 40% of the structure forms the segregated section, which can then behave as a primarily rigid block on top of a flexible structure. For retrofit or structural upgrade applications, additional storeys being added to the structure could be utilised in this way to achieve the same effect.

The segregated section can be attached to the main structure by passive spring damper systems. This configuration supplies reaction forces to the main structure. The reaction forces are generated by the relative motion between the structure and the segregated section. These passive TMD systems are effective at improving the structure response for a narrow range of structure frequencies centered around the design frequency (Sadek et al. [1997]).

Therefore, it is proposed to replace the passive spring damper system with semi-active resetable device based systems. The result is a semi-active resetable tuned mass damper system (RTMD). These sytems use feedback control to alter or manipulate the reaction forces, effectively re-tuning the system depending on the structural response. They thus can offer a broader more adaptable solution than passive tuning. The RTMD concept can be equally well utilised for both segregated structure or traditional additional mass systems.

Figure 6.1 schematically depicts the segregated storey configuration for a seven storey structure. The connections between the segregated section and main structure can be either passive for a TMD system or resetable for a RTMD system. For this study, the segregated section for the RTMD is assumed to be vertically supported on (relatively) frictionless bearings to allow restricted sliding with minimal dissipation compared to that offered by the resetable device components.

The aim of this analysis is to statistically quantify the *qualitative* benefit of RTMD systems over TMD systems. The results examine both the efficacy of the segregated configuration and the use of resetable devices in that approach. This study does *not* show exact design criteria. Rather, it is presented to encourage reassessment of structure control methods and to provide a further potential avenue of implementation for resetable devices. It is thus a qualitative, rather than a quantitative assessment.
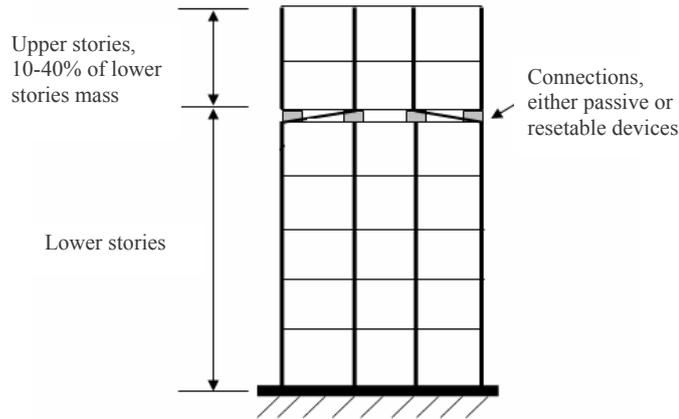
Figure 6.1   Schematic of a segregated structure where 10-40% of the structural mass is utilised as the tuned mass for either a TMD or RTMD system.

6.2   Study Methods

The structure is modelled as a two degree of freedom (2DOF) system as the response of the main structure is assumed to be first mode dominated, which is typical of many multi-storey civil structures. The segregated stories are modelled as a rigid, lumped mass. All results are normalised to the uncontrolled structure case for comparison. The three models used in this study are determined:

- **Uncontrolled structure**, modelled as a single degree of freedom system with 5% structural damping, as shown in Figure 6.2.

- **TMD system**, modelled as a 2DOF system with 10% equivalent viscous damping in the connections, and 5% structural damping in the flexible lower storeys, as shown in Figure 6.3.

- **RTMD system**, modelled as a 2DOF system similar to that of the TMD, but with the reaction forces provided by a resetable device, as shown in Figure 6.4.

Note that in each case the base structure or first degree of freedom is the same. The only changes are thus in the form of added storeys (mass) and their use as an energy absorber. This approach facilitates direct comparison between passive and semi-active approaches, as normalised to the uncontrolled case.
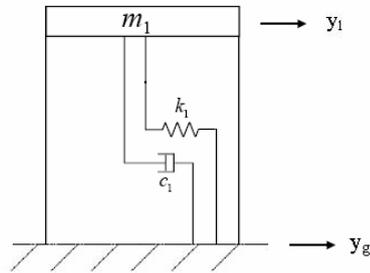
Figure 6.2   Uncontrolled structure, where m_1 is the mass, c_1 is the structure damping coefficient, k_1 is the column stiffness, $\ddot{y}_g$ is the ground acceleration, and y_1 is the motion of the structure mass relative to the ground.
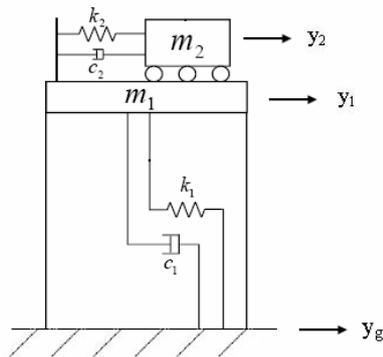
Figure 6.3   TMD system, where m_2 is the added tuned mass or segregated storey mass, y_2 is the motion of the tuned mass relative to the ground, k_2 is the tuned stiffness, c_2 is the tuned mass damping coefficient set to 10% viscous damping in the second degree of freedom.
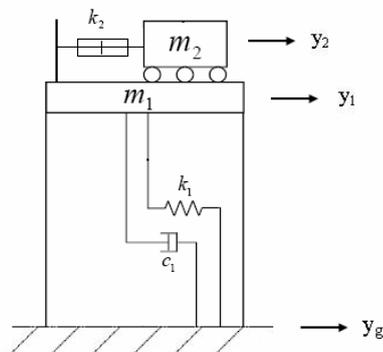
Figure 6.4   RTMD system, where k_2 in this case is the resetable device stiffness.

Linear structure models give a good indication of the overall structure response. However, a structure can enter the non-linear response range during strong earthquake excitation. Various hysteretic models have been proposed for modelling the inelastic restoring force in structures (Baber and Noori [1985]). The model used for this study is the Bouc-Wen smooth varying hysteretic model (Wen [1976]). The Bouc-Wen model incorporates a number of parameters, allowing a representation expressing several hysteretic properties. Therefore, following a thorough linear analysis and comparison, the non-linear Bouc-Wen hysteresis model is used to determine the response of the main structure for a non-linear analysis using these approaches. This last comparison examines performance due to realistic non-linearities that might be readily found under strong ground motion excitation.

Finally, note that the base uncontrolled structure has less total mass than the augmented systems of Figures 6.3 and 6.4. In this case it is assumed that extra storeys are being added as a TMD or RTMD. For more direct comparison results are compared for the base or first degree of freedom structure having the same period. With 20% added mass for m_2 the fundamental period changes only by 8 to 13%. Hence, there is not likely to be a significant change in structural response for any given structural motion. However, this point should also reinforce the qualitative nature of the comparison versus a strictly quantitative assessment.

6.2.1   Equations of Motion

6.2.1.1   Linear Equations

The general linear equations of motion for the three models are defined:

$$M\ddot{Y} + C\dot{Y} + KY = F(t) = -M\ddot{y}_g \qquad (6.1)$$

where M,C and K are the mass, damping and stiffness matrices, respectively, of the 1-2 DOF system, and $F(t)$ is the external load on the system. In this case, $F(t)$ arises from a ground motion acceleration $\ddot{y}_g$.

Thus, the equation of motion for the uncontrolled case of Figure 6.2 is defined:

$$m_1\ddot{y}_1 + c_1\dot{y}_1 + k_1 y_1 = -m_1\ddot{y}_g \tag{6.2}$$

where m_1 is the mass, c_1 is the damping coefficient, k_1 is the stiffness, $\ddot{y}_g$ is the ground acceleration, $\ddot{y}_1$ is the acceleration of the mass, $\dot{y}_1$ is the velocity of the mass, and y_1 is the motion of the mass relative to the ground.

For the TMD system in Figure 6.3, the equation of motion is defined:

$$\begin{bmatrix} m_1 & 0 \\ 0 & m_2 \end{bmatrix} \begin{pmatrix} \ddot{y}_1 \\ \ddot{y}_2 \end{pmatrix} + \begin{bmatrix} c_1+c_2 & -c_2 \\ -c_2 & c_2 \end{bmatrix} \begin{pmatrix} \dot{y}_1 \\ \dot{y}_2 \end{pmatrix} + \begin{bmatrix} k_1+k_2 & -k_2 \\ -k_2 & k_2 \end{bmatrix} \begin{pmatrix} y_1 \\ y_2 \end{pmatrix}$$
$$= \begin{bmatrix} -m_1 & 0 \\ 0 & -m_2 \end{bmatrix} \begin{pmatrix} 1 \\ 1 \end{pmatrix} \ddot{y}_g \tag{6.3}$$

where y_1 and y_2 are the structure mass and tuned mass system motions relative to the ground, m_1 and m_2 are the mass of the structure and mass of the tuned system, c_1 and c_2 are the structural and tuned mass system damping coefficients, and $\ddot{y}_g$ is the ground motion acceleration

Finally, for the RTMD system in Figure 6.4, the equation of motion is defined:

$$\begin{bmatrix} m_1 & 0 \\ 0 & m_2 \end{bmatrix} \begin{pmatrix} \ddot{y}_1 \\ \ddot{y}_2 \end{pmatrix} + \begin{bmatrix} c_1 & 0 \\ 0 & 0 \end{bmatrix} \begin{pmatrix} \dot{y}_1 \\ \dot{y}_2 \end{pmatrix} + \begin{bmatrix} k_1 & 0 \\ 0 & 0 \end{bmatrix} \begin{pmatrix} y_1 \\ y_2 \end{pmatrix}$$
$$= \begin{bmatrix} -m_1 & 0 \\ 0 & -m_2 \end{bmatrix} \begin{pmatrix} 1 \\ 1 \end{pmatrix} \ddot{y}_g + \begin{pmatrix} 1 \\ -1 \end{pmatrix} F_{spring} \tag{6.4}$$

where the terms are as previously described, except $F_{spring} = \Delta y\, k_2$ where $\Delta y = y_2 - y_1$, and k_2 is the resetable device stiffness.

6.2.1.2   Non-linear Equations of Motion

The restoring force (F_R) in the non-linear hysteretic system is broken down into two components. A non hysteretic, elastic component (F_E) that is a function of the instantaneous structure displacement and velocity, and a hysteretic component (F_H) that is a function of the time history displacement response. Thus, the restoring force for the non-linear system is defined:

$$F_R = F_E + F_H = K_E Y + K_H Z = \alpha K_T Y + (1 - \alpha) K_T Z \qquad (6.5)$$

where α is the yield stiffness ratio, K_T is the pre-yielding stiffness, Z is the relative displacement, and Z is the variable introduced to describe the hysteretic component.

The hysteretic component variable (Z) is described by:

$$\dot{Z} = \dot{y} \left[1 - 0.5 \left(1 + \text{sign}(\dot{y}Z) \right) \left(\frac{y}{Z} \right)^n \right] \qquad (6.6)$$

where n controls the smoothness of the curve, with $n = \infty$ resulting in a true, sharply cornered elastoplastic system. For this study values of $\alpha = 0.1$, $n = 2$, $Y = 0.045$ are used as they produce a smooth, realistic transition between elastic and plastic behaviour. The value of $\alpha = 0.1$ provides a post yield stiffness of 10%.

Overall, the general form of the equations of motion for the non-linear system model is defined:

$$M\ddot{Y} + C\dot{Y} + K_E Y + K_H Z = F(t) \qquad (6.7)$$

Thus, the non-linear TMD system has an equation of motion defined:

$$
\begin{bmatrix} m_1 & 0 \\ 0 & m_2 \end{bmatrix} \begin{pmatrix} \ddot{y}_1 \\ \ddot{y}_2 \end{pmatrix} + \begin{bmatrix} c_1+c_2 & -c_2 \\ -c_2 & c_2 \end{bmatrix} \begin{pmatrix} \dot{y}_1 \\ \dot{y}_2 \end{pmatrix} + \begin{bmatrix} k_{E1} & 0 \\ 0 & 0 \end{bmatrix} \begin{pmatrix} y_1 \\ y_2 \end{pmatrix}
$$
$$
= \begin{bmatrix} -m_1 & 0 \\ 0 & -m_2 \end{bmatrix} \begin{pmatrix} 1 \\ 1 \end{pmatrix} \ddot{y}_g - \begin{bmatrix} k_{H1} & 0 \\ 0 & 0 \end{bmatrix} \begin{pmatrix} z_1 \\ z_2 \end{pmatrix}
$$

(6.8)

where k_{E1} and k_{H1} are the elastic and hysteretic stiffness of the structure, and z_1 and z_2 are the hysteretic components of the Bouc-Wen model for the structure and tuned mass.

Similarly, the non-linear RTMD system has an equation of motion defined:

$$
\begin{bmatrix} m_1 & 0 \\ 0 & m_2 \end{bmatrix} \begin{pmatrix} \ddot{y}_1 \\ \ddot{y}_2 \end{pmatrix} + \begin{bmatrix} c_1 & 0 \\ 0 & 0 \end{bmatrix} \begin{pmatrix} \dot{y}_1 \\ \dot{y}_2 \end{pmatrix} + \begin{bmatrix} k_1 & 0 \\ 0 & 0 \end{bmatrix} \begin{pmatrix} y_1 \\ y_2 \end{pmatrix}
$$
$$
= \begin{bmatrix} -m_1 & 0 \\ 0 & -m_2 \end{bmatrix} \begin{pmatrix} 1 \\ 1 \end{pmatrix} \ddot{y}_g + \begin{pmatrix} 1 \\ -1 \end{pmatrix} F_{spring} - \begin{bmatrix} k_{H1} & 0 \\ 0 & 0 \end{bmatrix} \begin{pmatrix} z_1 \\ z_2 \end{pmatrix}
$$

(6.9)

where all of the terms are described previously.

If the relative displacement of the upper isolated storeys and the main structure is used in defining the equations of motion, as opposed to the relative motion of each section to the ground, the equation of motion of the RTMD system is:

$$
\begin{bmatrix} m_1 & 0 \\ 0 & m_2 \end{bmatrix} \begin{pmatrix} \ddot{y}_1 \\ \Delta\ddot{y} \end{pmatrix} + \begin{bmatrix} c_1 & 0 \\ 0 & 0 \end{bmatrix} \begin{pmatrix} \dot{y}_1 \\ \Delta\dot{y} \end{pmatrix} + \begin{bmatrix} k_1 & 0 \\ 0 & 0 \end{bmatrix} \begin{pmatrix} y_1 \\ \Delta y \end{pmatrix}
$$
$$
= \begin{bmatrix} -m_1 & 0 \\ 0 & -m_2 \end{bmatrix} \begin{pmatrix} 1 \\ 1 \end{pmatrix} \ddot{y}_g + \begin{pmatrix} 1 \\ -1 \end{pmatrix} F_{spring} - \begin{bmatrix} k_{H1} & 0 \\ 0 & 0 \end{bmatrix} \begin{pmatrix} z_1 \\ z_2 \end{pmatrix}
$$

(6.10)

This last definition in Equation 6.10 is used for analysing some additional semi-active device controllers that use different resetting criteria.

6.2.2   Control Laws

This study examines three specific resetable devices laws:

1. Reset the device when the relative velocity between the structure and the segregated storeys is zero, $\Delta \dot{y} = 0$. This law is the 1-4 control law described in Chapter 2.

2. Reset when the main structure velocity is zero, $\dot{y} = 0$.

3. A hybrid law where the first law is used until the relative displacement between the structure and the mass reaches a given value of 80-100% of the maximum device stroke, whereupon it is switched to the second law for the remainder of the record.

The third control law results from restrictions on the available device stroke (Fukuzumi et al. [2001]). More specifically, this hybrid law allows reseting of the device during large relative motion where a reset may not occur under the first law. Resetting the device dissipates structural energy. Hence, this hybrid law aims to maximise the energy dissipation for a wide range of structural motion. In addition, it minimises excessive upper storey motion and thus avoids any excessive overturning moments for safety and practicality in designing the tuned mass and main structure connections.

6.2.3   System Parameters

This study is intended to qualitatively investigate the additional benefits to structural response using resetable, rather than passive, devices between the main structure and segregated storeys. Therefore, variables such as the resetable stiffness and percentage of segregated mass are examined independently. It is therefore necessary to vary some parameters, while keeping others constant, for each section of this analysis. The choice of the constant parameters does not indicate an optimum selection, rather they are chosen as reasonable values, or as the value that gave the best response in a previous analysis.

6.2.4   Time History Analysis and Spectra

The structural response is analysed using the three suites of ground motions from the SAC project (Sommerville et al. [1997]). Spectra are created by varying the mass of the main structure (m_1). In each case, the mass of the upper isolated stories, or tuned mass, is modified to maintain the main structure-tuned mass ratio. The response is calculated for natural structural frequencies of 0.1Hz and 0.2 to 5.0Hz, in 0.2Hz increments.

These frequencies correspond to periods of 0.2-5.0s and 10s. The 0.2-5.0s range covers the primary range considered for seismic analysis, and the 10s value is added for completeness. The overall goal is to create or define the general shape of the spectra.

Time histories for each earthquake record are obtained using a Newmark-Beta numerical integration scheme (Clough and Penzien [1993], Humar [2002]). A time step of 0.005s ensures accurate simulation without excessive computational effort and removes the need to iterate within a time step. For each record, the absolute maximum and absolute mean structural displacement values are recorded. The results are compiled to obtain median and standard deviation values over each structural period in the spectra and then for each suite of ground motions.

6.3   Results

All results are normalised to the un-segregated, uncontrolled structure case. To indicate the spread of results the 16th, 50th and 84th percentiles are presented using lognormal statistics (Limpert et al. [2001], Hunt [2002]) where the 16th and 84th percentiles represent ± 1 lognormal standard deviation and the middle 68% of results. These percentile values indicate the relative improvement over the un-controlled case where a value of 100 represents the uncontrolled level of response. Tabulated results give the geometric mean and bandwidth ($\hat{x}\beta - \left(\frac{\hat{x}}{\beta}\right)$) at a structural natural frequency of two seconds ($T_n = 2s$). This period is important in seismic design and represents, in a single number, the qualitative efficacy of the control scheme for easy comparison between schemes. Note that the variation around this period, in the seismically critical one to three second period range,

is not generally large. Finally, the RTMD response as a percentage of the TMD response is presented in the tabulated results. This last comparison allows a direct comparison between the traditional passive TMD approach and the newly proposed RTMD approach.

6.3.1 Linear Structure Results

Structural displacement response time histories for two earthquakes from each suite are presented to show typical results in Figures 6.5 to 6.7. In most cases, the TMD and RTMD systems are effective at reducing the peak displacements of the structure, particularly following any initial larger peaks due to strong motion. However, in some cases the structure displacement is amplified compared to the uncontrolled case, particularly for the TMD case. Thus, it is vitally important to address the range of response over suites of earthquake ground motion records to avoid bias from using one, or a few particular ground motions.

Figures 6.5 to 6.7 also show a first very clear difference between the passive TMD and semi-active RTMD approaches. Specifically, the TMD response clearly shows a far different dominant structural period of response compared to the uncontrolled case. This difference is due to the TMD tuning effectively modifying the fundamental frequency with the added tuned mass spring system, and is thus an expected result. In contrast, the RTMD system has effectively the same dominant structural response period with the slight 8 to 13% difference attributed to the different total mass between the uncontrolled and RTMD cases. Overall, this difference clearly shows that the passive TMD and semi-active RTMD designs developed reduce structural response by different mechanisms.

Figure 6.8 shows an example response spectra demonstrating the 16th, 50th, and 84th percentiles. In the spectra presented in this chapter, TMD system structure response is indicated with a dashed line, while RTMD system response is shown by a solid line. The bandwidth is the difference between the 16th and 84th percentile values.
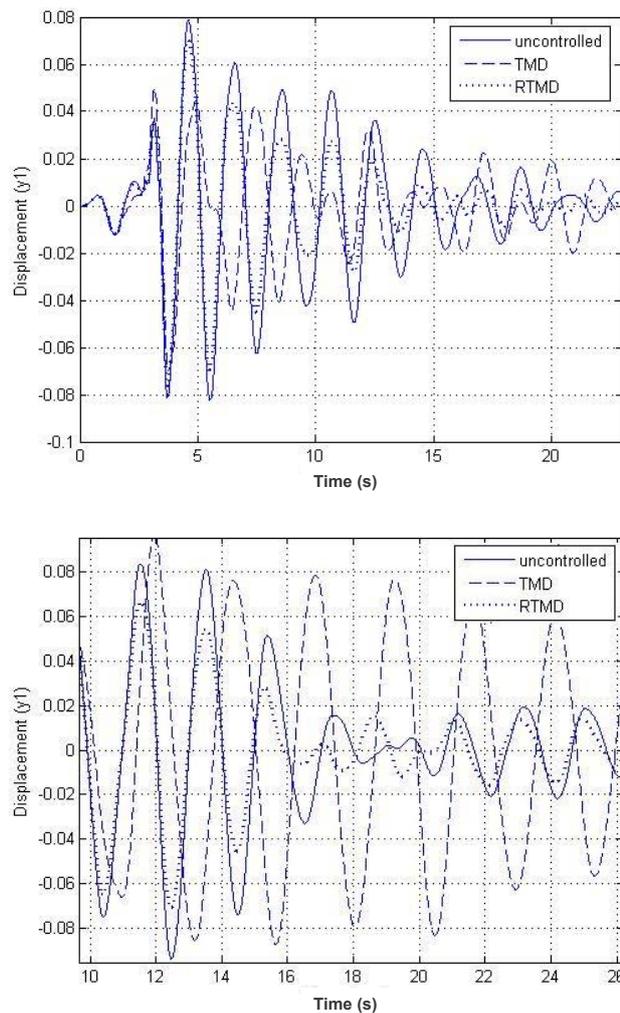
Figure 6.5 Displacement of the structure for selected strong motion to transient portions of two low suite ground motions.

6.3.1.1   Examination of Resetable Device Stiffness

Resetable devices are able to respond to a wide range of structural motion, as opposed to passive devices which are tuned to a particular frequency motion. Moreover, the tuning of TMD systems results in a very specific stiffness requirement for the passive devices, optimised for the expected structural natural period. However, if the structural analysis to determine the tuned stiffness is incorrect or the actual device stiffness is not the required value, the TMD system will no longer be correctly tuned, resulting in degraded results.

Therefore, this section examines the impact of the semi-active device stiffness used in the RTMD system. The analysis follows from the assumption that exact tuning is not always possible, either initially or for the duration of a structure's
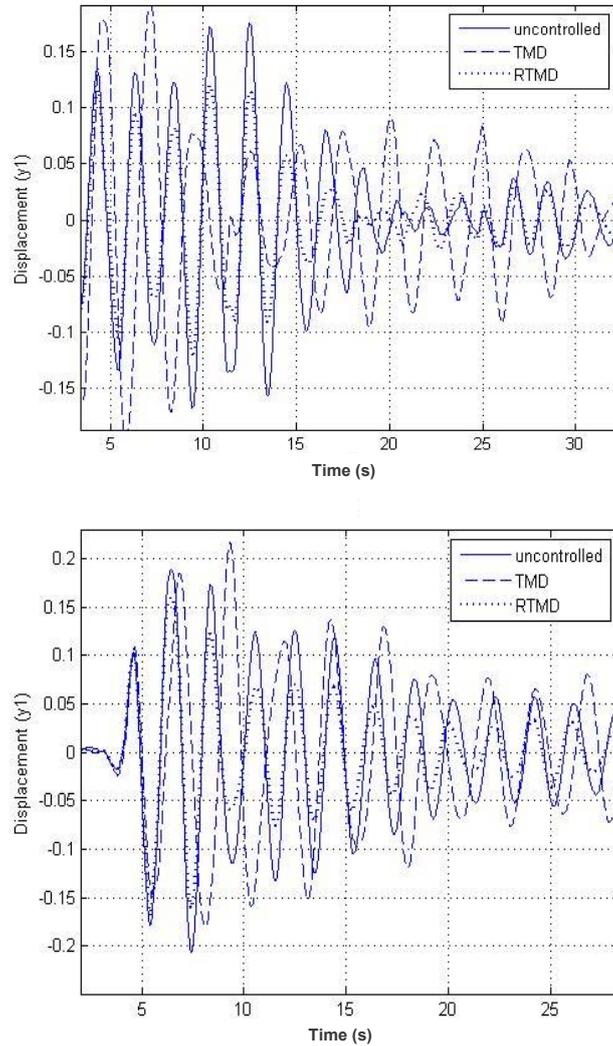
Figure 6.6 Displacement of the structure for selected strong motion to transient portions of two medium suite ground motions.

service. Hence, this section determines a tuning method for selecting the device stiffness required for a RTMD system and the robustness of the value obtained to variation.

RTMD system stiffness values are examined for values of k_2, $\frac{k_2}{2.5}$, $\frac{k_2}{5}$, $\frac{k_2}{8}$, and $\frac{k_2}{13}$, where k_2 is the tuned or optimised stiffness value. The assumption is that lower stiffnesses will allow more device motion and thus dissipate more energy than a stiffness greater than k_2. The segregated storey mass is kept constant at 20% of the structure mass. Tables 6.1 to 6.3 present the results for the low, medium and high suites, respectively.

Response for the three suites show very similar qualitative results. In addition, the maximum and mean displacements are very similar for each suite. A
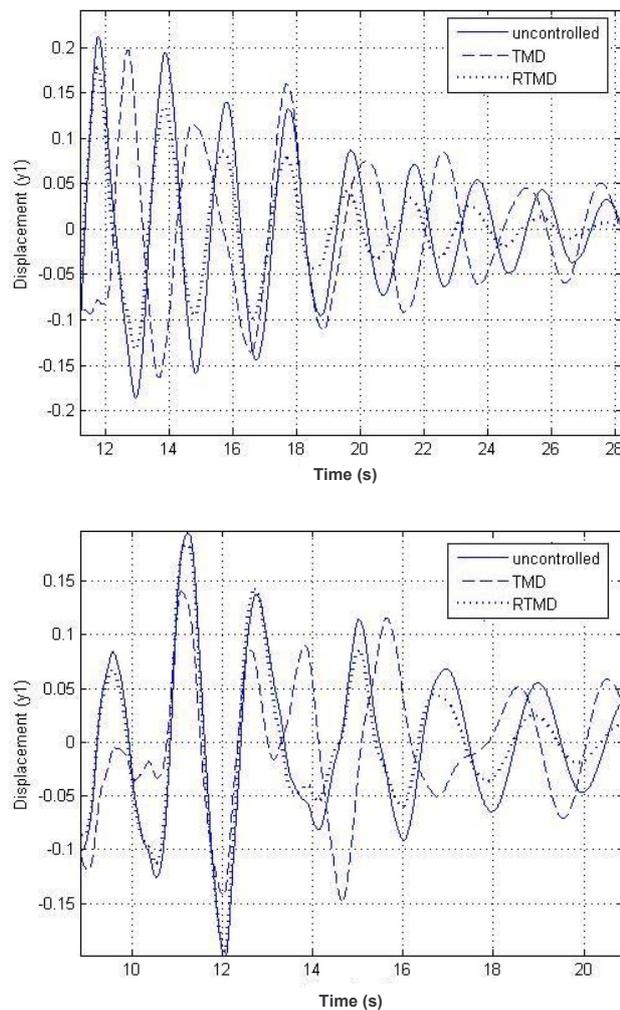
Figure 6.7   Displacement of the structure for selected strong motion to transient portions of two high suite ground motions.

large amount of data is presented so only general conclusions will be discussed. A RTMD system stiffness of $\frac{k_2}{2.5}$ generally gives the best reduction for the 50th percentile. The lowest stiffness value examined $\left(\frac{k_2}{13}\right)$ gives the smallest bandwidth or range between 16th and 84th percentiles, both as an absolute value and percentage of the TMD case. Hence, lower stiffness values for the resetable device provide better results than the optimal TMD (k_2) stiffness. Second to that result, lower stiffness gives a tighter range while higher stiffness gives a lower 50th percentile, indicating a clear tradeoff.

These results indicate that using a stiffness value, for the RTMD system, that is *lower* than the 'tuned' value has significant potential to produce good results. Thus, with a RTMD system it is not necessary to either calculate the *exact* tuned stiffness required or demand that the devices produce the exact
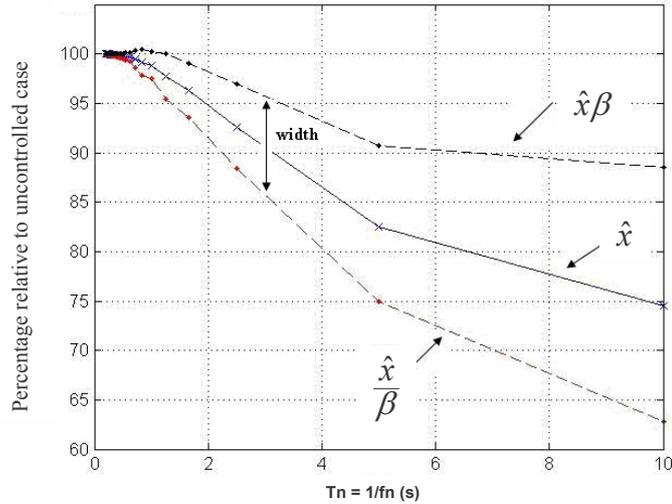
Figure 6.8 Example of a structural response spectra indicating the 16th ($\frac{\hat{x}}{\beta}$), 50th ($\hat{x}$), and 84th ($\hat{x}\beta$) percentile results. The spectra are relative to the uncontrolled structure case and converted to 100%. The width is the middle 68% ($16 - 84^{th}$ percentil) range and is measured at T=2.0s. The statistics used are lognormal, as appropriate for structural response analysis (Limpert et al. [2001], Hunt [2002]).

design stiffness. This result saves time and effort in the design procedure and dramatically simplifies design, as *any* stiffness lower than k_2 or $\frac{k_2}{2}$ will produce good results for the RTMD. More specifically, a RTMD stiffness value of $\frac{k_2}{5}$ represents a good compromise in reducing the mean value and bandwidth across the three suites. In addition, a stiffness value of $\frac{k_2}{5}$ should be a reasonable stiffness value to achieve with resetable devices.

Response spectra for the low, medium and high suites using a RTMD stiffness of $\frac{k_2}{5}$ are presented in Figures 6.9, 6.10, and 6.11, respectively. These spectra are intended to graphically illustrate the efficacy of the RTMD system at reducing and bounding the structural response. In addition, these spectra show the frequency dependency of the TMD system with a noticeable increase in the 84th percentile line around $T_n = 2s$, that is not present for the RTMD response. A narrow bandwidth across the spectra indicates the RTMD system is able to stay 'in-tune' with the structure, *independent* of the interaction/ratio between the ground excitation and structural natural frequency. In addition, the narrow bandwidth with few or no ground motion amplifying response over 100%, in contrast to the TMD, shows how the RMTD can provide good response attenuation regardless of the frequency content of the ground motion input.

Table 6.1 Low suite results of comparative stiffness analysis. Results are presented for k_2, $\frac{k_2}{2.5}$, $\frac{k_2}{5}$, $\frac{k_2}{8}$, and $\frac{k_2}{13}$. The 16th percentile ($\frac{\hat{x}}{\beta}$), 50th percentile ($\hat{x}$), and 84th percentile ($\hat{x}$ x β) results are presented for the TMD and RTMD cases along with the bandwidth. In addition, the bandwidth and 50th percentile as a percentage of the TMD are presented.

			$\frac{\hat{x}}{\beta}$	$\hat{x}$	$\hat{x}$ x β	band width	bandwidth % TMD	$\hat{x}$ % TMD
y_1 max		TMD (passive)	63.6	83.7	110.1	46.5	100.00%	100.00%
	k_2	reset when $\Delta \dot{y}_1 = 0$	83.6	96.2	110.7	27.1	58.30%	114.90%
		reset when $\dot{y}_1 = 0$	68	86.9	110.9	42.9	92.30%	103.80%
	$\frac{k_2}{2.5}$	reset when $\Delta \dot{y}_1 = 0$	79.7	90.3	102.2	22.5	48.40%	107.90%
		reset when $\dot{y}_1 = 0$	72.9	83.7	96.2	23.3	50.10%	100.00%
	$\frac{k_2}{5}$	reset when $\Delta \dot{y}_1 = 0$	84	91.5	99.6	15.6	33.50%	109.30%
		reset when $\dot{y}_1 = 0$	83.2	90	97.8	14.6	31.40%	107.50%
	$\frac{k_2}{8}$	reset when $\Delta \dot{y}_1 = 0$	89	93.5	98.2	9.2	19.80%	111.70%
		reset when $\dot{y}_1 = 0$	89	93.5	99	10	21.50%	111.70%
	$\frac{k_2}{13}$	reset when $\Delta \dot{y}_1 = 0$	92.65	95.55	98.5	5.85	12.60%	114.20%
		reset when $\dot{y}_1 = 0$	93.2	96.1	99.15	5.95	12.80%	114.80%
y_1 mean		TMD (passive)	61.2	83.3	114.6	53.4	100.00%	100.00%
	k_2	reset when $\Delta \dot{y}_1 = 0$	75.7	88.1	102.8	27.1	50.70%	105.80%
		reset when $\dot{y}_1 = 0$	57.45	77.6	105	47.55	89.00%	93.20%
	$\frac{k_2}{2.5}$	reset when $\Delta \dot{y}_1 = 0$	68.5	79.3	91.85	23.35	43.70%	95.20%
		reset when $\dot{y}_1 = 0$	56.4	70.7	88.75	32.35	60.60%	84.90%
	$\frac{k_2}{5}$	reset when $\Delta \dot{y}_1 = 0$	74.4	82.4	91.3	16.9	31.60%	98.90%
		reset when $\dot{y}_1 = 0$	71.5	81.6	93.2	21.7	40.60%	98.00%
	$\frac{k_2}{8}$	reset when $\Delta \dot{y}_1 = 0$	81	87	93.8	12.8	24.00%	104.40%
		reset when $\dot{y}_1 = 0$	81	88	95.5	14.5	27.20%	105.60%
	$\frac{k_2}{13}$	reset when $\Delta \dot{y}_1 = 0$	87.4	91.5	96	8.6	16.10%	109.80%
		reset when $\dot{y}_1 = 0$	88	92.6	97.3	9.3	17.40%	111.20%

Table 6.2 Medium suite results of comparative stiffness analysis. Results are presented for k_2, $\frac{k_2}{2.5}$, $\frac{k_2}{5}$, $\frac{k_2}{8}$, and $\frac{k_2}{13}$. The 16th percentile ($\frac{\hat{x}}{\beta}$), 50th percentile ($\hat{x}$), and 84th percentile ($\hat{x}$ x β) results are presented for the TMD and RTMD cases along with the bandwidth. In addition, the bandwidth and 50th percentile as a percentage of the TMD are presented.

			$\frac{\hat{x}}{\beta}$	$\hat{x}$	$\hat{x}$ x β	band width	bandwidth % TMD	$\hat{x}$ % TMD
y_1 max		TMD (passive)	72.7	86.55	103.2	30.5	100.00%	100.00%
	k_2	reset when $\Delta\dot{y}_1 = 0$	88.7	98.4	109.2	20.5	67.20%	113.70%
		reset when $\dot{y}_1 = 0$	72.2	91.6	110.2	38	124.60%	105.80%
	$\frac{k_2}{2.5}$	reset when $\Delta\dot{y}_1 = 0$	83.6	90.9	98.85	15.25	50.00%	105.00%
		reset when $\dot{y}_1 = 0$	73.8	84.9	97.8	24	78.70%	98.10%
	$\frac{k_2}{5}$	reset when $\Delta\dot{y}_1 = 0$	84.6	90.25	96.3	11.7	38.40%	104.30%
		reset when $\dot{y}_1 = 0$	81.4	89.45	98.35	16.95	55.60%	103.40%
	$\frac{k_2}{8}$	reset when $\Delta\dot{y}_1 = 0$	88.1	92.2	96.6	8.5	27.90%	106.50%
		reset when $\dot{y}_1 = 0$	87	92.6	98.75	11.75	38.50%	107.00%
	$\frac{k_2}{13}$	reset when $\Delta\dot{y}_1 = 0$	93.3	94.4	97.6	4.3	14.10%	109.10%
		reset when $\dot{y}_1 = 0$	91.6	95.2	99	7.4	24.30%	110.00%
y_1 mean		TMD (passive)	64.5	85.05	112.7	48.2	100.00%	100.00%
	k_2	reset when $\Delta\dot{y}_1 = 0$	74.9	86.9	101.3	26.4	54.80%	102.20%
		reset when $\dot{y}_1 = 0$	57.6	74	95.9	38.3	79.50%	87.00%
	$\frac{k_2}{2.5}$	reset when $\Delta\dot{y}_1 = 0$	66.05	74.7	84.6	18.55	38.50%	87.80%
		reset when $\dot{y}_1 = 0$	53	63.9	77.2	24.2	50.20%	75.10%
	$\frac{k_2}{5}$	reset when $\Delta\dot{y}_1 = 0$	71.2	77.9	84.9	13.7	28.40%	91.60%
		reset when $\dot{y}_1 = 0$	68	76.3	85.6	17.6	36.50%	89.70%
	$\frac{k_2}{8}$	reset when $\Delta\dot{y}_1 = 0$	78.8	83.35	88.2	9.4	19.50%	98.00%
		reset when $\dot{y}_1 = 0$	78.45	84	90	11.55	24.00%	98.80%
	$\frac{k_2}{13}$	reset when $\Delta\dot{y}_1 = 0$	85.8	89.9	92	6.2	12.90%	105.70%
		reset when $\dot{y}_1 = 0$	86.3	89.9	93.6	7.3	15.10%	105.70%

Table 6.3 High suite results of comparative stiffness analysis. Results are presented for k_2, $\frac{k_2}{2.5}$, $\frac{k_2}{5}$, $\frac{k_2}{8}$, and $\frac{k_2}{13}$. The 16th percentile ($\frac{\hat{x}}{\beta}$), 50th percentile ($\hat{x}$), and 84th percentile ($\hat{x}$ x β) results are presented for the TMD and RTMD cases along with the bandwidth. In addition, the bandwidth and 50th percentile as a percentage of the TMD are presented.

			$\frac{\hat{x}}{\beta}$	$\hat{x}$	$\hat{x}$ x β	band width	bandwidth % TMD	$\hat{x}$ % TMD
y_1 max		TMD (passive)	75.6	88.8	104.4	28.8	100.00%	100.00%
	k_2	reset when $\Delta\dot{y}_1 = 0$	90.9	104.4	111	20.1	69.80%	117.60%
		reset when $\dot{y}_1 = 0$	83.5	95.1	108.4	24.9	86.50%	107.10%
	$\frac{k_2}{2.5}$	reset when $\Delta\dot{y}_1 = 0$	85.5	92.1	99.1	13.6	47.20%	103.70%
		reset when $\dot{y}_1 = 0$	80	87	94.5	14.5	50.30%	98.00%
	$\frac{k_2}{5}$	reset when $\Delta\dot{y}_1 = 0$	86	91	96	10	34.70%	102.50%
		reset when $\dot{y}_1 = 0$	86	91	96	10	34.70%	102.50%
	$\frac{k_2}{8}$	reset when $\Delta\dot{y}_1 = 0$	89	92.7	96.5	7.5	26.00%	104.40%
		reset when $\dot{y}_1 = 0$	90.3	93.75	97.4	7.1	24.70%	105.60%
	$\frac{k_2}{13}$	reset when $\Delta\dot{y}_1 = 0$	92.5	94.9	97.5	5	17.40%	106.90%
		reset when $\dot{y}_1 = 0$	93.5	95.9	98.4	4.9	17.00%	108.00%
y_1 mean		TMD (passive)	68.4	94.8	131.9	63.5	100.00%	100.00%
	k_2	reset when $\Delta\dot{y}_1 = 0$	77.1	90.9	107.7	30.6	48.20%	95.90%
		reset when $\dot{y}_1 = 0$	56.7	76.5	104.1	47.4	74.60%	80.70%
	$\frac{k_2}{2.5}$	reset when $\Delta\dot{y}_1 = 0$	64.5	74.1	85.5	21	33.10%	78.20%
		reset when $\dot{y}_1 = 0$	53.1	63.2	76	22.9	36.10%	66.70%
	$\frac{k_2}{5}$	reset when $\Delta\dot{y}_1 = 0$	69	76	83.9	14.9	23.50%	80.20%
		reset when $\dot{y}_1 = 0$	67.8	75.55	84.4	16.6	26.10%	79.70%
	$\frac{k_2}{8}$	reset when $\Delta\dot{y}_1 = 0$	77.1	82.1	87.45	10.35	16.30%	86.60%
		reset when $\dot{y}_1 = 0$	78.45	83.7	89.4	10.95	17.20%	88.30%
	$\frac{k_2}{13}$	reset when $\Delta\dot{y}_1 = 0$	84.7	88	91.5	6.8	10.70%	92.80%
		reset when $\dot{y}_1 = 0$	86.1	89.6	93.2	7.1	11.20%	94.50%
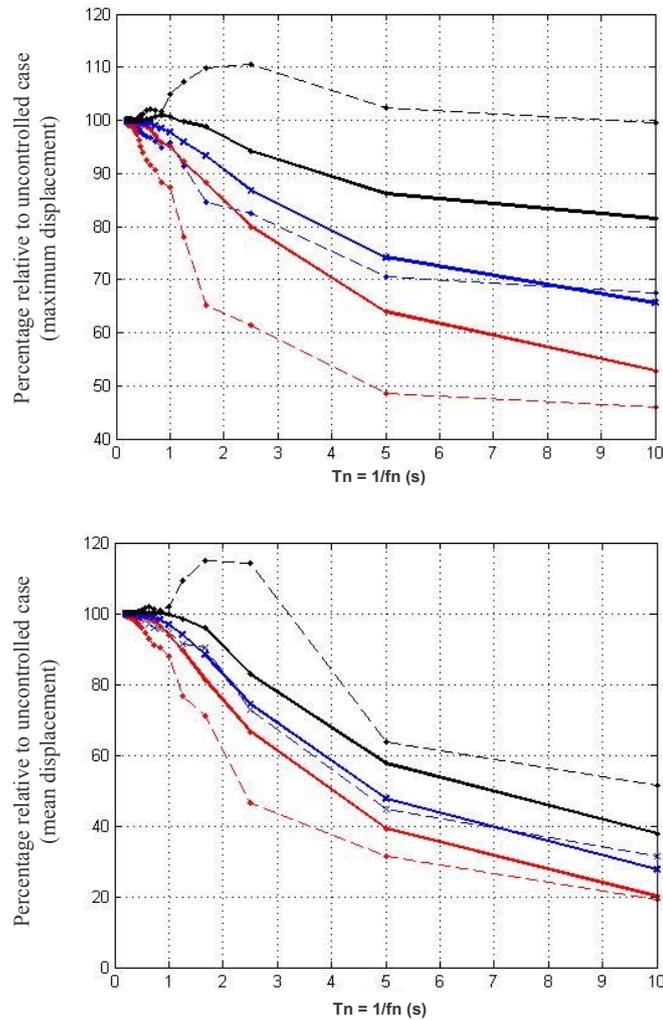
Figure 6.9 Low suite spectra. TMD system stiffness (k_2) exactly tuned to structure, RTMD system stiffness $\frac{k_2}{5}$. Tuned mass is 20% of structure mass. The dashed lines indicate the TMD system while the solid lines indicate the RTMD system. The upper line for both cases is the 84th percentile, the middle line the 50th percentile, and the lower line the 16th percentile.

6.3.2 Non-linear Structure Results

Non-linear structural response is likely to occur during ground motion excitation, particulary for large earthquake ground motion when structures are more likely to exceed their elastic limits. Non-linear modelling of the first degree of freedom section (lower storeys in the segregated structure case) results in more realistic structural response. Therefore, the remainder of this TMD and RTMD comparative study utilises non-linear structural response modelling. Figure 6.12 give typical examples of displacement time histories of the uncontrolled structural response as well as the TMD and RTMD cases for a ground motion from each of the three suites. The difference in response between the TMD and RTMD is not
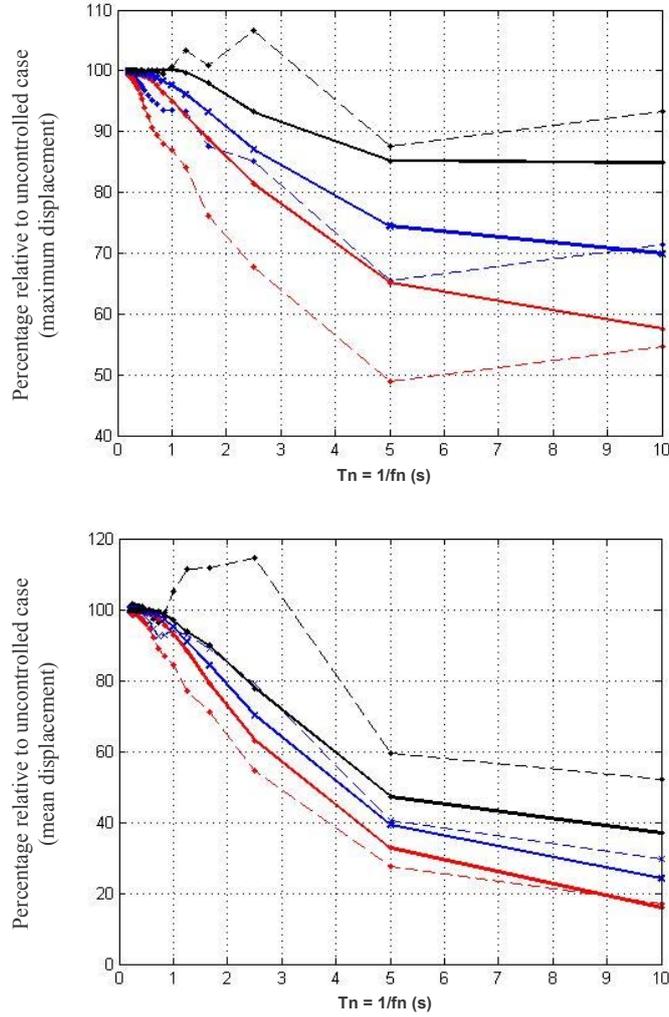
Figure 6.10   Medium suite spectra. TMD system stiffness (k_2) exactly tuned to structure, RTMD system stiffness $\frac{k_2}{5}$. Tuned mass is 20% of structure mass. The dashed lines indicate the TMD system while the solid lines indicate the RTMD system. The upper line for both cases is the 84th percentile, the middle line the 50th percentile, and the lower line the 16th percentile.

as pronounced as for the linear structure case (Figures 6.5 to 6.7) although the change in structural period is still evident for the TMD case.

6.3.2.1   Examination of Segregated Storey Mass

This section examines the effect of the percentage of segregated storey mass on the structure response for TMD and RTMD systems. Results are presented for values of 10 to 40%, in 10% increments, of the structure mass (m_1). The RTMD stiffness has a value of $\frac{k_2}{5}$ based on results from the comparative stiffness linear
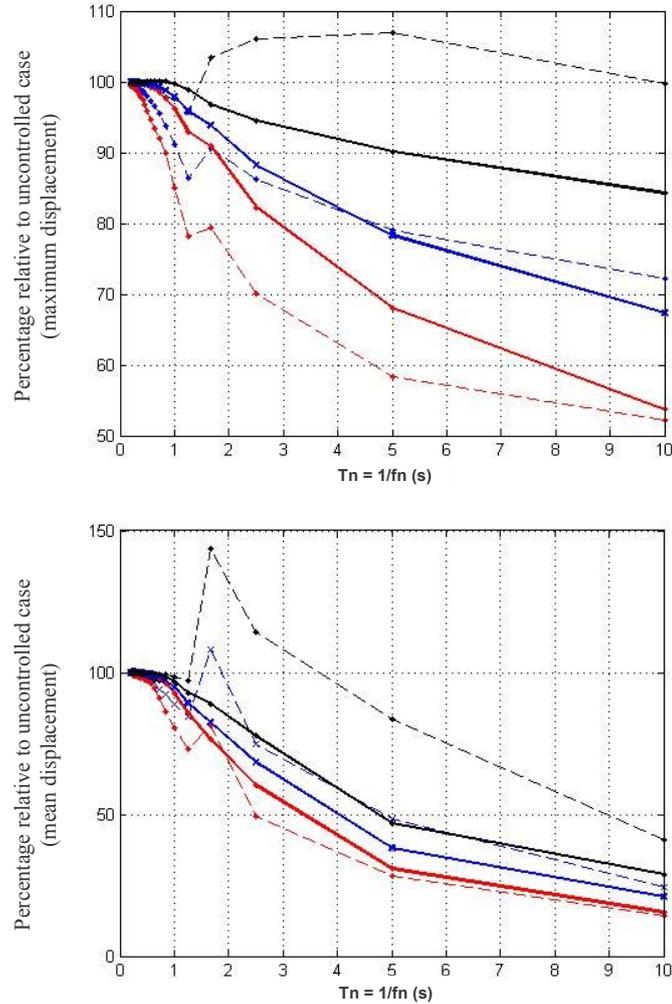
Figure 6.11   High suite spectra. TMD system stiffness (k_2) exactly tuned to structure, RTMD system stiffness $\frac{k_2}{5}$. Tuned mass is 20% of structure mass. The dashed lines indicate the TMD system while the solid lines indicate the RTMD system. The upper line for both cases is the 84th percentile, the middle line the 50th percentile, and the lower line the 16th percentile.

analysis. Results are largely suite invariant. Therefore, Table 6.4 shows the maximum and mean displacement results for the low suite only for clarity. In addition, the 72 year return period for the low suite events represent the most credible design case for this analysis.

Similar to the device stiffness analysis, a compromise between reducing the mean response *and* the bandwidth is required to choose the most effective mass percentage. For the passive TMD system the greatest reduction in the mean value results with $m_2 = 20\% m_1$ and for maximum displacements with $m_2 = 30\% m_1$. For the RTMD system, $m_2 = 40\% m_1$ results in the best reduction in the absolute mean value. However, $m_2 = 10\% m_1$ results in the best absolute bandwidth value,

while $m_2 = 20\%m_1$ shows the smallest bandwidth as a percentage of the TMD system.

Spectra with $m_2 = 20\%m_1$ and $m_2 = 30\%m_1$ are presented in Figures 6.13 and 6.14. These spectra, unlike Table 6.4, show the response over a range of structural periods. Examination of these spectra indicate a segregated mass of 30% of the structure mass gives the greatest response reductions in mean values across a range of structural periods, as well as minimising the bandwidth across the spectra. It is also a middle ground choice from the compromises seen at $T = 2.0s$ in Table 6.4.

6.3.2.2   Examination of Control Laws

Given a structural segregated mass of 30%, and a device stiffness of $\frac{k_2}{5}$, this section examines the three control laws for the RTMD system. Tables 6.5 to 6.7 show the results for the low, medium and high suites, respectively. Non-linear analysis is still used for this study. All three suites are used to see if varying the control has a variable effect over the different suites. The third, or hybrid control law switches from the first to the second law at $\Delta y = 0.2$m, of segregated storey stroke, which is a realistic TMD stroke.

The medium and high suite results show qualitatively similar results for the lowest mean response, percentage bandwidth and percentage mean values. For these two suites, the greatest reduction in mean values results from the second control law, which resets when $\dot{y} = 0$. In addition, this control law at least halves the bandwidth compared to the first control law.

In contrast, the low suite shows different results, with the mean value being the most reduced for the first, relative displacement control law. This first control law is the normal or typical resetable device control law (Bobrow and Jabbari [2002], Figure 2.9). The second control law that only depends on the structural velocity for reset points is analogous to the resetable devices being attached between the top of the main structure and the *ground*. Thus, reductions in structural dynamic motion using the first two control laws is dependent on the ground motion as well as structural response.

The third, or hybrid control law has the most bounded response, as the system is able to dissipate structural energy for all types of structural motion. The bandwidth is particularly narrow for the medium and high suites indicating the efficacy of the hybrid law during large relative motion. Overall, as expected, the hybrid law provides a best compromise or result from the two control laws.

6.4 Summary

RTMD systems show significant promise for applications of structural control, particularly for cases where extra storeys might be added. They offer advantages over passive TMD systems in the consistent response reductions seen over a range of structural natural frequencies. In particular, the use of reduced stiffness versus a tuned passive TMD system creates a simple, far more robust design solution. In addition, the RTMD systems improve structural performance even when the stiffness of the system is *not* the tuned stiffness. These results are in stark contrast to passive TMD system design where a slightly out of tune system can amplify the structure response or have significantly degraded performance. Thus, RTMD systems are more robust than their TMD system counterparts.

This specific analysis aims to encourage reassessment of control methods. More specifically, it has accentuated the efficacy of a novel structure design approach utilising semi-active control systems. Using the top section of a structure as the tuned mass alleviates the requirement of a large, predominantly redundant additional mass. In addition, the deliberate un-tuning of the resetable device stiffness chosen gives good results, while also reducing the complexity of the control system design.

Overall, a novel implementation is presented and an initial analysis offered to show its potential. Segregating storey mass for control offers a significant opportunity for seismically active urban areas, where the only avenue of expansion is upwards. A similar approach might also be considered for new high rise structures. Finally, the approach presented offers an insight into how rethinking typical solutions with new technology can offer dramatic improvements that might not otherwise be expected.

Table 6.4   Non-linear structure displacement statistics to low suite for the TMD and RTMD configurations normalised to the uncontrolled case.

			$\frac{\hat{x}}{\beta}$	$\hat{x}$	$\hat{x}$ x β	band width	bandwidth % TMD	$\hat{x}$ % TMD
y_1 max	$m_2 = 10\%$	TMD (passive)	85.35	93.7	102.9	17.55	100.00%	100.00%
		reset when $\Delta \dot{y}_1 = 0$	94.45	96.8	99.2	4.75	27.10%	103.30%
		reset when $\dot{y}_1 = 0$	93.3	97	100.7	7.4	42.20%	103.50%
	$m_2 = 20\%$	TMD (passive)	74.7	89.2	106.5	31.8	100.00%	100.00%
		reset when $\Delta \dot{y}_1 = 0$	90.3	94	97.9	7.6	23.90%	105.40%
		reset when $\dot{y}_1 = 0$	87.7	94.1	101	13.3	41.80%	105.50%
	$m_2 = 30\%$	TMD (passive)	68.8	86.9	109.65	40.85	100.00%	100.00%
		reset when $\Delta \dot{y}_1 = 0$	86.4	91.5	98.8	12.4	30.40%	105.30%
		reset when $\dot{y}_1 = 0$	83.4	91.8	100.95	17.55	43.00%	105.60%
	$m_2 = 40\%$	TMD (passive)	67.2	87.7	114.35	47.15	100.00%	100.00%
		reset when $\Delta \dot{y}_1 = 0$	82.7	89	95.9	13.2	28.00%	101.50%
		reset when $\dot{y}_1 = 0$	80.1	89.6	100.3	20.2	42.80%	102.20%
y_1 mean	$m_2 = 10\%$	TMD (passive)	76.8	91.4	109.1	32.3	100.00%	100.00%
		reset when $\Delta \dot{y}_1 = 0$	92.1	95.3	98.7	6.6	20.40%	104.30%
		reset when $\dot{y}_1 = 0$	92.4	96.2	100.2	7.8	24.10%	105.30%
	$m_2 = 20\%$	TMD (passive)	71.9	89.5	111.9	40	100.00%	100.00%
		reset when $\Delta \dot{y}_1 = 0$	85.2	91.4	98	12.8	32.00%	102.10%
		reset when $\dot{y}_1 = 0$	85.2	92.5	100.45	15.25	38.10%	103.40%
	$m_2 = 30\%$	TMD (passive)	71.8	90.3	114.1	42.3	100.00%	100.00%
		reset when $\Delta \dot{y}_1 = 0$	79.5	88.1	97.8	18.3	43.30%	97.60%
		reset when $\dot{y}_1 = 0$	80.4	89.6	99.8	19.4	45.90%	99.20%
	$m_2 = 40\%$	TMD (passive)	67.7	90	119.7	52	100.00%	100.00%
		reset when $\Delta \dot{y}_1 = 0$	74.3	85.2	97.6	23.3	44.80%	94.70%
		reset when $\dot{y}_1 = 0$	76.2	86.7	98.75	22.55	43.40%	96.30%

Table 6.5   Comparison of RTMD control methods for the low suite.

		$\frac{\hat{x}}{\beta}$	$\hat{x}$	$\hat{x} \times \beta$	band width	bandwidth % TMD	$\hat{x}$ % TMD
y_1 max	TMD (passive)	72	98	129	57	100%	100%
	reset when $\Delta \dot{y}_1 = 0$	83.6	96.2	110.7	27.1	48%	98%
	reset when $\dot{y}_1 = 0$	90.25	94.6	99.1	8.85	16%	97%
	hybrid (switch $\Delta y = 0.2$)	90.7	95	99.4	8.7	15%	97%
y_1 mean	TMD (passive)	70	99	141	71	100%	100%
	reset when $\Delta \dot{y}_1 = 0$	75.7	88.1	102.8	27.1	38%	89%
	reset when $\dot{y}_1 = 0$	82.3	89	96.3	14	20%	90%
	hybrid (switch $\Delta y = 0.2$)	84.45	89.45	94.8	10.35	15%	90%

Table 6.6   Comparison of RTMD control methods for the medium suite.

		$\frac{\hat{x}}{\beta}$	$\hat{x}$	$\hat{x} \times \beta$	band width	bandwidth % TMD	$\hat{x}$ % TMD
y_1 max	TMD (passive)	79.5	99	122.5	43	100%	100%
	reset when $\Delta \dot{y}_1 = 0$	88.7	98.4	109.2	20.5	48%	99%
	reset when $\dot{y}_1 = 0$	88.5	93.7	99.15	10.65	25%	95%
	hybrid (switch $\Delta y = 0.2$)	91.8	94.8	97.9	6.1	14%	96%
y_1 mean	TMD (passive)	77.75	108	145.9	68.15	100%	100%
	reset when $\Delta \dot{y}_1 = 0$	74.9	86.9	101.3	26.4	39%	80%
	reset when $\dot{y}_1 = 0$	79.8	85.1	90.9	11.1	16%	79%
	hybrid (switch $\Delta y = 0.2$)	83.6	97.2	90.95	7.35	11%	90%

Table 6.7   Comparison of RTMD control methods for the high suite.

		$\frac{\hat{x}}{\beta}$	$\hat{x}$	$\hat{x} \times \beta$	band width	bandwidth % TMD	$\hat{x}$ % TMD
y_1 max	TMD (passive)	83	102	124	41	100%	100%
	reset when $\Delta \dot{y}_1 = 0$	90.9	104.4	111	20.1	49%	102%
	reset when $\dot{y}_1 = 0$	91.5	94.7	97.9	6.4	16%	93%
	hybrid (switch $\Delta y = 0.2$)	93.25	96	98.8	5.55	14%	94%
y_1 mean	TMD (passive)	84	120	173	89	100%	100%
	reset when $\Delta \dot{y}_1 = 0$	77.1	90.9	107.7	30.6	34%	76%
	reset when $\dot{y}_1 = 0$	79.8	84.9	90.5	10.7	12%	71%
	hybrid (switch $\Delta y = 0.2$)	84.5	88.3	92.2	7.7	9%	74%
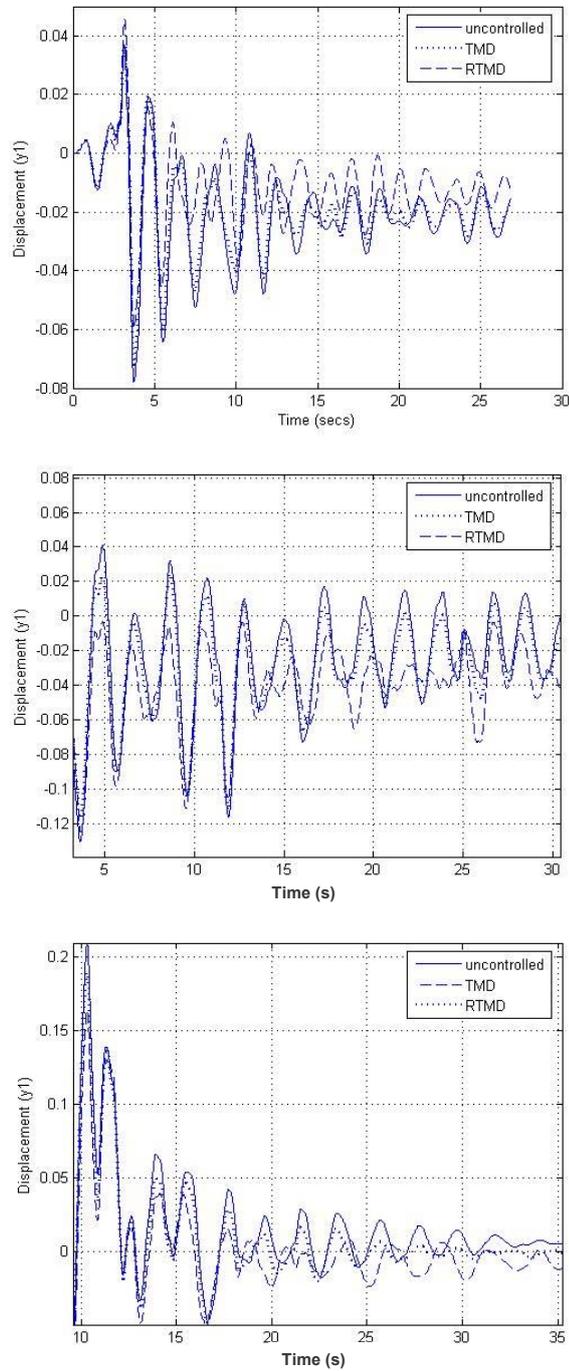
Figure 6.12   Non-linear structure displacement response to a ground motion record from the low, medium and high suites for the uncontrolled, TMD and RTMD configurations.
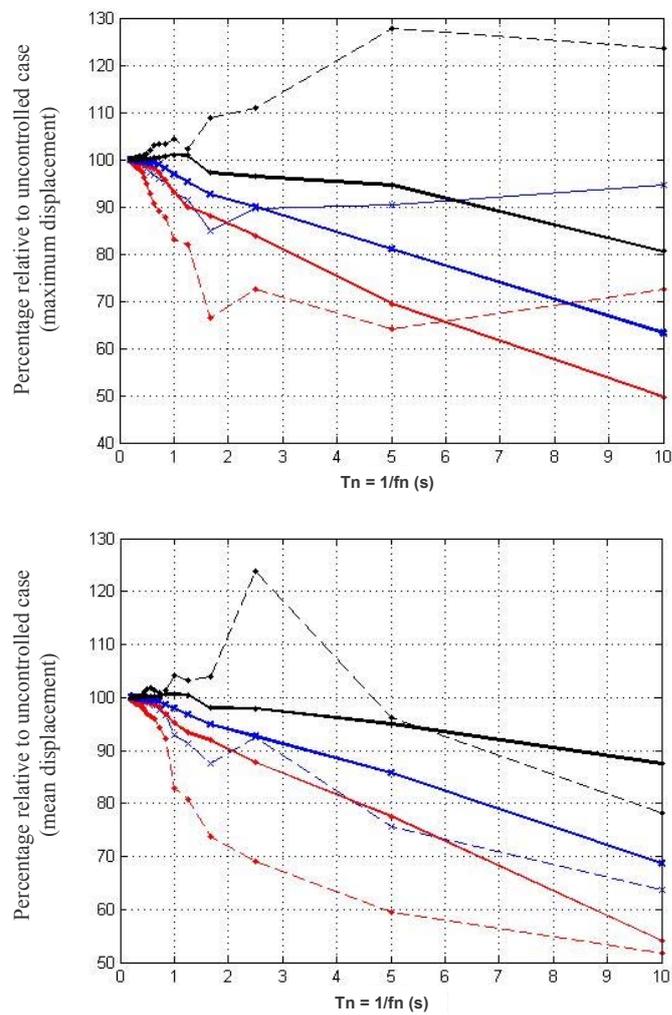
Figure 6.13   Non-linear reduction factors of structure displacement response to low suite for the TMD and RTMD configurations normalised to the uncontrolled case, segregated mass is 20% of structure mass.
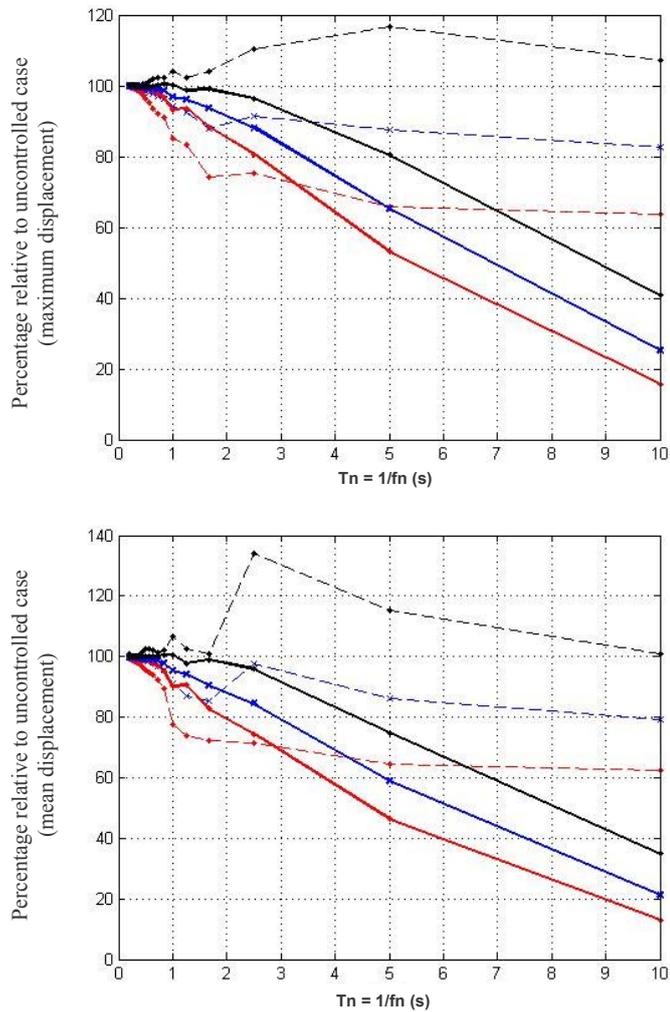
Figure 6.14   Non-linear reduction factors of structure displacement response to low suite for the TMD and RTMD configurations normalised to the uncontrolled case, segregated mass is 30% of structure mass.

Chapter 7

Hybrid Test System and Applications

7.1   Introduction

The step from analytical modelling to full-scale testing is a large one within structural control and structural engineering research. Full-scale tests provide accurate results, but are time consuming and expensive. In contrast, analytical studies enable rapid design development, but do not necessarily capture all of the effects and dynamics that can occur. There is also no replacement for full or large-scale validation testing no matter the level of analytical studies undertaken. Therefore, an intermediary step is required that bridges this gap and provides a stepping stone between analytical studies and expansive full-scale testing. Such a stepping stone would significantly ameliorate the risk in full-scale testing due to its significant cost and time requirements.

The overall test procedure when developing new structural control methods would thus have a pyramid shape. A large number of analytical tests forms the base of the pyramid and provides significant confidence in the fundamental methods developed. The peak of the pyramid is the full structural experimental tests conducted to validate the extensive analytical modelling. The middle section is an intermediate point that extends the extensive analytical testing into the real world, while still maintaining the rapid turnaround and adaptability associated with analytical testing and modelling. It thus builds further confidence towards investing in full-scale testing, reducing the associated risks of these tests.

This chapter outlines the process for this intermediary step. The process used is not limited in application to semi-active resetable device testing. The same

process can be used to test any sub-structure within a structural system, be it a control device or a new structural connection method. The process devised is termed the Hybrid testing procedure, and is an extension of pseudo-dynamic testing (Takanashi et al. [1975]). Mechatronics researchers refer to this intermediary step as Hardware-in-the-loop (HILT) systems (Chase et al. [2007]).

Hybrid or real-time pseudo-dynamic tests couple virtual structures under dynamic loading with physical sub-structures or devices in a dynamic test rig. The use of sensors and actuators in a closed-loop feedback system maintains the dynamic equilibrium of the overall system, comprising of the physical test article and virtual modelled structure.

Hybrid testing thus alleviates much of the time and cost associated with full-scale testing. It also enables tests that would be infeasible or very difficult as complete full-scale structural tests. However, these advantages come with a significant cost in complexity, and hybrid test systems are difficult and expensive to develop. Until now this complexity and the lack of real-time system expertise in the broader structural engineering community has restricted its wider utilisation in structural engineering research.

This chapter presents a simple, low-cost, robust hybrid test system, and outlines solutions to the major issues faced in developing any hybrid system. A single degree of freedom structure with a resetable device added is utilised to develop and illustrate this hybrid test system. Chapter 8 presents a rocking wall system to demonstrate the efficacy of the hybrid test system in rapidly conducting a number of tests (Mulligan et al. [2006b]).

7.2   Hybrid Test System

The purpose of the hybrid testing procedure is to test elements or sub-structures as if they were physically in place in a real structure without having to create the actual full-scale structural system. A test procedure for new sub-structures or elements that allows them to be rapidly tested in a variety of structural applications is a useful and adaptable tool for the structural engineering researcher. It is particularly useful for testing new methods of design, construction or finishing, as well as for investigating novel devices or systems. More rapid testing turnaround

for full-scale testing with fewer resources required ensures more systematic testing
and thus greater certainty in the final full-scale experimental application, reducing the associated risk of a poor or unexpected result. To achieve this goal the
requirements are two-fold:

1. A detailed, potentially non-linear, model that captures the essential dynamics of the main structure at the proper level of detail so that a real-time numerical integration can be performed.

2. A real-time system capable of melding this model with the test system actuators and sensors in a seamless fashion.

To achieve these requirements, a Hybrid Testing Procedure (HTP) has been
developed that allows rapid implementation of a hybrid experimental set up
(Chase et al. [2007]). This approach utilises the dSpace$^{\circledR}$ real-time feedback control system to create this system, both rapidly and without error. This system is
flexible and widely used for rapidly prototyping control and instrumentation in
a number of industries.

In the case presented here, it is necessary to use a real time testing procedure
as the control of the physical semi-active control device being tested is determined
by the dynamic, real-time response of the main structure. Hence, it is essential
that the test be carried out in real-time, because the resetable device will have
to perform in real-time when in place. Therefore, the system must be able to
operate both the device and virtual structure, as well as all the interacting sensors
and actuators, at a rate much higher than the structural response to avoid issues
with equilibrium stability (Mulligan et al. [2006a]).

The NEES project (Takahashi and Fenves [2005], Pan et al. [2006]) offers a
similar type of testing, with the additional feature of being connected over the
web. Thus, the different aspects of the setup can be located over different geographic locations. However, this feature adds complexity and the project focuses
on the geographic distribution of the test sub-structures. It also significantly
slows the system to 0.1 to 0.5s cycles, which is too slow for real-time hybrid
testing and thus only useful for quasi-static cases. The NEES system therefore
allows greater potential collaboration but at a cost of excluding real-time highly
dynamic systems and devices from consideration.

In contrast, the process described here was developed with the focus on the dynamic, real-time implementation of a number of applications that would benefit structural research. This research presents a novel process based on commercially readily available real-time systems products that use the well known Matlab® and Simulink® programs. This reliance on well accepted modelling tools and a commercially validated system ensures that the overall approach is repeatable and minimises errors. The goal is to present a system that could be readily recreated in any lab without any unnecessary effort, while also offering the ability to collect all the data required with minimal programming or development effort.

The overall approach of the hybrid test system is centered on the dSpace real-time control system development tool. System and process programming is easily accessible through the Simulink block diagram framework, which offers extensive functionality and flexibility. This approach therefore enables rapid implementation of varying test systems and experimental situations. Hence, it enables faster research turnaround and thus potentially greater insight can be obtained.

The major issues in developing a hybrid system are minimal signal processing lag, optimised sensing resolution and bandwidth, and efficient model computation. All three issues affect the ability of the system to maintain dynamic equilibrium of the overall virtual-physical system in real-time, and thus provide an accurate and stable test. Hence, the sensors must be optimised across resolution, noise and range, while the computational methods must compromise between model realism and minimal complexity. The final system presented here can readily accommodate non-linear-multi-degree-of-freedom models and a 1kHz operating bandwidth.

7.2.1   HTP Test Method Development

The process is based upon and similar to the pseudo-dynamic testing methods (Takanashi et al. [1975], Bayer et al. [2002]). More specifically, the structural model which has known dynamics is computationally modelled, while the subsystem or device is physically built. The two systems are coupled through a dynamic test rig or actuators that provide the input displacement or force commands dictated by the main modelled structural response to earthquake or other

input motion. In addition, response coupling is provided via sensors that measure and return the sub-system response to the main structural model input. This virtual-real interface is managed by the dSpace real-time control system development tool, which is also utilised as the data gathering and storage system.

For the applications examined in this research the motion input commands from the model to the sub-structure result in feedback forces. Sensors on the test structure measure the displacements and response forces. The motions are measured to ensure the command was received by the system and to guarantee precision in an inner feedback loop if required. The response forces become inputs from the physical structure into the main structural system model calculation in the next time step.

The entire process, along with data collection for off-line analysis, is executed in real-time. The process in this research is run at 1.0kHz, thus each time step is 0.1 ms. This rate ensures equilibrium is satisfied for the overall structural system without iteration within a time step due to the very small dynamic structural changes that occur over that time frame.

The details of the real time step-wise calculation process are illustrated in Figures 7.1 and 7.2. Figure 7.1 is a flow chart of the overall HTP process developed. Figure 7.2 shows the prototype semi-active device in the dynamic test rig with an illustration of the process.

The HTP process steps in detail are defined:

- **First time step**. External inputs to the main structure, such as forces due to a ground motion, are determined for the current time step. These external inputs must be known for the duration of the test.
  All other time steps. All inputs to the physical system are determined, including external inputs and returned responses from the sub-structure being examined. Response of the modelled structural system to these external inputs is calculated and the conditions at the interface of the sub-structure and device being examined are determined. Conversion factors due to scaling or changes in the type of motion, such as rotational to linear motion, are applied at this point.

- Input commands to the physical system, resulting from the previous model calculation stage, are sent to the test rig.

- The test rig implements these command inputs on the physical test device.

- The physical sub-structure or device response is measured, both forces and displacements. Forces are returned to the model for the next time step, displacements are returned to check tracking accuracy.

- The response from the sub-structure is returned to the computation system where the conversion factors, if any, are again applied. Accuracy and equilibrium are checked to ensure system stability and behaviour.

These steps are repeated in order for the duration of the hybrid test.
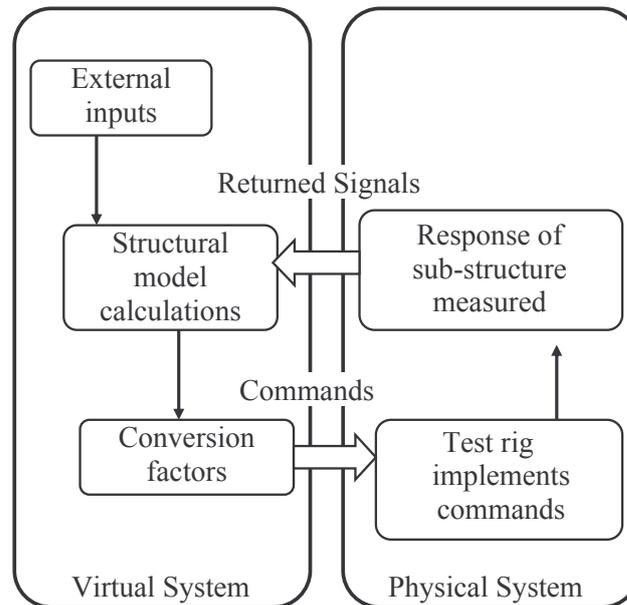
Figure 7.1   Flow chart of Hybrid Testing Procedure detailing the links in the step-wise procedure.

The virtual system response is computed using the absolute Newmark-β with constant average acceleration numerical integration scheme. This integration scheme is utilised as it can guarantee stability (Clough and Penzien [1993], Humar [2002]). The calculation time step is chosen to achieve accurate structural response calculations, while ensuring the hybrid system is capable of completing
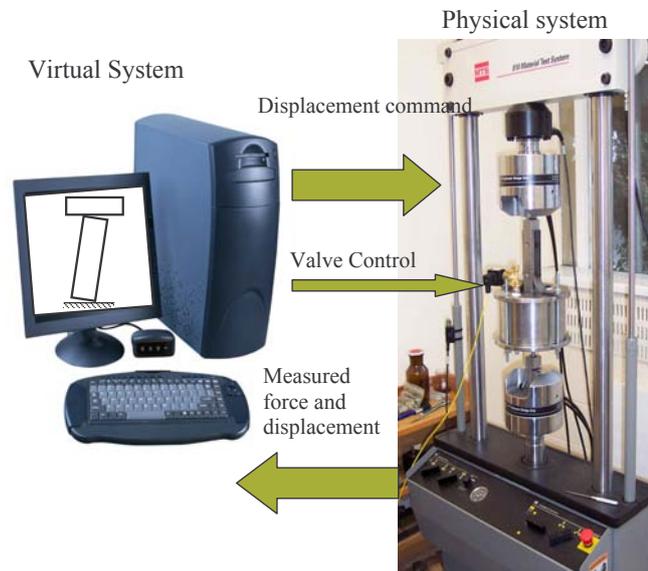
Figure 7.2   Photograph of a prototype device in the test rig and illustration of the virtual system.

each task within the time step. In particular, running this system at a rate at least ten times higher than the maximum structural system frequencies of interest can minimise the need to determine changes in equilibrium status in the midst of these steps. More specifically, if the rate is very high relative to the modelled test structure then equilibrium can be ensured with a reasonable tolerance without the need for iteration within a time step.

The dSpace system used is capable of running at least 10 input and 10 output channels at 1-10 kHz. This rate is far faster than any structural system or semi-active device requirements. Hence, no inner iterations are required to determine the necessary forces and displacements during each individual step, as is the case with many quasi-static test procedures.

7.3   Advantages and Limitations

The advantages and limitations of the hybrid testing procedure are illustrated utilising a single-degree-of-freedom (SDOF) structure as the test basis. Figure 7.3 shows a schematic of the (SDOF) structure with a resetable device between the structural mass and the ground. The SDOF structure is the virtual part

of the system, modelled in this case, using standard, linear equations of motion. However, non-linear equations could be used. The resetable device is the physical part of the system and is coupled to the virtual structure by a dynamic test rig and a series of sensors and command inputs.
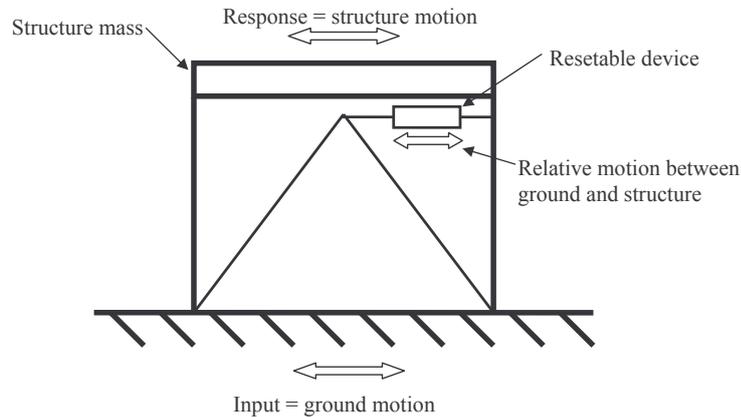
Figure 7.3   Schematic of the single degree of freedom structure with an attached resetable device. The relative motion between the structure mass and the ground is equal to the piston displacement of the resetable device.

A simple structural system was used to enable rapid analysis of the test results and to more readily illustrate the overall HTP developed. Therefore, the focus is on the test method development, rather than the particular response of a specific complex structural system. Thus, procedural problems and issues can be easily identified and solved. In addition, sinusoidal input ground motions were used for simplicity because it is easily recognisable during testing, giving direct feedback to the developer/operator that the command section of the process loop is operating correctly. Overall, this simple example is used in this chapter to easily illustrate the process and issues in developing this HTP.

7.3.1   Advantages

The benefits of using the Hybrid Testing Procedure include:

1. Real time dynamic analysis using the critical experiment hardware and sensors.

2. Easily set up experiments, and the ability to quickly change system parameters during experimentation.

3. Transportable. The system and approach can be widely applied and generalised to a variety of test systems and situations.

4. A wide variety of possible applications can be hybrid tested. The HTP is not restricted to semi-active devices.

5. It is a middle step between simulation and full- or large-scale experiments.

In addition, many applications can potentially be analysed and tested far more readily as a sub-system, or as a series of disconnected subsystems, than as full- or near full-scale experiments, and at a much lower total cost. These advantages stem from using the dSpace rapid prototyping system, which is contained within an easily transportable unit utilising well accepted programs and systems.

7.3.1.1   Real Time

Central to the whole process is the dSpace real-time control system. Due to the computational power of the dSpace system, fairly complex structural models can be used with no delays for data processing. Hence, the experiments can be run in real time. This real time analysis can be preferable to pseudo-dynamic testing as inertial effects do not have to be additionally incorporated into the virtual analysis, and a layer of significant approximation is thus removed. As a result, the tests also run much faster, allowing more time for further tests as required.

In addition, the dSpace system does not allow continuation in the calculation process if the preceding time step analysis has not been completed. This rigid real-time behaviour ensures the simulation follows in the correct order with inputs to the system corresponding to the correct point in time of the analysis. It is a significant condition that is markedly not enforced by the more commonly used LabView$^{\circledR}$ based systems (Welham [2004]).

7.3.1.2   Easy Set Up

Once again the easy set up is due to the real-time control system used. The virtual model is set up in simulink's block diagram framework, which allows easy access

to sections of the model. It also allows rapid implementation of any changes required during testing using the dSpace command desk. The dSpace system is also used for data gathering and storage. Hence, there is no need for a separate system for this purpose. In addition, connection to a variety of different sensors and measuring devices is straightforward, as any conversions and calibration can be incorporated into the virtual experiment layout and adjusted in real time from the command desk. Finally, the reliance on the well known, well accepted and well tested Matlab and Simulink products provides a well documented and reliable software implementation pathway for any test designer and thus readily modified by even a moderately experienced user.

7.3.1.3   Easily Transportable

The computation, virtual-real interface and the data recording and storage systems are all contained within the dSpace unit. Thus, the whole system and approach is easily transportable to different test locations or environments. In this case, a wheeled unit is used to take dSpace to any specific lab area required. Similarly, dSpace based experiments can be saved and electronically transferred to other users for their application, and will require little or no modification to local requirements or conditions.

7.3.1.4   Variety of Applications

Due to the flexibility of the procedure a variety of structural systems can be implemented. The implementation of any structural system is dependent only on the ability to model the main, virtual, structural system sufficiently to capture the necessary structural dynamics and on an external testing machine or actuators that can supply the necessary commands, dictated by the response analysis of the virtual structure to the sub-structure. The applications tested to date are a single-degree-of-freedom system with a device attached between the structure mass and the ground, and a rocking wall panel where the device acts as a 'smart' tendon to control the rocking dynamics of the wall.

7.3.1.5 Middle Step

This middle step between analytical and full-scale testing using the HTP increases the confidence that primary hardware and in this case sensor systems will work in full-scale tests. Reduction in time and financial investment while improving confidence before full-scale tests results in a better use of equipment and funding. The HTP ensures that the tests chosen to take to full-scale testing provide good validation and insightful results of the technique, device or structural system being investigated.

7.3.2 Limitations

The problems associated with development of this, or any, HTP can include:

1. Signal processing lag

2. Optimising sensing resolution

3. Bandwidth, and efficient model computation

All three of these issues relate to the lag created in sensing and computation. These lags affect the ability to create a stable and real-time hybrid system without computationally expensive inner iterations in each time step. The last of these issues is largely a trade-off between model complexity and the desired realism or accuracy, versus fast computation that requires a minimum of computational power and bandwidth.

7.3.2.1 Signal Processing Lag

Signal processing lag is the time difference between completion of the computation and sending a command signal for a particular time step and when the signals from the external physical system are received. These two signals are both required before the subsequent time step calculation can commence. Figure 7.4 shows this delay between the command and returned displacement signals for the

SDOF structure case with a value of ∼0.07s. In addition, Figure 7.5 illustrates the sequential steps included in this total delay.
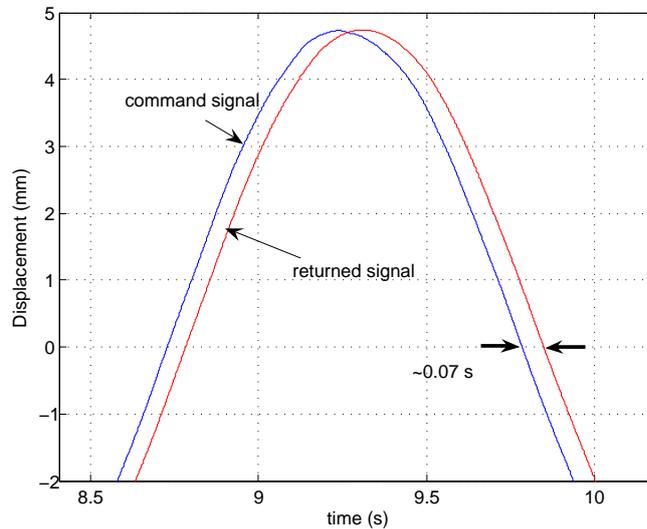
Figure 7.4   Plot of command displacement and returned displacement signal. The delay in this case is approximately 0.07s.
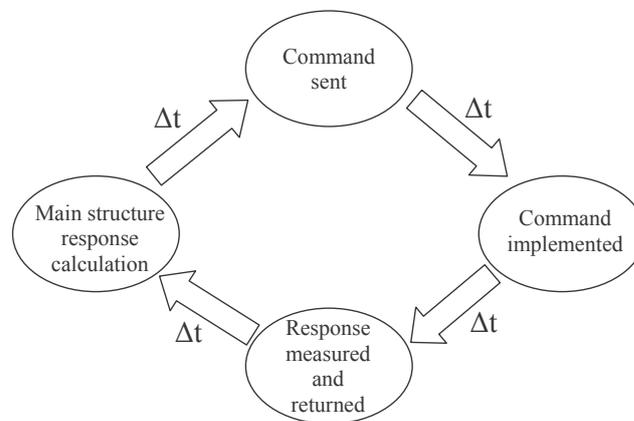
Figure 7.5   Illustration of total delay between a command signal sent to the test rig, implemented, response measured by the sensors, and the response returned to the virtual system for calculation in the next time step.

If the command and returned signals are not synchronized, the overall system may become unstable, particularly if the full hybrid system is run at a relatively slower rate (Franklin et al. [2002]). Commencing a time step, the start values are read by the computational system. If these start values are a mixture of command and returned signals corresponding to different points in the analysis, a change of state may have occurred that is not yet registered.

An example of this change of state leading to instability can occur with the simple single-degree-of-freedom structure with a single displacement based structure control device attached between the ground and the structural mass. If the virtual structure is calculated to have changed direction and the external signal from the physical device lags behind this change, it will appear to the virtual system that the device, instead of resisting the structural motion, is pushing the structure. Hence, it will add energy to the overall virtual structural system and result in rapid growth in the peak structural displacement.

This simple and spurious condition can be removed by using only returned sensor signals in an internal feedback loop instead of a combination of computed and measured signals. However, no computation can proceed in this approach until all sensor signals are returned, which can potentially increase the overall lag. Overall, this approach ensures the main virtual structure and physical substructure conditions are consistent at the start of each time step calculation minimising any lag relative to the periods of interest.

7.3.2.2 Optimising Sensor Resolution and Band-width

The clarity of the feedback signals can have a significant effect on the stability and quality of the analysis. If the returned signals have excess noise associated with them it is very difficult to determine the actual sensor signal. In addition, if the returned signals are filtered to provide clearer data, the lag between the calculated response and the corresponding returned values increases and the possibility of instability, as discussed previously, increases.

Figure 7.6 shows a zero measurement signal from the LVDT of the MTS dynamic test rig utilised and the FFT of the data. The frequency peaks in the FFT add odd multiples of 50Hz and are typical of interference from mains power on unshielded cables. The noise floor level was unacceptable because the filtering required to obtain a smooth signal introduced a large time lag over 0.1 seconds, which is too close to the structural periods of interest.

The LVDT signal from the dynamic test rig also had a tendency to drift up to values of 1 to 2mm, even when no actual displacement was occurring. External linear potentiometers were therefore used as an alternative to the internal

LVDT signal resulting in a lower noise floor and stable measurements. The noise level reduction was achieved because the cables for the linear potentiometers are shielded, whereas the dynamic test rig is not. These potentiometers have the additional advantage of allowing manual calibration and zeroing, something that was not as readily possible with the internal displacement measurement. Figure 7.7 shows a comparative potentiometer zero measurement and the FFT. Note the absence of frequency peaks indicating mains power interference. In addition, the approximately 50% lower rms noise level allowed a much shorter and subsequently lower lag filter to be used.

An external load cell was also utilised to measure the force developed in the resetable device. This external load cell has a range of ±20kN as opposed to the internal load cell range of ±50kN. Thus, the external load cell has a better resolution for the expected 1 to 10kN device response. This resolution example is important in ensuring accurate forces are returned to the virtual structure without significant error, thus ensuring a more accurate and realistic hybrid test.
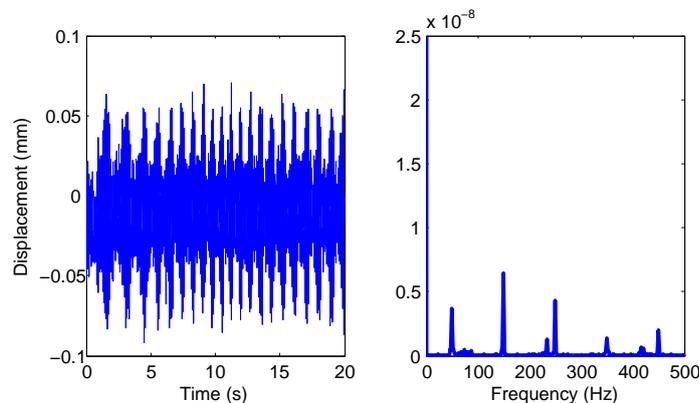
Figure 7.6   Internal LVDT displacement signal and the FFT showing peaks associated with mains power interference.

7.3.2.3   Efficient Model Computation

The efficacy of the model is a trade off between rapid calculation and enough detail to accurately represent the dynamic response of the structure being modelled. The computational power of the dSpace system utilised has not, to date, been challenged. Its current computational capacity includes the use of up to two 850MHz PowerPC chips with optical networking between I/O devices and these chips.
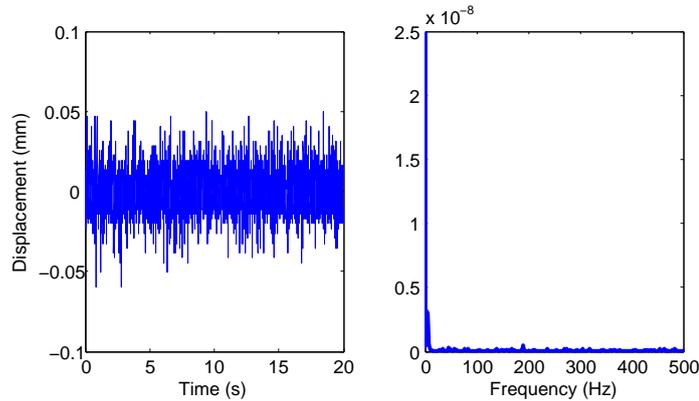
Figure 7.7 External linear potentiometer signal and the FFT showing lower noise level and absence of peaks associated with mains power interference.

If large complex models were required to accurately represent the virtual structure, the structure calculations and data gathering and storage systems could be separated onto two dSpace systems, thus allowing maximum computational power to calculate the response of the structure. Overall, this issue can also be ameliorated by ensuring an efficient model at the resolution desired and that enough computational resources are made available.

7.4 Summary

The hybrid test method developed utilising well known programs and systems provides the ability to easily and rapidly conduct hybrid tests at relatively low cost. The procedure centered around the dSpace control system configuration results in a transparent system that can be readily adapted prior to and during testing. Applications are variable and not limited to structural control method development presented in this research. The only necessary components are an efficient model of the virtual system, a physical sub-system to test, and a dynamic coupling test system. Chapter 8 illustrates the application of the the hybrid testing procedure developed to an experimental semi-active device used in a virtual non-linear rocking wall control problem.

Chapter 8

Semi-Active Rocking Wall Panels - Hybrid and Simulation Analysis

8.1   Introduction

Rocking motion during seismic events results in structural systems withstanding larger motion than would otherwise be expected (Housner [1963]). Rocking wall systems utilise this type of response and are an effective method of dissipating seismic response energy and mitigating structural damage. Resetable devices have the potential to dissipate energy, customize hysteretic behavior and reduce damage. Hence, the combination of a semi-active resetable device with a rocking wall could significantly further improve the overall energy management of these systems and the overall structure during seismic events.

A scaled semi-active rocking wall system, designed for a large open structure, is analysed using the hybrid testing procedure. The resetable devices are controlled with the 1-3 control law. Thus, the devices supply supplementary resistance only for the upward rocking motion of the wall, providing semi-active energy dissipation over half of each cycle. The system then relies on radiation damping on impact with the ground for the other half. The hybrid analysis is supported by an analytical study over suites of ground motions and device stiffnesses to create basic design guidelines for semi-active rocking walls.

8.2   Hybrid Experimental Set-up

The rocking wall system analysed using the hybrid testing procedure is a scaled version of a wall designed for a large, open structure (Abdul Hamid [2006]). The basic dimensions are 0.45m x 5.0m with a mass of 2802kg. Each rocking wall supports a portion of a lumped roof mass, as shown in Figure 8.1. The resetable device can be located within hollow sections of the wall for efficient packaging and aesthetics.

The addition of a resetable device to this rocking wall is an improvement or alteration to an already existing form of damping system using yielding tendons to reduce large rocking motion. These yielding tendons are designed to provide additional energy dissipation on large rocking cycles. Resetable devices, on the other hand, are able to provide additional energy dissipation on *each* cycle rather than just the few large cycles as with the yielding tendons. Thus resetable devices have the potential to improve and control the overall performance of the rocking system.

The rocking wall system response is examined for free vibration and the odd half of the medium suite of ground motions from the SAC project (Sommerville et al. [1997]). This 10 ground motion suite is used because it contains a range of near and far field ground motions of size sufficient to cause significant rocking. Thus, this choice represents a compromise over the range of magnitudes and ground motion types possible.
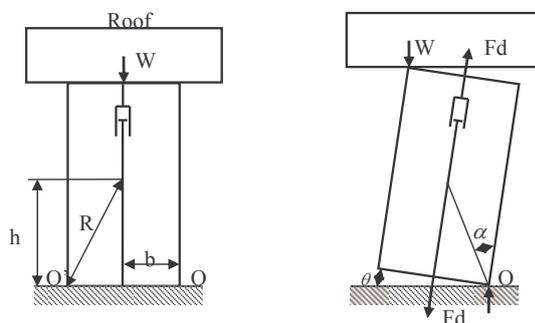
Figure 8.1   Rocking wall schematic showing roof mass and location of resetable device. Note: this analysis uses one resetable device in the center for simplicity, however other configurations are conceivable, for example a device on either end/side of the rocking panel.

The resetable device provides an added resistive restoring force on the upward rocking motion of the wall. When the wall reaches its peak rotation for any

cycle, the stored energy is released, and the wall then rocks downward purely under self weight. On impact with the ground 15% of the wall's rocking energy is assumed to be absorbed, based on velocity (Housner [1963]). Hence, allowing free return without added resistance enables maximum energy dissipation from radiation damping on impact combined with the enhanced semi-active dissipation on upward motion. If the remaining energy is sufficient the wall rocks up in the opposite direction when the resetable device once again provides a restoring force.

The linearised equation of motion of the wall rotating about rocking point O or O' in Figure 8.1 is defined:

$$I\ddot{\theta} - MgH\theta \mp MgB + F_{act}b = F(t)h \qquad (8.1)$$

where I is the mass moment of inertia, $\ddot{\theta}$ is the rotational acceleration about the rotation point, M is the total mass of the system, g is acceleration due to gravity, H is the height to the effective centre of mass, θ is the rotation about O or O', B is the width of the wall, F_{act} is the semi-active force, and $F(t)$ is the applied force due to ground motion.

The analysis is carried out using the real-time high-speed hybrid testing procedure developed in Chapter 7 of this thesis. The rocking wall is the virtual system represented by a computational model. The resetable device used is the first prototype and represents the physical sub-structure in a dynamic test rig, as seen in Figure 7.2. The specific steps for this hybrid testing application are detailed for this specific application:

1. Wall model calculations determine the rotation of the wall depending on the ground motion and other forces.

2. Rotation of the wall is converted into the linear displacement the resetable device would experience when contained within the wall.

3. Displacement command signal is sent to the dynamic test rig.

4. Valve command is determined based on the current relative device displacement and control law defined.

5. The dynamic test rig supplies the displacement to the physical resetable device.

6. Measured response force developed in the device is returned to the virtual system to be used in the subsequent time-step calculation.

The process is repeated step-wise for the complete ground motion record. A time step of 0.001s (1kHz servo-rate) was chosen for the entire process. The error in each time step is small enough that no equilibrium iteration is required for any time step. This overall approach enables a rapid and simple test procedure, as detailed in Chapter 7.

8.2.1   Free Rocking Motion

The virtual rocking wall panel was given an initial 0.2m/s rotational velocity to induce rocking motion. Figure 8.2 shows the uncontrolled rocking response induced without the resetable device, and the controlled rocking motion using the prototype device. The resistive forces provided by the resetable device on the upward rocking motion significantly reduce the rocking amplitude and response attenuation time. The controlled peak rocking amplitude is decreased by ∼20% for the initial peak and between 30 and 50% for the subsequent cycles, compared to the uncontrolled case. The maximum peak rotation for the uncontrolled case is ∼2.6 degrees which is reduced to ∼2.0 degrees with the resetable device. These rotations translate to ∼20mm and ∼15mm maximum corner lift of the wall, respectively, which represents a significant reduction in response.

8.2.2   Forced Rocking Motion

This hybrid study examines the rocking motion response to the suite of earthquake ground motions. Figure 8.3 presents the Imperial Valley earthquake record from the medium suite, the uncontrolled and controlled rocking motion response, and the resulting semi-active resetable device control forces. Note that the wall does not rock until some time after the ground motion has begun. More specifically, the ground acceleration ($\ddot{X}_g$) is required to be greater than the wall slenderness ratio ($\frac{B}{H}$) multiplied by gravity, or $\ddot{X}_g > \frac{B}{H}g$, for rocking to occur (Housner
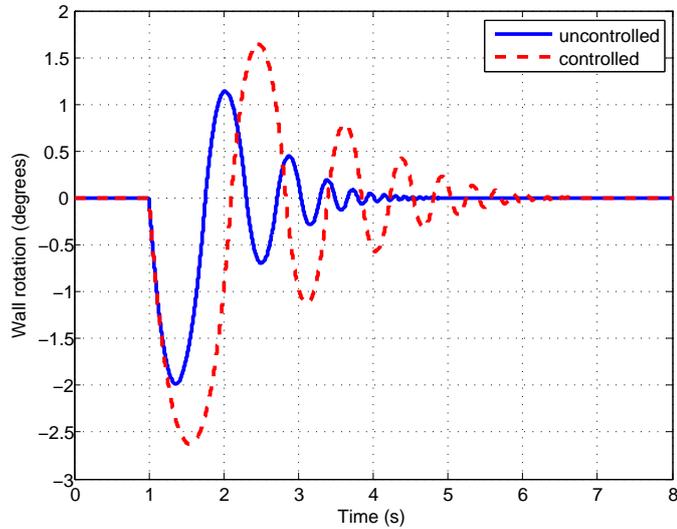
Figure 8.2   Free vibration of the rocking panel comparing the uncontrolled (without a resetable device) and controlled rocking motion. The wall is given an initial rotational velocity of 0.2rad/s at 1.0s.

[1963]). For the wall examined here a ground motion acceleration of 0.88m/s^2 is required for rocking to commence. However, once the wall is in motion the ground acceleration can be lower than this value and the wall will continue to rock provided there is sufficient rotational velocity after impact with the ground.

Figure 8.3 illustrates the efficacy of the resetable device at reducing forced rocking motion, with significant reductions quite evident. These reductions indicate that significant energy has been dissipated via the semi-active device, as desired. However, this is only one result using a particular ground motion. Therefore, results for the suite of ground motions are presented in Table 8.1. The results are presented as reduction factors compared to the uncontrolled case. The maximum peak reduction factor (R.F_{max}), and average absolute rotation reduction factor (R.F_{av}) represent the reduction in the maximum peak rotation and overall reduction in rotation for the duration of the record, respectively.

In some cases the maximum peak reduction is close to 1.0 indicating the maximum rotation is not reduced. However, in most of these cases the overall rocking motion is reduced, indicated by a value less than 1.0 for R.F_{av}. Reduction in overall rocking motion is beneficial to the wall system, as damage to the wall panel is reduced by reducing the velocity of ground impact, as well as reducing the number of rocking cycles. In addition, a reduced R.F_{av} indicates that significantly

more energy is dissipated compared to the uncontrolled case, even though overall the system rocks less. Thus, this difference in energy was dissipated via the semi-active device.
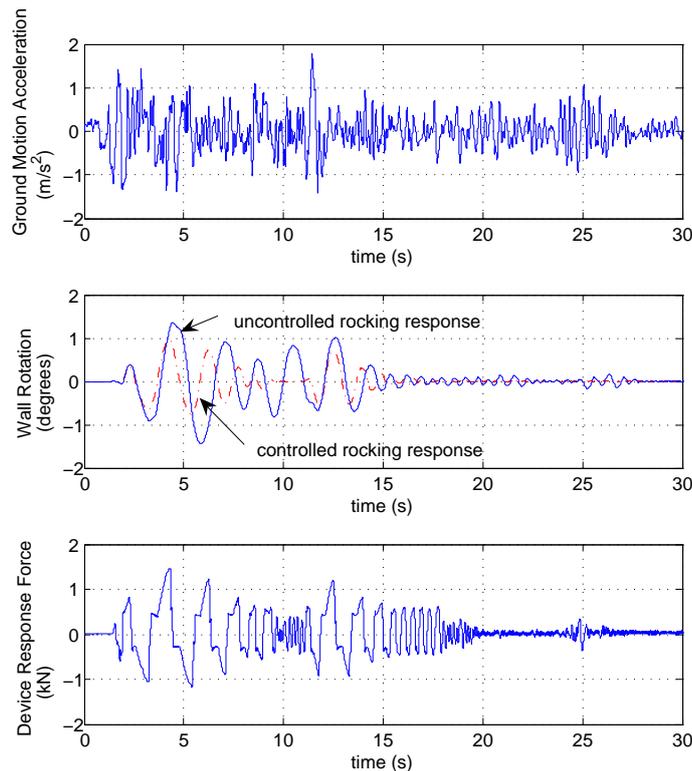
Figure 8.3   Rocking wall response to the Imperial Valley ground motion. The uncontrolled and controlled rocking response is shown as well as the additional resistive (control) forces provided by the resetable device.

In contrast, Table 8.1 indicates that the rocking response motion to the Imperial Valley (1979), array 5 ground motion increased for both the peak rotation and average rotation, indicated by a reduction factors greater than 1.0. Figure 8.4 shows the uncontrolled and controlled rocking responses in this case. The resetable device did not significantly limit the rocking response and between eight and nine seconds the controlled response is greater than the uncontrolled response.

This apparent contradiction is due to the ground motion itself, which between approximately five and nine seconds, shows a bias of acceleration in the positive

direction. The resetable device response forces during this time are insufficient to overcome the highly forced motion of the ground, literally moving away from underneath the wall for a considerable length of time. Hence, the addition of the semi-active device has non-linearly modified the rocking period and response such that the ground is moving away from the structure, increasing rotation in this case. This behaviour is an example of how semi-active systems may give different responses for different ground motions, necessitating the use of suites of ground motions to obtain a valid overall performance assessment.

Table 8.1   Rocking wall panel response to the odd half of the medium suite. Results are presented as maximum peak reduction factor (R.F$_{max}$), and average rotation reduction factor (R.F$_{av}$).

Earthquake record	R.F$_{max}$	R.F$_{av}$
Imperial Valley (1979)	0.67	0.48
Imperial Valley (1979), array 5	1.1	1.3
Imperial Valley (1979), array 6	0.83	0.77
Landers (1992)a	1.0	0.77
Landers (1992)b	1.0	0.67
Loma Prieta (1989), Gilroy	1.0	0.83
Northridge (1994)a	1.83	0.77
Northridge (1994)b	1.0	1.0
Northridge (1994), Sylmar	1.0	1.0
North Palm Springs (1986)	1.0	0.63

In addition, the absolute rocking motion is small (<1 degree) in comparison to other cases. The result is small relative device motion and therefore small device forces. Thus, the resetable device is only providing forces primarily from friction effects for a large percentage of the earthquake record and little effect would therefore be expected for this case. Note that while reduction factors are good for assessing relative performance, they do not account for such absolute differences.

8.2.2.1   Change in Rocking Period

Figure 8.5 illustrates the effect of changes in the rocking response period between the uncontrolled and controlled rocking wall systems. In this illustration the rocking response between 20 and 21s shows the difference between the uncontrolled

and controlled responses, with the controlled response having a shorter period of rocking motion. When the large pulse occurs the uncontrolled wall is moving towards the center position whereas the controlled wall is moving *away* from the center position. Hence, the large pulse effectively results in the ground moving to more rapidly return the uncontrolled wall to the center position. However, the same pulse results in the ground moving away from underneath the wall for the controlled case, thus increasing the rocking response for this and the subsequent cycles.
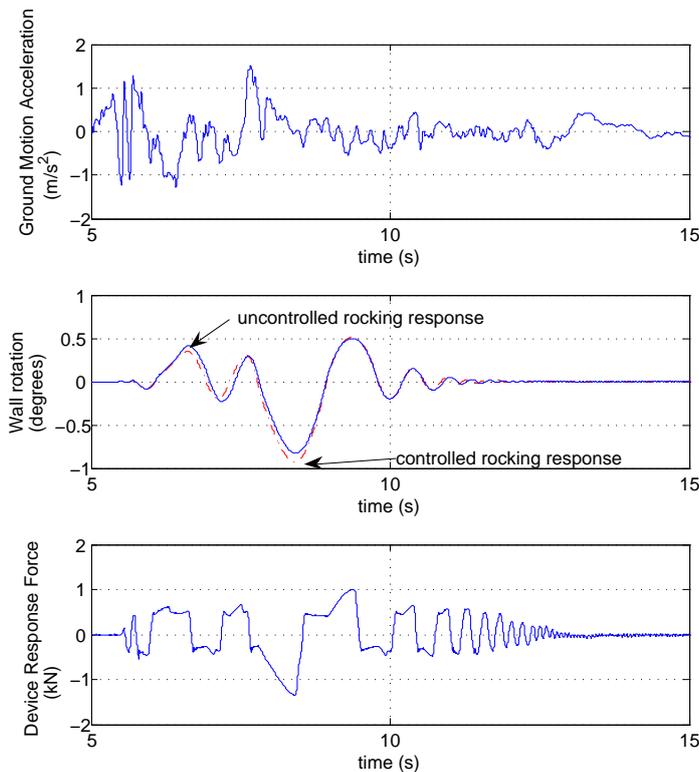
Figure 8.4   Rocking wall response to the Imperial Valley, array 5 ground motion. The uncontrolled and controlled rocking response is shown as well as the additional resistive (control) forces provided by the resetable device.

Typically, the addition of a supplemental damping system to a rocking wall panel system changes the rocking period. The overall rocking response of these rocking systems is therefore a function of the aspect ratio, the type of additional supplemental damping system and the interaction between the rocking period

and the ground motion input. This interaction between the rocking period and the ground motion input can result in enhanced or detrimental rocking response. This point further illustrates the need to examine the response of structural systems to a variety of input ground motion types and present the results for a number of response metrics, both to avoid bias in the results presented.
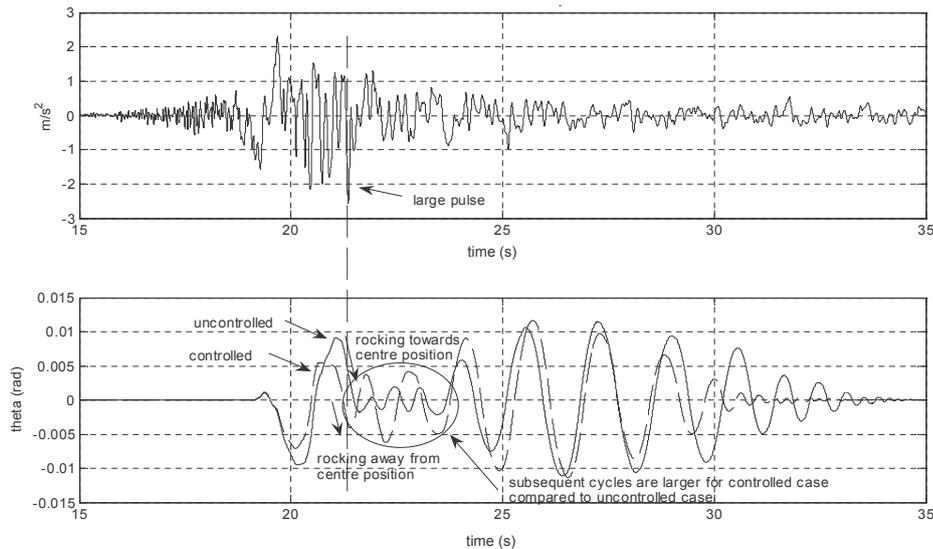
Figure 8.5 Rocking wall response to the Loma Prieta, Gilroy ground motion. The change in rocking period between the uncontrolled and controlled responses are clearly shown. When the large ground motion pulse occurs the uncontrolled wall is moving towards the center position, whereas the controlled wall is moving away from the center position. Hence, the large pulse results in increased motion for the controlled response on the subsequent cycles which does not occur in the uncontrolled response.

8.3 Large Scale Rocking Wall

The hybrid testing experimental results from the previous section indicate resetable devices can improve the energy dissipation of a rocking wall panel for a variety of ground motions. However, the resetable device was unable to provide forces large enough to produce significant reductions (R.F $\leq$ 0.48) due to the low nominal device stiffness value compared to the full-scale structural system demands. Therefore, the response of a larger rocking panel with semi-active devices is examined analytically given the hybrid proof-of-concept. This approach also allows design considerations to be analysed by parametrically examining three device stiffnesses (1000, 5000, and 10000kN/m). Note that with a fixed

semi-active resetable device prototype such a parametric study could not occur without unrealistic scaling of the rocking panel.

The larger rocking panel has dimensions of 1.2x8 m^2. It has an effective seismic mass of 19.93T at a height of 8m (Abdul Hamid [2006]). This larger rocking panel is studied for analytical design of semi-active rocking walls as its dimensions are more realistic for structures currently using these systems. Such structures would typically include storage and commercial warehouses requiring large, unobstructed open spaces.

The response of this larger scale wall is examined analytically utilising a validated non-linear model of the resetable device in the rocking wall system. Figure 8.6 shows a hybrid test result and modelled result comparison for the smaller rocking wall. The model accurately captures the controlled wall rocking response. The initial peak error and resulting lag are due to the physical device response being less than the modelled device response for this first motion cycle. More specifically, during a hybrid test the initial measured force response value is set to zero. In contrast the device model incorporates the friction value response from the beginning of the motion. Hence, the modelled response has a slightly greater resistive force than the hybrid case for the first half motion cycle.
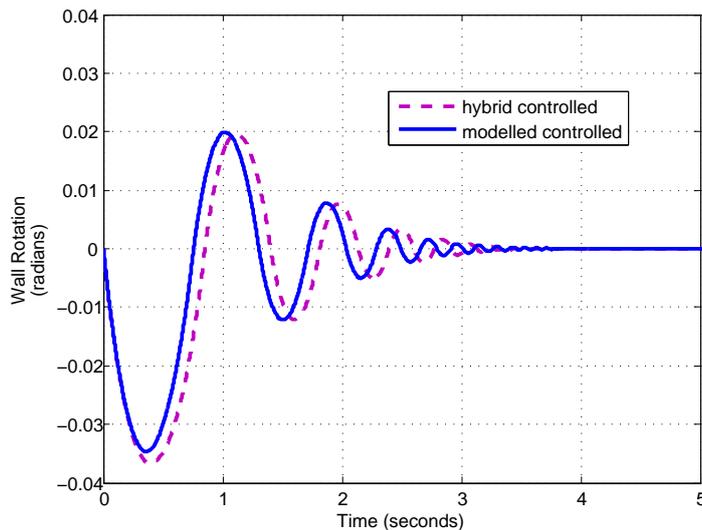
Figure 8.6   Comparison of the hybrid testing procedure and modelled results for a rocking wall panel under free vibration. The model accurately captures the rocking response dynamics.

First, free vibration response of the rocking system with various initial conditions was examined. This response is examined to confirm the model and analysis

procedures, as the expected qualitative results are known from previous hybrid test results from the small scale wall in Sections 8.2.1 and 8.2.2. The stiffness values for the semi-active device are chosen empirically to give a range of times for the wall to cease rocking. The stiffness values used are 1000kN/m, 5000kN/m and 10000kN/m, which for a typical rotation of 0.02 rad represent maximum device forces of 12kN, 60kN and 120kN respectively. These force levels are achievable with appropriate device design as discussed in Chapters 2, 4, and 10.

Second, response of this larger wall system is examined for the odd half of the medium suite of ground motions. This suite-based analysis approach offers the opportunity to classify the system response to a wider variety of ground motions. In addition, statistical analysis of the response over the suite of ground motions incorporates the results of these studies into metrics that are currently used in performance-based design methods. Finally, use of this specific suite also allows qualitative comparison to the hybrid results for additional insight and validation.

All results are normalized to the uncontrolled case and are presented as peak reduction factors, R.F, equivalent viscous damping, ξ, and area enclosed, A, in the shear capacity, Cc vs θ curve for the largest peak motion. The enclosed area, A, is illustrated in Figure 8.7 and is dependent on the slope which is a function of device stiffness. Hence, the device stiffness is the major determining factor of this metric along with the resulting maximum peak rotation. The device stiffness slope in Figure 8.7 is normalized to the uncontrolled case, which has a slope of -1. Hence, the area is defined:

$$
\begin{aligned}
A &= \frac{\theta_{max}}{S} - \frac{\theta_{max}}{2S}|-\theta_{max} - \theta_{max}S| \quad \text{if} \quad S < 1 \\
A &= \frac{1}{2}(\theta_{max}^2 + \theta_{max}^2 S) \qquad \text{if} \quad S \geq 1
\end{aligned}
\tag{8.2}
$$

where A is the area enclosed, θ_{max} is the maximum angle obtained by the rocking panel, and S is the absolute normalised slope.

Note that the area actually represents a complex tradeoff of device stiffness and resulting response. A stiff device will have a larger area for a fixed rotation. However, stiffer devices also limit the peak rotation, reducing the area for a given stiffness. The optimal device for this metric will thus be stiff enough to dissipate
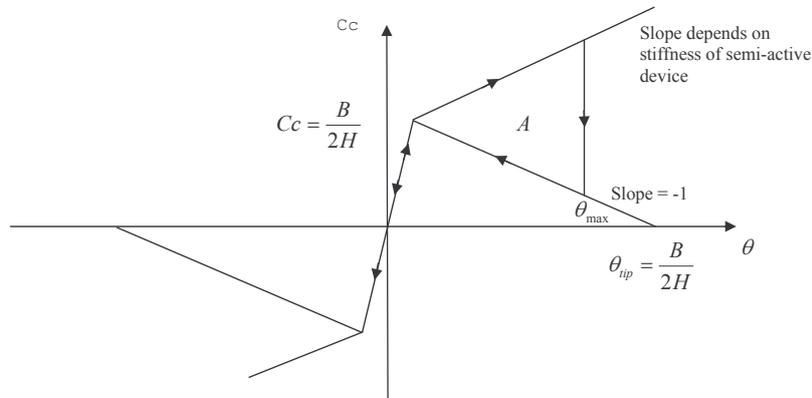
Figure 8.7   Cc vs θ curve to illustrate calculation of metric enclosed area, A.

more energy, while being flexible enough to allow the reasonable rocking motion to occur that results in device motion and energy dissipation.

8.3.1   Free Vibration Response

The peak rotation responses of the rocking system with the three semi-active devices are normalized to the uncontrolled response for free vibration tests. The wall was given an initial rotation of 1 to 5 degrees and released, as shown for the five degree case in Figure 8.8. The normalized peak values (R.F.) show decreased peak responses for all three devices and all initial angles, as summarized in Table 8.2. These reductions represent mean effective additional damping of 6.3%, 10.2%, 14.1% for the 1000kN/m, 5000kN/m and 10000kN/m devices respectively. In this case, the stiffer devices do better because the initial rotation is fixed. Hence, the stiffer devices provide larger resistive forces on each upward rocking motion.

The reduction factors for the free vibration response are all less than 1.0. The reduction factor reduces for larger initial rotations because the relative displacement across the resetable device is larger. Thus, the device provides larger reaction forces in each cycle. In addition, the reduction factors decrease for higher stiffness devices. A higher stiffness device provides a greater response force for a given relative displacement, therefore providing larger resistive forces to the rocking wall panel and greatly reducing the rocking amplitude for each cycle.
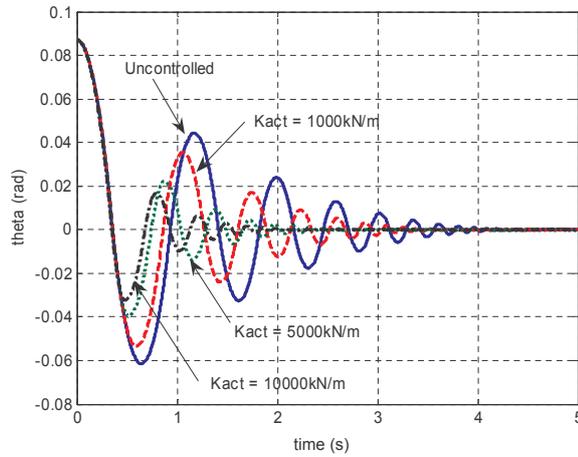
Figure 8.8   Free vibration response of large rocking wall panel with an initial rotation of five degrees (0.087 radians).

Table 8.2   Large rocking wall panel free vibration response to different initial angles of rotation. Results are presented as reduction factors (R.F) and equivalent viscous damping (ξ).

Initial angle	Kact = 1000kN/m		Kact = 5000kN/m		Kact = 10000kN/m	
(degrees)	R.F	ξ	R.F	ξ	R.F	ξ
1	1.0	5.0	1.0	5.2	1.0	5.5
2	0.90	5.8	0.77	9.3	0.67	13.0
3	0.90	6.6	0.71	11.5	0.63	16.7
4	0.90	7.0	0.67	13.2	0.56	20.0
5	0.83	7.2	0.63	14.8	0.53	23.1
Geometric mean	0.90	6.3	0.77	10.2	0.67	14.1
Mult.var.	0.90	1.1	0.83	1.4	0.77	1.7

8.3.2   Forced Vibration

The response of the rocking system to the suite of 10 earthquakes shows the ability of the semi-active resetable devices to reduce rocking amplitude and dissipate energy for real input motions. Reduction factors less than 1.0 indicate beneficial reductions in the peak rocking angle, helping avoid excessive rocking or tipping. More importantly, lower peak (and generally average) rotations reduce the shear and other structural forces on the rocking wall system. These reductions also provide additional response dissipation to the wall and the overall structure, which is made up of a number of wall panels, only some of which might be semi-active.

For the 1000kN/m device, seven of the 10 records show reduction factors equal to or greater than 1.0. However, three of these results are very near to 1.0 and effectively unchanged, as shown in Table 8.3. The exception is the reduction factor for the Northridge (1994) Sylmar record, which has a reduction factor of 1.43.

This result for Northridge (1994) indicates that the addition of the actuator significantly increased the maximum rocking angle. However, this reduction factor does not indicate that the addition of the damper was detrimental to the system, as the reduction factor is based on the maximum peak angle. In fact, reductions in subsequent rocking angles were still reduced. In addition, the area enclosed in the Cc vs curve is 2.1x10-5 in this case, which is close to the geometric mean for the entire suite of 2.54x10-5, and the effective added viscous damping, while low, is positive, indicating additional damping in the system over the whole record when compared to the uncontrolled case. More likely, the peak increased in this case due to an unfortunate interaction of the semi-active rocking period, with the actual ground motion that results in an enhanced peak value, as discussed in Section 8.2.2.1.

Table 8.3   Large rocking wall panel forced vibration response with a resetable device stiffness of 1000kN/m. Results are presented as reduction factors (R.F), equivalent viscous damping (ξ) and area enclosed on a Cc vs. θ plot.

Earthquake record	R.F	ξ	Area x10-5
Imperial Valley (1979)	0.91	6.2	3.8
Imperial Valley (1979), array 5	1.0	5.1	1.8
Imperial Valley (1979), array 6	0.91	6.7	2.5
Landers (1992)a	1.0	4.7	2.4
Landers (1992)b	1.0	4.9	5.7
Loma Prieta (1989), Gilroy	0.90	5.8	7.0
Northridge (1994)a	1.0	4.9	1.7
Northridge (1994)b	1.0	5.2	2.1
Northridge (1994), Sylmar	1.43	1.6	2.1
North Palm Springs (1986)	1.0	5.2	0.9

Results for the 5000 kN/m device in Table 8.4 show six of the 10 R.F. values are greater than 1.0 and the geometric mean is greater than the same value for the 1000 kN/m device, as shown in figure 8.6. Once again the Northridge (1994) Sylmar record resulted in the greatest reduction factor. The equivalent viscous

Table 8.4   Large rocking wall panel forced vibration response with a resetable device stiffness of 5000kN/m. Results are presented as reduction factors (R.F), equivalent viscous damping (ξ) and area enclosed on a Cc vs. θ plot.

Earthquake record	R.F	ξ	Area x10-5
Imperial Valley (1979)	0.77	9.3	9.6
Imperial Valley (1979), array 5	1.0	4.9	4.8
Imperial Valley (1979), array 6	0.5	31.3	2.3
Landers (1992)a	1.0	4.9	0.8
Landers (1992)b	1.0	4.9	19.5
Loma Prieta (1989), Gilroy	0.77	10.6	15.0
Northridge (1994)a	1.0	4.8	6.0
Northridge (1994)b	0.91	6.0	6.5
Northridge (1994), Sylmar	1.67	0.5	9.9
North Palm Springs (1986)	1.0	5.5	2.9

Table 8.5   Large rocking wall panel forced vibration response with a resetable device stiffness of 10000kN/m. Results are presented as reduction factors (R.F), equivalent viscous damping (ξ) and area enclosed on a Cc vs. θ plot.

Earthquake record	R.F	ξ	Area x10-5
Imperial Valley (1979)	0.67	12.9	7.3
Imperial Valley (1979), array 5	0.91	6.2	4.1
Imperial Valley (1979), array 6	0.3	106.2	0.7
Landers (1992)a	1.0	5.5	0.7
Landers (1992)b	1.0	5.5	18.0
Loma Prieta (1989), Gilroy	0.53	24.3	7.2
Northridge (1994)a	1.0	5.0	5.8
Northridge (1994)b	0.91	6.9	5.8
Northridge (1994), Sylmar	0.25	2.7	5.3
North Palm Springs (1986)	0.91	6.1	2.7

damping values are generally greater for the 5000kN/m stiffness case. The areas enclosed for the peak cycle are greater than for the lower, 1000kN/m stiffness case. These results illustrate the tradeoff between reducing rocking to limit damage by using a stiffer device, while still allowing some rocking, which is the a substantial energy dissipation mechanism of these semi-active rocking systems.

Finally, the results for the 10000kN/m device in Table 8.5 show reduction

factors all less than 1.0 except for the Northridge (1994) Sylmar record, which indicates that this record is particularly demanding for this specific wall geometry and mass. Again, all the equivalent viscous damping values and areas were improved versus the uncontrolled case. Overall, it is clear that it is important to consider a suite of seismic motions, rather than a single input when evaluating the design effectiveness of this type of semi-active system. This conclusion is further illustrated in the variation seen in the values reported in Tables 8.3 to 8.5.

The additional damping, ξ, provided by the three semi-active devices are all around or above the 2-5% damping provided naturally by the wall in the uncontrolled case via energy absorption on impact with the foundations. Table 8.6 summarizes the resulting damping values obtained from the analyses presented. As expected, the 10,000 kN/m device provides the greatest additional geometric mean damping of 7.1% due to the larger energy stored and dissipated by this highest stiffness device. These results indicate that the semi-active devices are providing the dominant form of energy dissipation, rather than impact, because the trend of the results would not otherwise so clearly follow the device stiffness values.

The area enclosed by the normalised Cc vs ξ curve is also an indication of the energy absorbed by the semi-active device. The area is a trade off between the additional stiffness provided and the peak rotation that results in the presence of that added stiffness. If the additional stiffness provided is relatively low the absolute slope on the Cc vs curve is less than 1.0, and the resulting area enclosed is small. Conversely, if the stiffness of the device is relatively high, as for the

Table 8.6 Summary of the rocking response of the large scale wall with three different resetable device stiffnesses.

Metric	K=1000 kN/m	K = 5000 kN/m	K= 10000kN/m
R.F geometric mean	1.0	0.91	0.83
R.F multiplicative variance	0.91	0.77	0.71
ξ geometric mean	5.1	5.5	7.1
ξ multiplicative variance	1.2	2.1	2.3
A geometric mean	2.5	5.6	3.9
A multiplicative variance	1.8	2.6	2.8

10000kN/m device, the peak rotation values are greatly reduced and consequently, the area enclosed is reduced. As might thus be expected, the 5000kN/m device has the greatest enclosed area for the suite of ground motions, thus providing the best tradeoff between high stiffness and reduced amplitudes of the three values examined.

The standard lognormal multiplicative deviation values for the reduction factors, R.F., effective additional damping and area enclosed are also shown in Table 8.6. The 10000kN/m device standard deviations are larger than those for the other two devices. This result is due to the ability of the large stiffness device to noticeably change the period of the rocking structure, as discussed previously and illustrated again in Figure 8.9. Hence, the peak rotation of the rocking system occurs at a distinctly different time than in the uncontrolled case.

When the peak value occurs, the current direction of ground motion may either cause the wall to return quickly to its upright position or make it rock to a greater extent than the uncontrolled case. This significant change in system period therefore can lead to a much more variable result, particularly for the 10000kN/m stiffness device.

In this case then, the interaction of semi-active wall period and ground motions is most clearly illustrated in the standard deviation or variability in results seen across the suite. More specifically, in some ground motions this interaction is helpful and in others it degrades performance. Stiffer devices enforce greater changes in response that may result in greater variabilities. Finally, similar results would be expected for rocking systems with similar aspect ratios but different overall sizes and comparable device stiffness values.

The results reported show the efficacy of resetable devices at providing additional damping to the rocking wall system. The advantage of using a resetable device, instead of a yielding tendon (Ajrab et al. [2004]), is that the semi-active device works for each cycle, whereas tendon yielding provides additional damping on only 1-2 large motion cycles. The result is significantly increased damping being added to the system because the resetable devices are able to reduce response energy for every cycle.
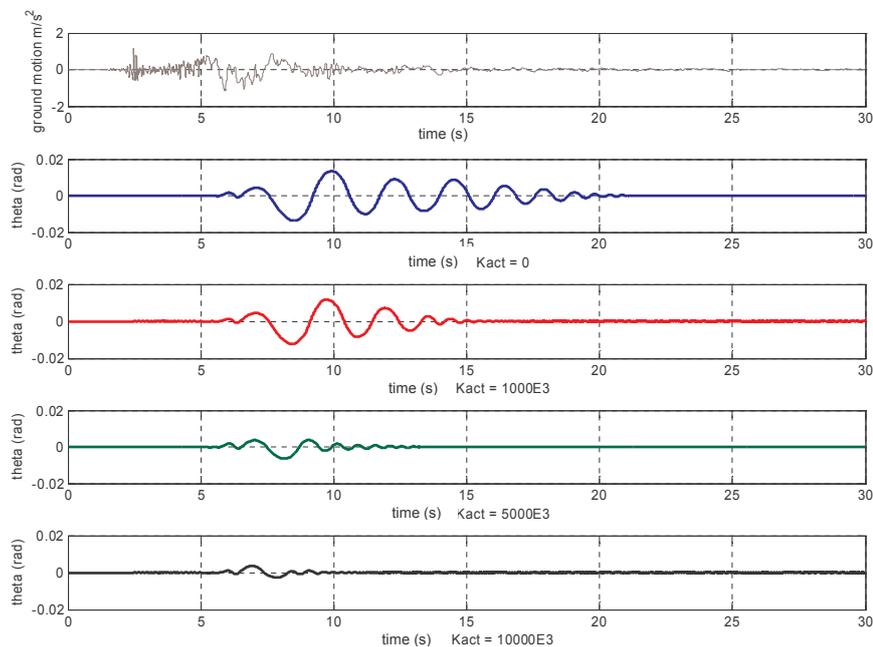
Figure 8.9   Large scale rocking wall panel response to the Imperial Valley (1979), array 6 ground motion. Note: as the device stiffness increases from 1000kN/m to 10000kN/m the rocking motion period is noticeably altered compared to the uncontrolled (K=0kN/m) case.

8.4   Summary

Semi-active resetable devices can be used to significantly enhance the energy dissipation of rocking wall systems while also reducing the peak rotations. The free vibration responses of the rocking system with the semi-active devices added clearly shows the efficacy of the combination of a rocking wall and semi-active device in dissipating energy from the entire structural system. Similarly, analysis using a suite of ground motions indicates the added energy dissipation is available for realistic large seismic events. In particular, the variation in results seen over this suite also indicates that, for a given rocking wall, the results are very dependent on the specific ground motion, indicating that suites of events must be used to better identify the overall efficacy of the entire semi-active system. More specifically, for the case analysed, a medium value 5000kN/m device provided the best design compromise as seen in the resulting reductions in the peak angle of rotation and a large area enclosed on the Cc vs curve. Finally, the use of suites of ground motions with appropriate lognormal statistics (Hunt [2002], Limpert et al. [2001], Barroso et al. [2003b]) provides a framework for encapsulating reduction

factors and performance directly into currently used performance based design methods. Overall, the methods presented in this chapter, both hybrid and analytical, are readily generalisable to a variety of similar rocking wall systems and provide a framework for approaching the general semi-active structural control design problem (Rodgers et al. [2007b]).

Chapter 9

One-fifth Scale Semi-Active Structural Control: Experimental Validation

9.1 Introduction

This chapter examines the performance of a $\frac{1}{5}^{th}$ scale semi-active moment resisting steel frame building using a resetable device structural control system. Two equivalent semi-active resetable devices are located on the structure, which has total dimensions of 2.1 x 1.2 x 2.1m^3 (Kao [1998]). A total of 27 earthquake records, with a range of intensity measures, are used as input ground motions to the structure in shake table tests. The results are presented relative to the uncontrolled and failsafe modes.

9.2 Method

The $\frac{1}{5}^{th}$ scale steel moment resisting frame structure has three floors and a roof level. The elevation is comprised of two bays, one long and one short. The structure was designed to have the same natural frequency of a full scale building, of approx 0.6s, rather than a natural frequency defined by laws of similitude (Kao [1998]). To achieve the same natural frequency, a larger amount of added mass on each floor level is required. Structural connections are designed with yielding fuses to accurately represent this full-scale structural behaviour. Figure 9.1 shows a schematic of the structure indication the devices and instrumentation, and Figure 9.2 shows a photograph of the structure with the resetable devices attached. Additionally, Figure 9.3 shows a close up of one of the resetable devices.
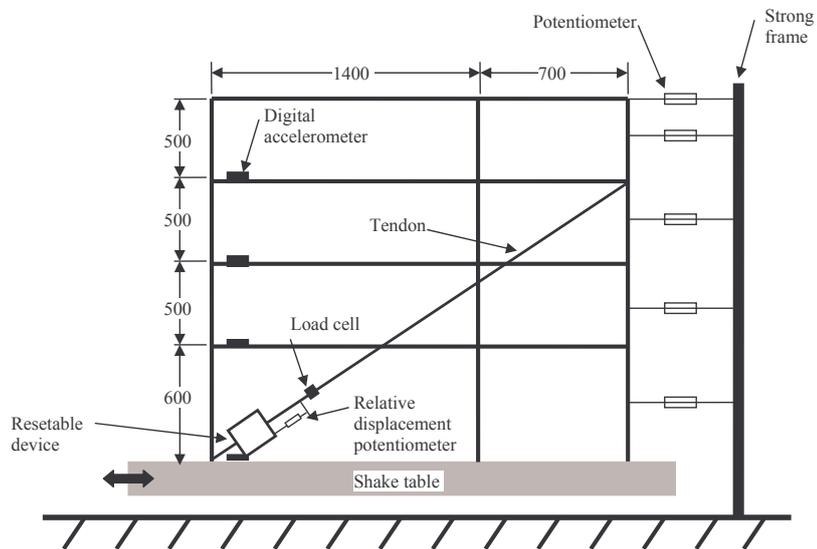
Figure 9.1   Schematic of the test structure indicating the instrumentation configuration. All dimensions are in millimeters.

Figure 9.2   Photograph of the test structure on the shake table with a resetable device attached to each side of the structure via rigid tendons.

Figure 9.3   Closeup of a resetable device installed on the test structure.

9.2.1   Instrumentation

Two resetable devices are installed on the structure, one on each long side, as shown in Figures 9.1 and 9.2. The devices are attached from the ground to the third floor via a rigid tendon. Thus, the device and tendon span the entire length of the long side of the structure. This control architecture was chosen after extensive non-linear finite element simulation in Ruamoko (Anaya et al. [2007]). The relative displacement across each device is measured by a potentiometer and a load cell measures the force reacted by each device.

A digital accelerometer was placed on each floor of the structure. These accelerometers record data at 2kHz. In addition a digital accelerometer is attached to the shake table. Five linear potentiometers up the height of the structure, sampled at 1kHz, measure the absolute horizontal displacement of the mid point of each storey and the roof. The shaking table absolute displacement is measured with a linear potentiometer sampled at 1kHz. Each floor displacement is found by linearly interpolating the displacement measured by the potentiometer above and below the corresponding floor level. These derived displacements were verified to be accurate representations of the floor displacements by comparison with the double integration of the digital accelerometer data for each floor, and results of other studies (Kao [1998]).

The high sampling rates were used to ensure all noise could be filtered without aliasing. The 2kHz accelerometer sampling rate was used to ensure all mains power noise sources up to 700Hz could be filtered (Chase et al. [2004b]). The

potentiometers are unaffected by mains power and were thus sampled at a more standard 1kHz.

The relative displacement data across the device used as the control law input was filtered in real time using the same method as described in Chapter 4. All recorded data was bandpass filtered in the 0.2 to 15.0Hz range after collection. The filter was designed in Matlab$^{\circledR}$ to have 0dB gain in the pass region and -80dB in the stop regions. A post processing zero-phase forward and reverse filtering method was used to avoid introducing any phase lag in the data.

9.2.2   Control Laws

Both the 1-4 and 2-4 control laws were tested and the specific law was applied to both devices in a given test to create the semi-active resetable device damping system. In addition, the structural system was tested with all the device valves open to give friction damping results. Finally, the fail-safe mode, where all valves are closed to give air spring results was also tested. The fail-safe mode is so termed because it is the state that occurs if power is lost to the damping system with this particular device design. The fail-safe mode is chosen to be all valves closed rather than all valves open because reasonable supplemental reaction forces are provided with the valves closed. More specifically, the response forces resulting from valves closed are large enough to resist the structural motion, whereas the valves open case is analogous to a very low stiffness tendon, where response forces consist of static friction and viscous air damping (Section 4.4.2.2).

The uncontrolled structure response with the entire tendon arrangement re-moved was obtained for comparison. These results are limited to a selected fewer ground motions where structural yielding was not expected to occur based on preliminary finite element analysis (Anaya et al. [2007]). Therefore, the valves open case is used as a surrogate uncontrolled case for comparison of all results even though the tendon arrangement provides some additional stiffness to the system.

9.2.3 Ground Motion Inputs

Four earthquake records at various intensity levels were used during the experiments, for a total of 27 input ground motions. These records are detailed in Table 9.1. The input motions were selected such that the minimum and maximum percentages for each different record utilised had similar peak ground accelerations and intensity measures. In between, either 5%, 10% or 20% increments of peak ground acceleration were used for each record. The intensity measure is the spectral displacement of a structure with a fundamental frequency of 2.5Hz. Note that the recorded peak ground acceleration (PGA) for the Sylmar 5% record is significantly greater than the 10 and 15% values for the same record. This large value is due to a very short pulse that was not present in the original record and hence is most likely due to a spurious motion of the shake table. An approximated value derived from the original input acceleration record is shown in brackets. PGA values are presented as recorded values as opposed to original acceleration record values because these recorded values best represent what the test structure experienced during testing.

Some minor modification was used to ensure the records could be accurately tracked by the shake table. Specifically, the limiting factor for accurately tracking the displacement input motion is the maximum table velocity, before servo-valve saturation occurs, of 0.24m/s. Therefore, the earthquake records are modified such that the velocity does not exceed this saturation level, while retaining as much of the acceleration record as possible. The modification method is similar to that detailed in Chase et al. [2004b]. This modification should thus ensure no unexpected acceleration spikes occur while also ensuring optimal (<0.1mm) tracking of the table reference input.

9.2.4 Performance Metrics

The response metrics of interest are the 3rd floor maximum acceleration, the 3rd floor maximum relative displacement and the maximum total base shear. These metrics indicate the damage done to the occupants and non-structural elements of the structure, the structure itself, and the foundations of the structure, respectively. A reduction in one of these metrics can result in an increase in

Table 9.1 Ground motion records used for shake table analysis of a $\frac{1}{5}^{th}$ scale structure with a resetable device damping system. El Centro, Kobe, Taft and Sylmar records were used with different percentages of each record. The magnitude of each record is determined by the percentage of the original record, the peak ground acceleration (PGA) recorded during the test, and the spectral displacement (SD) intensity measure for a single-degree-of-freedom structure with a natural frequency of 2.5Hz.

	% of record	PGA (recorded)	SD (2.5Hz)
El Centro	10	0.8451	0.0024
	20	1.06	0.0048
	30	1.29	0.0073
	40	1.45	0.0097
	50	1.68	0.0121
	60	2.14	0.0145
	70	2.64	0.0170
	80	2.96	0.0194
	90	3.04	0.0218
	100	3.51	0.0242
Kobe	5	0.88	0.0045
	10	1.15	0.0090
	15	1.51	0.0135
	20	1.82	0.0180
	25	2.17	0.0225
	30	2.54	0.0269
	35	2.85	0.0314
Taft	20	1.50	0.0028
	40	2.74	0.0056
	60	3.77	0.0083
	80	5.01	0.0111
Sylmar	5	1.35(0.44)	0.0040
	10	0.95	0.0081
	15	1.22	0.0121
	20	1.44	0.0162
	25	1.88	0.0202
	30	2.26	0.0242

another metric in some cases (Rodgers et al. [2007b]). For example, the added non-linear stiffness contribution by resetable devices often reduces displacements of all types, but at a cost of increased accelerations (Hunt [2002], Barroso et al. [2003b]). However, using customised control methods, such as those in this thesis, reductions in all metrics, or large reductions coupled with only small increases, can be achieved, as discussed in Chapter 3.

Results were then normalised by the intensity measure of the earthquake record allowing comparison across the different earthquake records used in the analysis. In addition, this normalisation allows comparison to previous spectral examinations of the semi-active devices. These results are reported as cumulative distribution functions as they are then more readily incorporated into a standard hazard analysis and performance based design (Barroso et al. [2003a], Rodgers et al. [2007b]).

9.3 Results and Discussion

The response metrics for each input motion are plotted vs the intensity measure of the record in Figure 9.4, along with the linear (displacement) or non-linear (base shear) least squares fit. Some plots do not show all 27 records as the structure was expected to yield at the higher intensity measures using some control types. Hence, these specific cases were not tested as part of the overall experimental protocol.

The structural response for all the control laws and the uncontrolled case are readily compared in Figures 9.5 and 9.6, which present the base shear and maximum 3rd floor displacement least squares fit for the data in Figure 9.4. The base shear capacity of the structure was designed to be 3kN. A pushover analysis by Kao [1998] using Ruamoko resulted in a base shear capacity of 6kN. This apparent discrepancy was caused by over-strength actions of the yielding fuses (Kao [1998]).The base shear of the structure including the resetable devices and tendons is approximated as 16kN from Figure 9.5. This value is far higher than prior analysis values and the discrepancy is most likely due to the altered structure, slightly different fuse designs in the test structure and increased strength of these fuses.

Figure 9.5 shows that the 2-4 control law provides the largest buffer between the demand and capacity base shear for a given intensity measure as expected by design of this control law. The 1-4 case has the smallest buffer with the fail-safe having similar results. The valves open case is approximately between the 2-4 and fail safe result.

Reduction in the base shear demand for a given intensity measure means the structural system can withstand larger ground motions without damage to the foundation and the base of the columns. This result is significant for buildings where large foundations are expensive or prohibited by site conditions. It is equally or more significant for retrofit of existing structures, where reducing the demand is preferable over expensive and potentially difficult foundation strengthening.
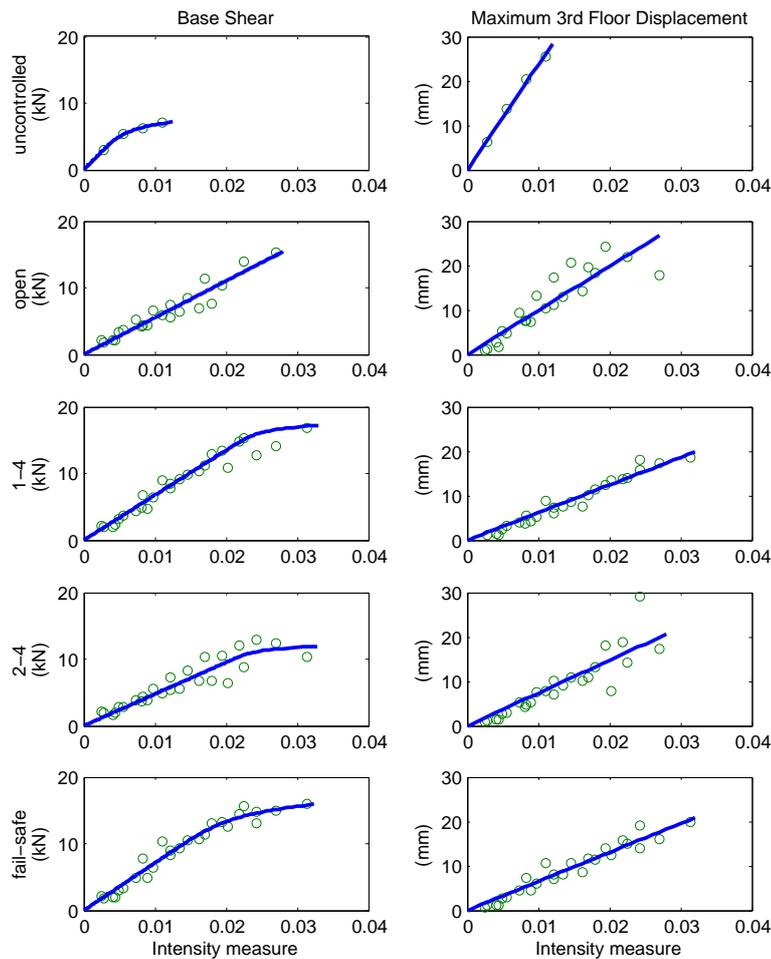
Figure 9.4 Base shear and maximum 3rd floor displacement for all control types and the uncontrolled case including the least squares fit relative to the spectral displacement intensity measure.

All the control laws show a reduction in maximum 3rd floor displacements compared to the uncontrolled case for a given intensity measure. The 1-4 and fail-safe cases have similar results with the best reductions. The 2-4 law shows significant reductions, which are very close to but not as great as the 1-4 and fail-safe cases. This hierarchy of displacement performance matches the spectral analysis in Chapter 3.
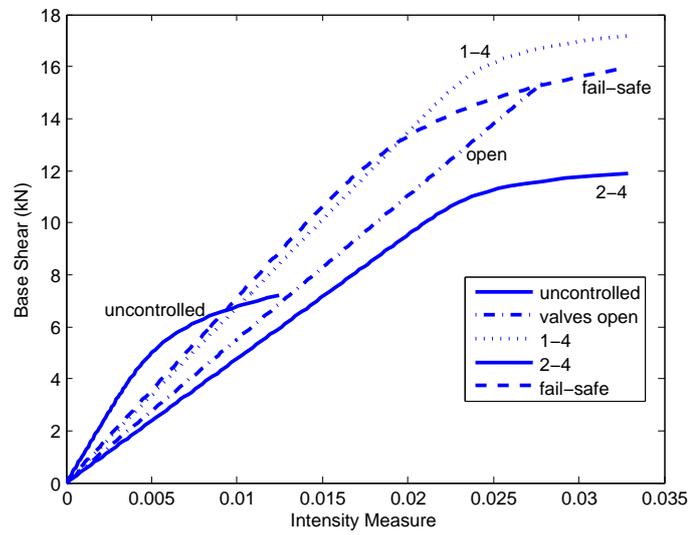
Figure 9.5   Least squares fit of base shear comparing all control types and the uncontrolled case relative to the spectral displacement intensity measure.
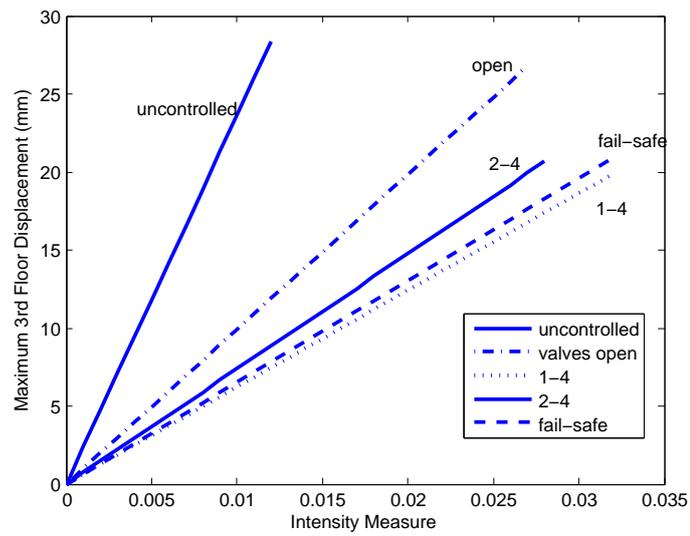
Figure 9.6   Least squares fit of maximum 3rd floor displacement comparing all control types and the uncontrolled case relative to the spectral displacement intensity measure.

Comparison of experimental test structure reduction factor results with the spectral analysis of Chapter 3 shows good correlation. Figure 9.7 shows displacement and base shear experimental reduction factors on the spectra for the 1-4 and 2-4 valve control cases. The experimental reduction factor is normalised for the valves open case, or surrogate uncontrolled condition, and averaged over all ground motions. The spectra results are presented as averages over the three suites of ground motions. This close correlation indicates the efficacy of the spectral analysis and the resetable device models used in the analysis in predicting the actual response of a test structure using the resetable device structural control system. In addition, these close correlations between analytical and experimental data validate the links between each development step and the tools and models used in analysis prior to the full-scale testing.
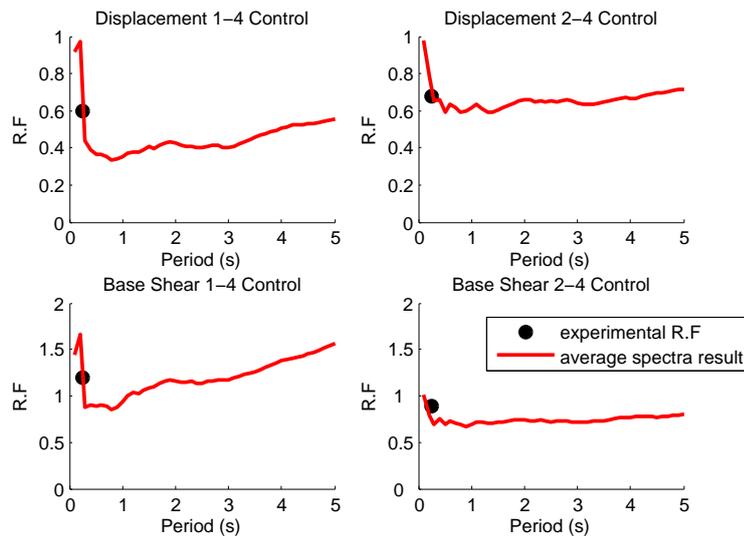
Figure 9.7 Experimental reduction factors for displacement and base shear on the spectra developed in Chapter 3 for maximum third floor displacement and base shear for the 1-4 and 2-4 control laws. These comparisons shows good correlations and validate the prior analytical work.

Cumulative distribution functions of the response metrics normalised to the ground motion intensity measure are shown in Figure 9.8. The fitted lognormal distributions for the base shear, maximum 3rd floor displacement, and maximum 3rd floor acceleration, are shown for each control law and the uncontrolled case in Figures 9.9 to 9.11. Each distribution contains the data for all records utilised for the specific control method examined. In addition, Table 9.2 shows the lognormal mean ($\hat{x}$) and multiplicative variance (σ) for all the data in Figures 9.8 to 9.11.
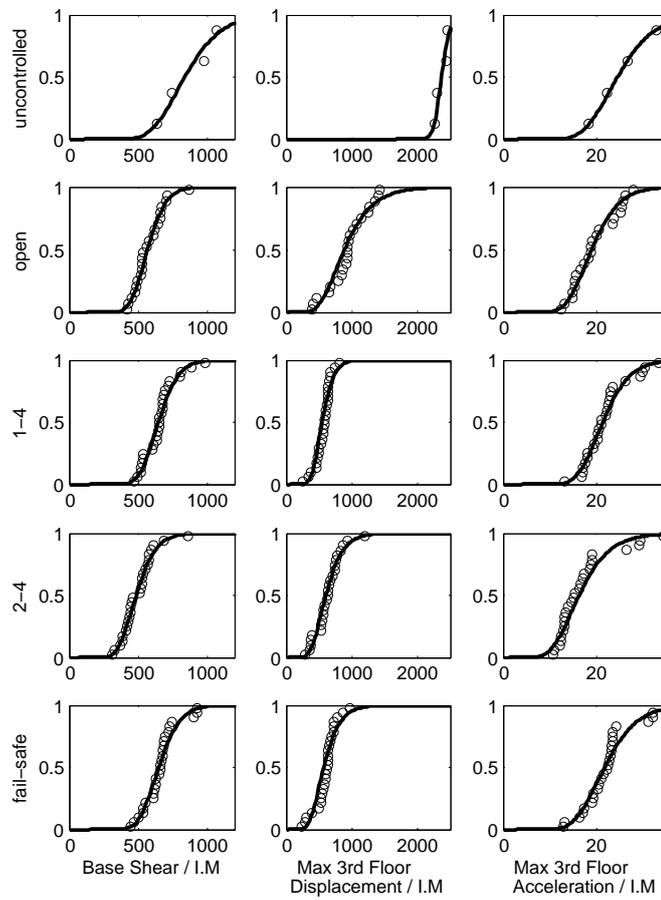
Figure 9.8   Lognormal base shear, maximum third floor displacement, and maximum third floor acceleration cumulative probability data points and functions.
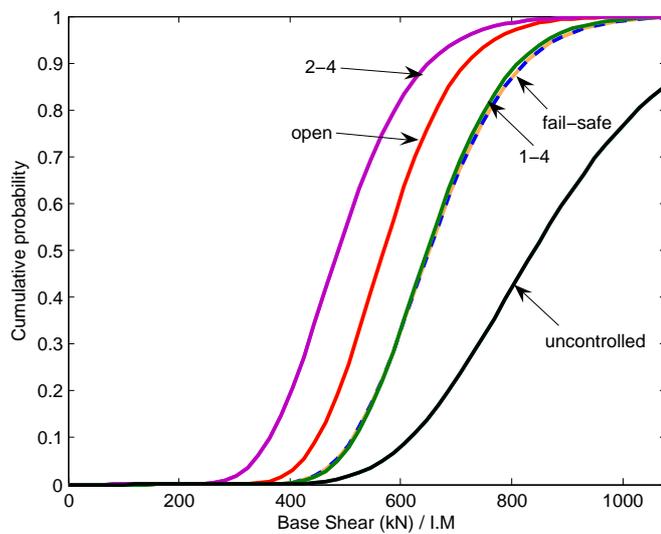
Figure 9.9   Lognormal base shear cumulative probability functions.
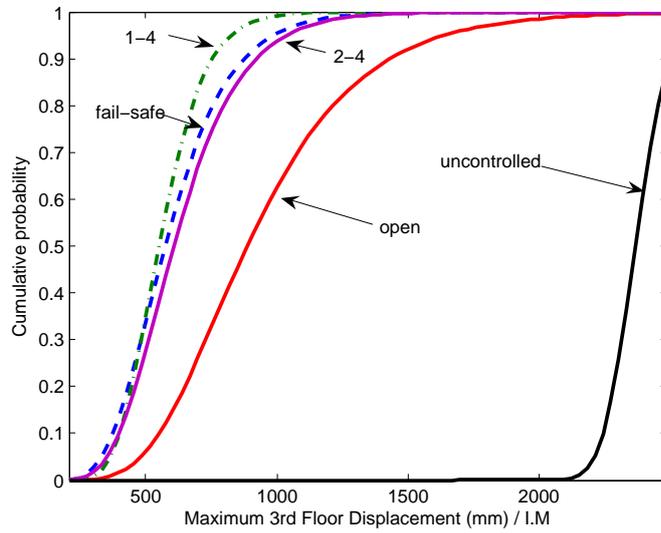
Figure 9.10   Lognormal maximum third floor displacement cumulative probability functions.
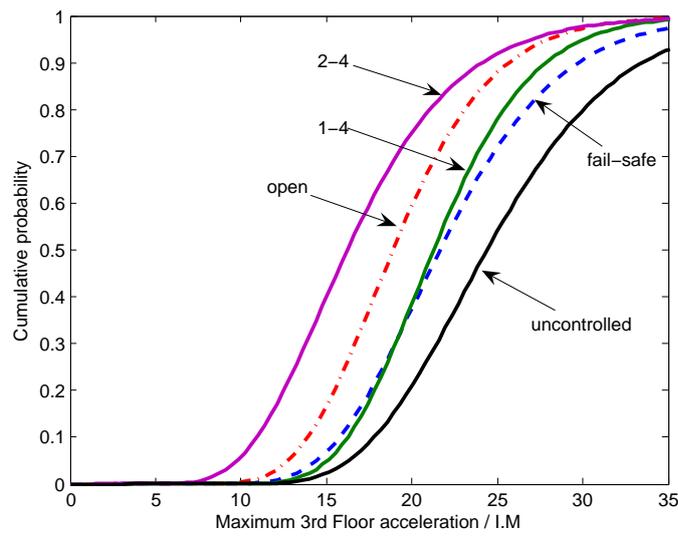
Figure 9.11   Lognormal maximum third floor acceleration cumulative probability functions.

Table 9.2 Lognormal mean ($\hat{x}$) and multiplicative variance (σ) for base shear, maximum 3rd floor displacement and acceleration for each control case.

	Base Shear		Maximum 3rd Floor Displacement		Maximum 3rd Floor Acceleration	
	$\hat{x}$	σ	$\hat{x}$	σ	$\hat{x}$	σ
uncontrolled	839	1.27	2368	1.04	24	1.28
open	568	1.20	887	1.45	19	1.27
1-4	647	1.19	549	1.28	21	1.23
2-4	486	1.25	605	1.39	16	1.36
fail-safe	650	1.20	573	1.39	22	1.28

The cumulative distribution functions of the 3rd floor maximum acceleration and displacements, and the base shear, relative to units of ground motion input intensity, show a lognormal distribution. The performance metrics are normalised to the ground motion intensity measure recorded during the experiment.

Ordinarily, the normalisation results from using ground motion records scaled for probability of exceedence for the region of interest. However, these shake table experiments utilised four ground motion records with varying levels of intensity, which were chosen to provide a range of inputs and so that the test structure did not yield. Thus, to create the cumulative probability results, the normalisation appears in the performance metrics rather than the ground motion records. This is in contrast to other studies (Hunt [2002], Hunt et al. [2002], Rodgers et al. [2007b]).

The cumulative probability plots indicate the probability of exceeding a given metric (per ground motion intensity) for each control method. Thus, the demand on the structural system is reduced as the cumulative probability function moves to the top left corner of Figures 9.9 to 9.11. An ideal curve is a vertical line at the left most limit of each plot that plateaus at a cumulative probability of 1.0. This ideal curve represents an assurance of not exceeding the performance metric for all ground motions or intensity measures examined. Table 9.2 presents the mean and multiplicative variance, or uncertainty of the results in Figures 9.9 to 9.11. A low multiplicative variance indicates low uncertainty in the result or small deviations away from the mean. Hence, a control case with a low mean *and* low multiplicative variance is the best case scenario and closest to the ideal curve.

All the semi-active control method results are to the left of the uncontrolled case (lower mean values) in the cumulative probability plots, indicating an improvement in performance with the addition of the semi-active resetable devices. This difference is particularly pronounced for the maximum 3rd floor displacement metric, where the mean probability for the 1-4 or 2-4 control methods gives a value of ~ 550 to 600mm/I.M which is at least three times less than that for the uncontrolled case (> 2000 mm/I.M).

Of particular note is the ability of the devices under 2-4 control to limit both the 3rd floor displacements and to significantly reduce the base shear and 3rd floor accelerations compared to the other control and fail safe cases, which typically increases the base shear demand. Thus, devices using the 2-4 control law are able to improve the structural performance for all metrics. In contrast, 1-4 control and the fail safe mode provide large reductions in one metric, usually displacement, with a concomitant increase or no change to other base shear or acceleration metrics. These results also quantitatively match the spectral analysis, as shown in Figure 9.7 (Rodgers et al. [2007b]). Additionally, the trends match analytical studies using the SAC suites scaled for probability of occurance (Hunt [2002], Chase et al. [2004a], Chase et al. [2005b]).

Reporting results as cumulative probability functions readily allows the findings to be incorporated into probabilistic performance based design methods (Barroso [1999], Barroso et al. [2003a], Rodgers et al. [2007b]), for example if the building codes state that a hospital requires a 90% certainty that the base shear demand will not exceed 700kN per unit of ground motion intensity due to a foundation design constraint. Using Figure 9.9 the valves open and 2-4 control law configurations meet this criteria. However, the 2-4 case has a much larger buffer between the allowance and response. In addition, the reduction in displacement response for the 2-4 control law far exceeds the reduction for valves open, as shown in Figure 9.10. Therefore, the 2-4 control law is the best option for this scenario.

Performance based design using these cumulative probability functions allows tradeoffs in design to be rapidly assessed. The broad view of a series of potentially contradictory performance metrics used here discourages narrow focus on one particular metric, avoiding potential errors or failures in the design procedure. In addition, probabilities of exceedence are a useful design tool where varying

levels of assurance of damage limits are dependent on different building uses. In combination, the overall method presented offers a generalisable and complete foundation for taking these resetable devices into regular design practice with confidence.

9.3.1   Switching Control Laws

The results presented show a significant trade off between reducing the maximum 3rd floor displacement and increasing the base shear. The 2-4 control law clearly has the lowest base shear value, while the 1-4 control law is the most effective at reducing the structural displacement. Switching the control law depending on the input ground motion and resulting structural dynamics can offer the benefits of both these control laws. Table 9.3 presents the maximum absolute base shear, cumulative base shear, and maximum absolute 3rd floor displacement for the El Centro 80% ground motion input. The cumulative base shear is the total base shear experienced by the structure for the duration of the ground motion and hence is an indication of cumulative damage to the structural system.

The results in Table 9.3 illustrate the benefits of switching the control law depending on the structural dynamics. In this particular case the control law is switched from 1-4 to 2-4 when the relative displacement across the resetable devices exceeds 7mm in both directions. This displacement value was chosen as it corresponds to relatively large structural motion for this particular test structure. Thus, the initial large structural motion is resisted with the 1-4 control law, reducing the maximum displacement, while the remainder of the record is resisted with the 2-4 control reducing the base shear. This switching control law result is a substantial improvement on using the same control law for the entire record and further emphasises the benefits to structural control applications of the novel semi-active resetable device ability to manipulate the reactive forces depending on the structural demands.

Table 9.3   Maximum base shear, cumulative base shear, and maximum 3rd floor displacement for the 1-4, 2-4 and switching control laws for the 80% El Centro ground motion record. Note, the switching control law changes from the 1-4 to the 2-4 case when the relative displacement across the device exceeds 7mm in both directions.

Control type	Maximum Base Shear (kN)	Cumulative Base Shear (kN)	Maximum 3rd Floor Displacement (mm)
1-4	13.5	76	12.4
2-4	9.6	63	18.0
switching 1-4 to 2-4	11.0	71	12.1

9.4   Summary

The addition of two semi-active resetable devices in a tendon arrangement greatly improves the structural performance of a $\frac{1}{5}^{th}$ scale moment resisting steel frame building under earthquake loading. The different control laws implemented generally result in an improvement in some performance metrics with a corresponding increase in other metrics. However, the most significant results are using the 2-4 control law. This control case presents favourable results that show improvements in *all* performance metrics, base shear, displacement, and acceleration, as expected from prior spectral and other analysis. This result is particularly important for retrofit applications where reductions in the structure displacement is necessary to reduce structural damage but the foundations may have insufficient strength to meet increased demand.

The tradeoff between improvements in some metrics with corresponding degradation in other metrics is addressed by switching control methods depending on the structural motion (resulting from the ground motion input). In particular, this switching method gives comparable results to the best improvements in all performance metrics obtained with the standard control methods. Hence, this switching control method further confirms the ability of the semi-active resetable devices developed in this research to adapt to changing structural demands due to non-linear behaviour from large ground motion pulses or structural degradation over time.

The fail-safe case presents the worst case scenario with a control system utilising resetable devices. This case occurs when the power to the devices fails

or the control system malfunctions. The structure dynamics with the fail-safe mode are still favourable over the uncontrolled or surrogate uncontrolled (valves open) cases, indicating the robust nature of resetable device control systems.

Overall, these shake table experiments have shown the efficacy of semi-active resetable devices as a structural control method. Results are presented in a format that can be readily and directly incorporated into performance based design methods that indicate the relative performance of each control method for the performance metrics. In addition, these experiments are the first large scale structural application of this type of semi-active resetable devices. They are also the first experiments to utilise and validate the customised hysteresis loops this novel design enables. Thus, the findings are an important step to realising full scale structural control with customised semi-active hysteretic behaviour using these novel semi-active resetable devices, or any other device capable of providing these unique capabilities.

Chapter 10

High Force, Next Generation Devices

10.1 Introduction

The semi-active resetable device prototypes and design curves developed are effective, but provide relatively modest forces and stiffnesses for the device volume. Therefore, increasing the semi-active resetable device response forces with the same volume would be beneficial and create or enable a broader range of structural applications. More specifically, the force-displacement response of the large-scale prototypes developed in this research do not reach the level of those assumed by Hunt [2002] and Barroso et al. [2003b].

In general, the assumption of the device force-displacement response in all prior work has been based on a set device stiffness and made prior to any complete understanding of the physical characteristics of resetable devices. In addition, increasing the peak response forces in relation to the physical size of the device would increase the energy dissipation capability of these devices without increasing the overall architectural footprint. However, the first of their kind design curves developed in this thesis allows these tradeoffs to be analytically examined and the appropriate force enhancement to be quantified directly, rather than estimated.

The hysteretic response of resetable devices is non-linear with the stiffness increasing as the piston approaches the maximum displacement, as seen for example in Figure 4.11. To achieve greater forces without changing the device dimensions it was proposed to shift the working range of the device into this higher stiffness region. This shift can be achieved by using either a different working fluid, or

more innovatively with a high pressure air source to charge the active chamber. This latter choice requires little modification to the device or control methods and effectively begins the force-displacement response at a higher pressure and thus stiffness.

The resetable device force response is dependent on the differential pressure between the two chambers. Hence, the greater this differential pressure the greater the resisting force produced. The base pressure is the pressure in the active chamber before the air is pressurised due to a change in chamber volume caused by piston displacement. Increasing the base pressure in the active chamber prior to any piston motion greatly increases the differential pressure between the chambers because the other chamber does not have the increase in base pressure. This increase shifts the entire hysterestic curve as it is as available through any subsequent piston motion.

The sculpting ability over the hysteretic response of the devices may also be further enhanced with the addition of a high pressure air source. The active chamber can either be pre-pressurised or allowed to work from atmospheric pressure. This level of chamber control and management raises the possibility of the device having differential response depending on the type or direction of motion.

It is important to note that this ability to add a high pressure source and to utilise it for differential response is only possible due to the independent chamber design presented. Charging the chambers with the standard connected chamber design of Bobrow and Jabbari [2002] would, by default, result in both the chambers being charged. Hence, the increase in differential pressure between the chambers supplied by the charging would be negated as both chambers would be once again starting from the same base pressure.

The analysis presented in this chapter resulted in some interesting and unusual hysteretic responses, not all of which immediately lend themselves to structural applications. However, this range of device hysteresis responses illustrates the full potential capabilities of hysteresis sculpting. It should also raise the idea that a very wide variety of responses are possible and thus encourage structural designers to extend their thoughts to what is desired, rather than what is possible and accepted today.

10.2   Device Setup

The prototype devices required only small modifications to enable pre-pressurising of each chamber. Pre-pressurising requires an additional controlled valve per chamber, creating a four valve device, as shown in Figure 10.1. This change was readily achieved as extra valve attachment points were incorporated for such cases during manufacture.

The additional valves are attached to a pressure regulator. For ease of supply, this regulator is attached to the mains high pressure supply in the testing lab. If this pre-pressurising configuration was to be installed in a structure the high pressure could be supplied by stand alone tanks attached to each device or via a central system as in the lab. There are typically only a few relatively large pulses during the strong motion part of an earthquake. Therefore, a sufficient pressure supply in a relatively small tank can provide the device with sufficient air mass and pressure for the duration of these pulses.
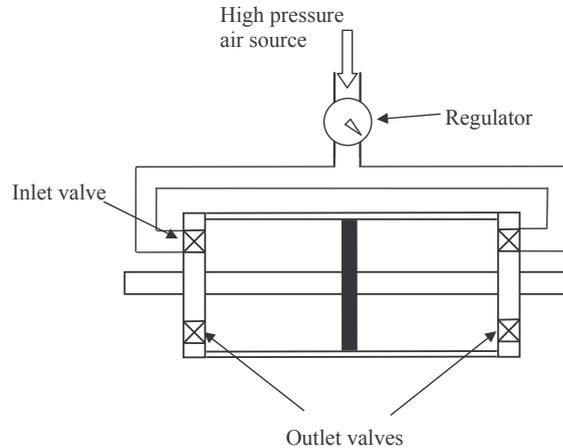
Figure 10.1   Schematic of four valve design incorporating a high pressure air source.

The four valve configuration allows significantly more complex valve control laws to be implemented than the original two valve prototype device configuration. The 1-4, 1-3 and 2-4 control laws are all investigated with added pressure along with other more complex cases. However, the complexity is increased by the relative timing between pre-pressurising the active chamber and the normal increase in pressure due to the active chamber volume decreasing with piston motion. Some configurations are obviously not beneficial such as having the inlet

and outlet valve of a chamber open at the same time allowing the high pressure air to flow through the chamber. In addition, the level or amount of added pressure input becomes an added variable in determining and modelling the overall device response.

The relative timing of pre-pressurising and pressure releasing of each chamber affects the response. There are basically three configurations developed for pre-pressurising the active chamber:

1. Pre-pressurise on the quarter cycle directly prior to total pressure and energy release.

2. Pre-pressurise on the quarter cycle directly following total pressure and energy release.

3. Pre-pressurise on all quarters that are not pressure and energy releasing.

Figure 10.2 illustrates the relative timing of charging and releasing pressure from the active chamber based on the 1-3 control law. The plot on the left of Figure 10.2 indicates the active chamber is pre-pressurised during the quarter cycle immediately prior to when the device is resisting piston motion. In contrast, the plot on the right indicates the active chamber is pre-pressurised immediately following pressure and energy release from the active chamber. The control used may fit into more than one of these options depending on the release configuration.

Pre-pressurising results in a rapid increase of the base pressure in the chamber, so it can be thought of as a stepwise increase in the pressure corresponding to a stepwise change in the total force response. Therefore, option 1 results in a stepwise change in the force immediately following a reset. Options 2 and 3 result in a stepwise change in the force immediately prior to a reset. The distinguishing feature between options 2 and 3 is that option 3 continues to pre-pressurise the chamber for the whole cycle when the pressure is not being released. Thus, this option results in the device response being heavily dependent on the value of the pressure source rather than on the piston displacement.
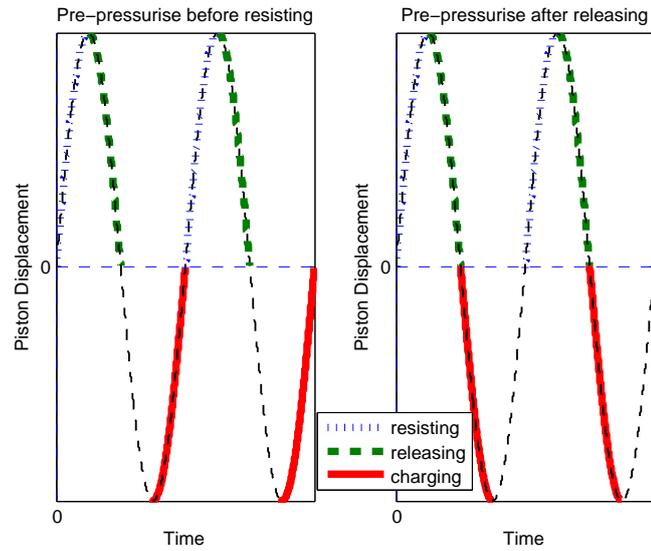
Figure 10.2   Relative timing of pressurising and releasing pressure from the active chamber.

10.3   Analysis Method

The experimental response of the second prototype device to an array of different valve control configurations and pressure source values was examined. The piston input motion is sinusoidal with varying amplitude and frequency. The range of possible control methods with four valves is extensive. Most valve control figurations were pre-determined based on either desired outcomes or systematic extensions from analysis of the two valve configuration. However, some of the valve control figurations were impromptu, which resulted in some interesting and unusual device hysteresis loops.

The comprehensive device model developed in Chapter 5 was further modified to incorporate the impact of the added high pressure source. The model was also extended to increase the understanding of how the high pressure source alters the device behaviour. Specifically, the validated model allows rapid examination of changes to the hardware of the device, such as the valve orifice size and opening rates that are fundamental to the device behaviour. The validated model captures the dynamics of this device configuration in most cases.

10.4   Results and Discussion

The addition of the high pressure air source had the desired effect of increasing the maximum forces produced by the device compared to working from atmospheric pressure. In general, the addition of 1.0atm (100kPa) of pressure to the active chamber, more than doubles the maximum force produced by the device. Figure 10.3 shows a comparison of the device under 2-4 control working from atmospheric pressure and with an additional 1 and 1.5 atmospheres of pressure. The maximum force increases from approximately 1.5kN for the atmospheric supply pressure case to 3.5kN and 5.6kN for the high pressure source cases. The additional pressure elongates the force-displacement response along the vertical force axis, thus increasing the force provided in the 2nd and 4th quadrants. The force in the 1st and 3rd quadrants does not change significantly.

The apparent delay between zero piston displacement and the rapid decrease in force increases as the additional pressure increase. This delay was discussed in Sections 4.5.2.2 and 5.3 and is further increased for these higher pressure devices due to larger pressure differentials between the active chamber and the external fluid reservoir pressures. More specifically, when the valve is opened at the zero crossing point the balance between the decreasing pressuring from air mass exiting the device and the pressure continuing to increase from the chamber volume decreasing takes longer to be dominated by the pressure release. Therefore, as the active chamber charging pressure increases this apparent delay increases.

In addition, increasing the initial pressure of the active chamber also results in increased energy release times. This increase is due to the time required for the additional mass of high pressure air to be released from the chamber. The energy release time thus becomes a dominating feature of the response, for even relatively low frequency input motions, as seen in Figure 10.4. The descending slopes from the maximum force to the constant force section, are significantly different for the 0.1Hz and 0.5Hz motion cases, indicating that the energy release time is a significant portion of the overall cycle time. The 0.5Hz case appears to have a slower release as a greater proportion of the 0.5 second quarter period is required to release all the compressed air from the chamber.

A significant energy release time, along with the ability to control the rate,
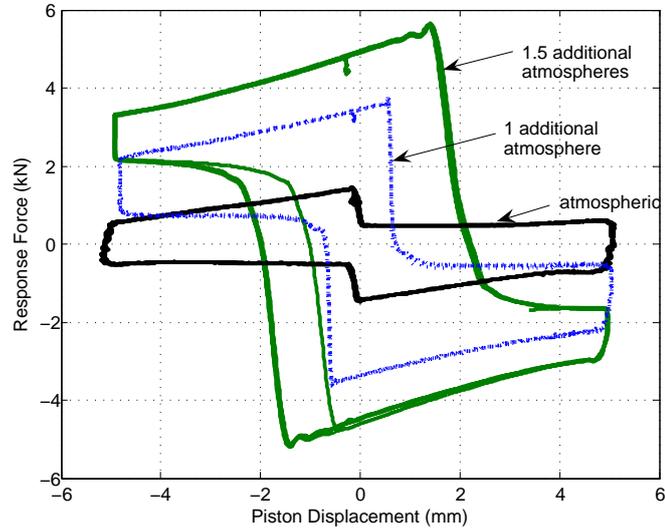
Figure 10.3 Force-displacement response of device with atmospheric, 1.0 additional atmosphere, and 1.5 additional atmosphere of pressure. The piston motion is sinusoidal with an amplitude of 5mm and frequency of 0.1Hz. Note the elongation of the response along the force axis.
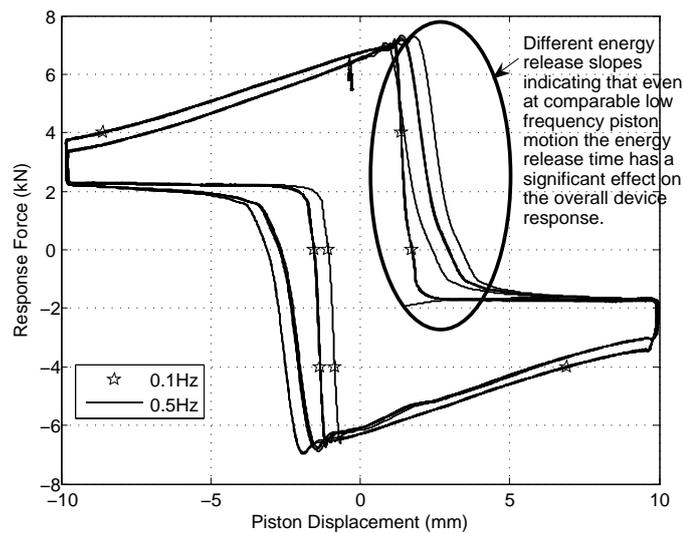
Figure 10.4 Force-displacement response of the device showing significant energy release time for even comparably low piston motion of 10mm at 0.1 and 0.5Hz. The high pressure supply is 1.5 additional atmospheres.

can be advantageous, as it allows further sculpting of the hysteretic behaviour of the device. This sculpting has the potential to produce more optimal device responses for different applications. More specifically, the energy release rate, and hence the slope of the hysteresis plot, can be controlled by the opening size or number of valves operated depending on the desired air flow rate out of the device. In addition, the flow rate can be manipulated during each release period, an area to be examined further. In these experiments, the outlet valves are fixed at the prototype design specification. However, larger valves would have decreased the release time, all else equal. These choices can be controlled via more complex valves or by designs including more valves.

The analytical model developed in Chapter 5 captures all the dynamics to accurately predict the experimental results. The energy release time is incorporated by modeling the open valve as an orifice with a variable size. Figure 10.5 shows the experimental and modeled results for the 2-4 control case with a piston displacement of 10mm at 0.5Hz, and the air supply at 2.0 additional atmospheres. The maximum forces and overall loop are well predicted along with the energy release slope. In addition, valve specific model parameters can be easily altered to account for different valve types, valve control or valve architectures.
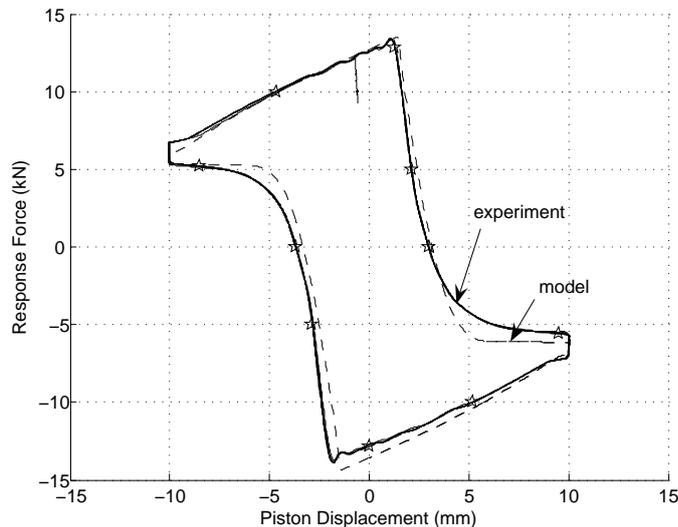
Figure 10.5   Force-displacement response of the device comparing experimental and modelled data. The piston input motion is sinusoidal with an amplitude of 10mm and a frequency of 0.5Hz. Note the model accurately captures the device response including the non-linear energy release rate.

Finally, the high pressure air supply resulted in some interesting hysteretic responses from the device. Figure 10.6 shows some unusual hysteretic shapes

along with the predicted response from the model enabled by this approach and design. In all cases shown, the supply pressure is 2.0 atmospheres. Some of these shapes are achieved by only pre-pressurising one chamber of the device and letting the other work from atmosphere, while others are achieved by holding one chamber closed. Both of these cases make the device effectively one sided, resulting in much higher forces in one displacement direction than the other, thus allowing unique differential behaviour from the device depending on displacement type or direction.
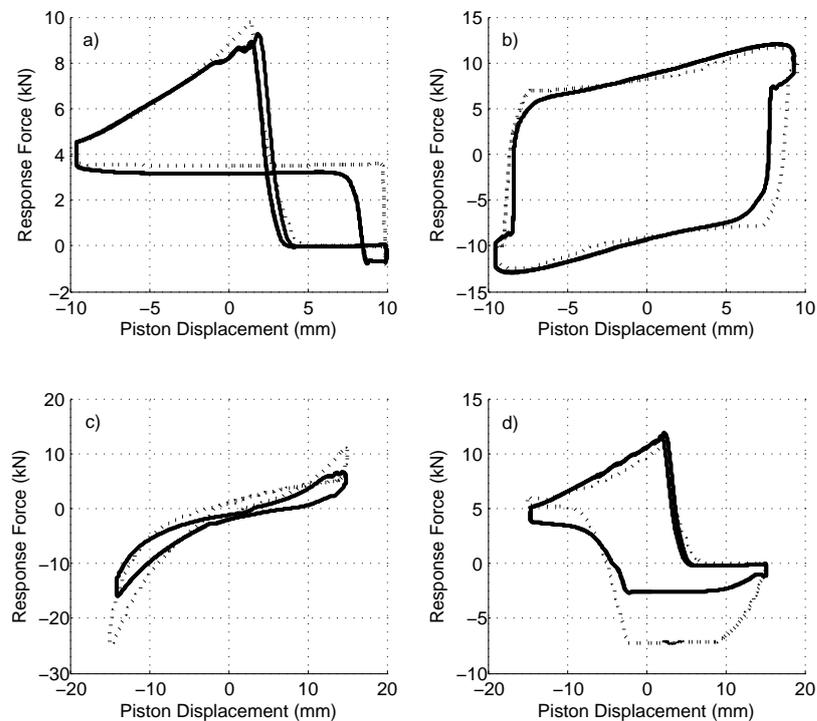
Figure 10.6 Force-displacement response of the device for a number of different valve control configurations including effectively one sided device response. The modelled prediction is shown with a dotted line, and the experimental results with a solid line. The piston input motions are all sinusoidal with a frequency of 0.5Hz.

Figure 10.6a is a one sided 2-4 controlled device where the active chamber is pre-pressurised immediately following pressure release giving the square response in the 2nd quadrant. Figure 10.6b is the device using 1-4 control with the active chamber pre-pressurised immediately prior to resisting motion, thus enlarging the area inclosed compared to the conventional device response with 1-4 control. Figure 10.6c is also based on the 1-4 control law, however the active chamber is pre-pressurised following pressure release. Finally, Figure 10.6d is another one sided device with the active chamber using the 2-4 control law. In this case the

active chamber is pre-pressurised immediately prior to resisting motion resulting in the 4th quadrant having a similar result to Figures 10.3 and 10.4.

10.5   Closure

The addition of a high pressure air source is an effective way of increasing the maximum forces produced by semi-active devices using air as the working fluid, without increasing the device size. The device response is further able to be sculpted, in comparison to the two valve design working at atmospheric pressure. In addition, some potentially useful and unusual hysteretic responses are obtained.

However, the energy release rate increased and is dependent on the number or size of outlet valves. Further, control over the air release rate would further add to the hysteretic sculpting ability of these devices. Such changes are made passively by design or via additional control elements actively modifying valve size and number.

The analytical model developed in Chapter 5 is able to accurately predict the experimental results, and contributes to the understanding of the device dynamics during operation. In addition, this model is generic and can be used for any devices with the same basic components. The experimental results presented thus serve to further validate this model. Finally, the unique hysteretic responses allow a far wider range of potential applications and customisation than currently available semi-active devices.

Chapter 11

Conclusions

Structural control is an effective method to reduce structural damage during large seismic events. Structural control methods have traditionally utilised passive devices for energy dissipation. Recently, the concept of active control methods has been developed that are able to adjust the structural response. However, these systems are complex and require large energy sources to operate. In contrast, semi-active control offers similar advantages to active control systems coupled with the simplicity and reliability of passive control systems. Thus, semi-active devices are emerging as the method of choice for the emerging consideration of structural control applications.

Semi-active structural control methods have the ability to significantly improve structural performance during seismic events. Cost effective solutions to structural control can be provided with resetable devices. The devices designed and extensively examined in this research are one of the first larger scale resetable devices created. They are the only ones to offer the unique abilities to re-shape structural hysteretic behaviour. The results indicate the simplicity and efficacy of these devices at managing and dissipating energy resulting from structural motion.

The resetable devices manufactured and examined utilise a new array of control laws resulting in unique abilities to manipulate structural hysteretic behaviour. Thus, the response of the semi-active control system can be tailored to each structural application in ways not possible prior to this research. This extensive manipulation widens the application scope of resetable devices to structural systems not previously considered, such as rocking wall panels. In addition, structural hysteretic response manipulation resulting from the new control methods

enables response improvement for more than a single response metric.
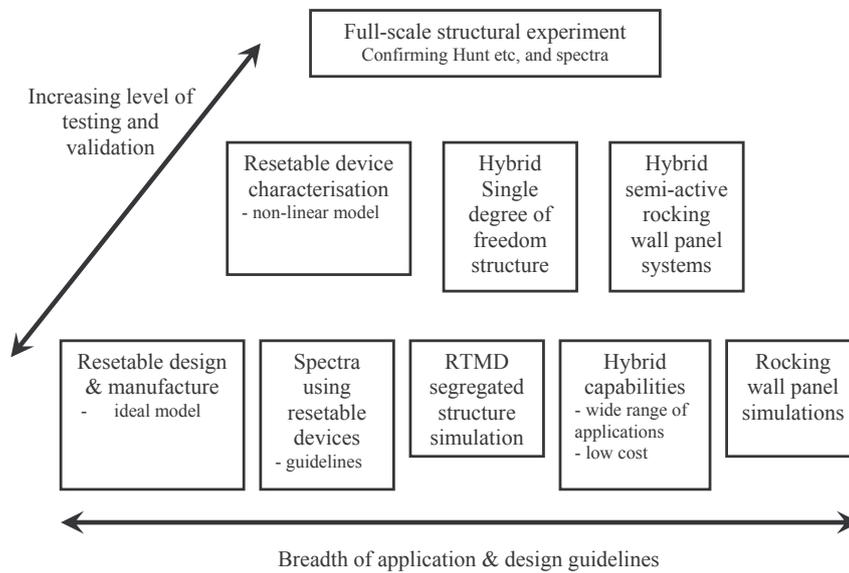
Figure 11.1   Pyramid shape of structural control method development.

The hysteretic sculpting ability presented, hopefully encourages structural engineers to consider what is required for a structural application, rather than using more limited or less effective control methods that are currently commonly considered. Tailoring the control system response to the structural application is further emphasised by using a range of response metrics to analyse the structural response during seismic events. Traditional energy dissipation design focuses strongly on maximum energy dissipation without much regard to the effect on other potentially degraded response metrics, such as base shear.

Intuitive methods of resisting all motion to limit displacements are challenged. In particular, the 2-4 control method developed provides new ways of looking at structural control. This case considers the overall structural response demands and provides improvement in *all* performance metrics rather than a selection. Hence, this control method is also particularly suited to retrofit applications.

Two prototype devices with the novel independent chamber design are designed and characterised using an extensive examination procedure. In addition, a validated realistic, non-linear model of these devices is developed that captures all the device dynamics. This validated model is used for analytical examination of semi-active resetable device structural control applications.

Figure 11.1 depicts the tiered levels in structural control method development as implicitly proposed in this thesis. This pyramid provides a pathway for designing, developing and implementing these resetable devices. The lower level represents the extensive analytical tests and simulations that provide the motivation and broad results for the structural control method being developed. The middle section is the intermediary step between analytical and full-scale testing. The hybrid testing procedure (HTP) was developed as this intermediary step for this research. The HTP reduces the overall design cycle by being relatively cheap and time efficient compared to full-scale tests, while providing many of the benefits. Therefore, the HTP ameliorates the risk in full-scale testing as a lot of the necessary development and potential errors can be identified and negated prior to full-scale testing. Finally, the highest tier or tip of the pyramid represents full- or large-scale experiments. These large-scale experiments are justified by, and validate the extensive analytical and hybrid test results that led to them.

As a package these results design, characterise, and validate the significant potential of resetable devices for semi-active civil infrastructure control and seismic damage mitigation. In particular, results are presented across a wide range of application spaces with a method for creating recognisable design guidelines for each unique structural application. They are then concluded or finalised via increasing levels of experimental validation for each result. Close correlation between analytical and experimental data validates the entire control method development process developed throughout this thesis.

In summary, the unique contributions this research and thesis make to the field of structural control include:

- Development of a novel resetable device design which provides the ability to manipulate the overall hysteretic response of a structural system leading to control systems that are tailored to each specific structural application. The significant outcome of this development is the potential to mitigate some of the response tradeoffs that can occur with structural control. Furthermore, this ability to manipulate the response encourages a paradigm shift towards development of optimised structural control systems.

- Full characterisation of large-scale resetable devices including a process that can be used for similar devices. This characterisation revealed some signif-

icant and important device dynamics that were not apparent and/or discussed in other studies.

- Development of a high-speed, real-time hybrid testing procedure specifically for structural applications provides a link between analytical and full experimental testing. Utilising widely used and accepted programs and equipment this method is readily implemented leading to an overall increase in testing of structural developments.

- Large-scale full experimental shake table tests which validate the devices developed, the analytical studies as well as proving the efficacy of resetable devices in structural control.

Chapter 12

Future Work

This research has shown the significant potential of semi-active resetable devices with air as the working fluid for structural control applications, thus meeting some of the objectives highlighted by Soong and Spencer [2000]. However, full-scale implementation of these devices is still limited due to moderate forces produced in comparison to the device size. This issue has partially been addressed in Chapter 10, but further work in this direction is required to achieve efficient, economic and flexible structural control designs.

Lead dampers (Rodgers et al. [2007a]) offer very large response forces for the device size. The combination of these high force devices with resetable devices that offer high response adaptability could ameliorate the moderate force response currently provided by purely resetable device structural control methods. This combination would therefore result in structural control systems that can dissipate large amounts of structural energy while tailoring the control system response to the structural system via limited extra semi-active elements. However, this approach requires analysis first per the initial (lower) level of the process or pyramid proposed.

Semi-active resetable devices also have significant promise as 'smart' dampers in existing structural control methods, such as the tuned mass damper systems. Chapter 6 presented a qualitative analysis of this type of system. However, to bring these structural control systems to full-scale implementation further studies focusing on a qualitative analysis are required, starting with hybrid testing. In addition, large-scale testing similar to the work presented in Chapter 9 would provide validation of these types of resetable device applications.

Recent work on optimised hysteretic response for structural control including base isolation has further served to highlight the increasing awareness of the advantages available with recent development in structural control devices. This awareness has fundamentally shifted the goals of structural research from using what is available to determining and discovering novel and innovative new ways to achieve optimum results. Therefore, future structural control method research, particularly using resetable devices, should begin from the base point of optimising the control system to the demands of each individual structural system.

The analyses in this research used suites of ground motion records. Most results were suite invariant. However, acknowledgement is given that suite invariant does not mean ground motion invariant. This dependency on ground motion is illustrated with some of the responses of the rocking structure in Chapter 8. The interplay between the ground motion and rocking wall at times created unpredictably large rocking responses. There is scope for further investigation into this ground motion structure interaction in future semi-active structural control research.

An overall summary of future directions would therefore include:

- Research of optimised structural control device response for a variety of structural applications.

- Research examining the efficacy of combining resetable devices with other damping devices to improve the overall structural control efficiency.

- Hybrid test analysis of resetable tuned mass damper (RTMD) systems leading to large-scale experiments.

- Large-scale rocking wall panel shake table tests utilising resetable devices to enhance the overall energy dissipation of these systems.

These directions would be the most likely to efficiently lead to a first full-scale implementation of semi-active resetable devices utilising the novel hysteresis sculpting behaviour to advantage.

References

Abdul Hamid, N. (2006). *Seismic Damage Avoidance Design of Warehouse Buildings Constructed Using Precast Hollow Core Panels.* Phd, University of Canterbury.

Ajrab, J., Pekcan, G., and Mander, J. B. (2004). Rocking wall-frame structures with supplemental tendon systems. *Journal of Structural Engineering*, 130(6):895–903.

Anaya, R., Carr, A., Mander, J. B., Chase, J. G., Mulligan, K., and Rodgers, G. (2007). Seismic testing of a model structure with semi-active resetable devices. Palmerston North, New Zealand.

Baber, N. and Noori, M. (1985). Modelling general hysteresis behavior and random vibration application. In *ASME Design Engineering Technical Conference*, Cincinnati, Ohio.

Barroso, L. R. (1999). *Performance Evaluation of Vibration Controlled Steel Structures Under Seismic Loading.* Doctor of philosophy, Stanford University.

Barroso, L. R., Chase, J. G., and Hunt, S. (2003a). Probabilistic seismic hazard analysis of semi-active controlled 9-story steel moment-resisting structure. In *16th ASCE Engineering Mechanics Conference*, University of Washington, Seattle.

Barroso, L. R., Chase, J. G., and Hunt, S. (2003b). Resettable smart dampers for multi-level seismic hazard mitigation of steel moment frames. *J. Struct. Control.*, 10:41–58.

Bayer, V., Dorka, E., Fullekrug, U., and Gschwilm, J. (2002). Realisation of real-time pseudo-dynamic sub-structure testing. In *2002 International Conference on Noise and Vibration Engineering*, pages 1713–1720, Leuven, Belgium. Katholieke Universiteit Leuven.

Bobrow, J. E. and Jabbari, F. (2002). Vibration suppression with resettable device. *Journal of Engineering Mechanics*, 128(9):916–924.

Bobrow, J. E., Jabbari, F., and Thai, K. (1995). An active truss element and control law for vibration suppression. *Smart Materials and Structures*, 4(4):264–269.

Brock, J. (1946). A note on the damped vibration absorber. *ASME Journal of Applied Mechanics*, 13:284.

Chase, J. G., Barroso, L. R., and Hunt, S. (2004a). A semi-active acceleration-based control for seismically excited civil structures including control input impulses. *Structural Engineering and Mechanics*, 18(3):287–301.

Chase, J. G., Hudson, N. H., Lin, J., Elliot, R., and Sim, A. (2004b). Nonlinear shake table identification and control 3 for near-field earthquake testing. *Journal of Earthquake Engineering,*, Vol. 9(No. 3):1–22.

Chase, J. G., Mulligan, K., Elliot, R., Mander, J. B., Keir, M., and Chen, X. (2007). Hardware-in-loop test for rapid development of structural control devices. In *IEEE Conference on Automation Science and Engineering*, Scottsdale, Arizona, USA.

Chase, J. G., Mulligan, K., Gue, A., Alnot, T., Rodgers, G., Mander, J. B., Elliot, R., Deam, B., Cleeve, L., and D, H. (2006). Re-shaping hysteretic behaviour using semi-active resettable device dampers. *Engineering Structures*, 28(10).

Chase, J. G., Mulligan, K., Gue, A., Mander, J. B., Alnot, T., Rodgers, G., Deam, B., Cleeve, L., and Heaton, D. (2005a). Resetable devices with customised performance for semi-active seismic hazard mitigation of structures. In *Planning and Engineering for Performance in Earthquakes*, Wairakei, New Zealand. New Zealand Society for Earthquake Engineering Incorporated.

Chase, J. G., Mulligan, K., Hunt, S., Barroso, L. R., and Deam, B. (2005b). Actuator-actuator interaction and instability in decentralised control of nonlinear seismically excited tall structures. In *9th International Conference On Structural Safety and Reliability*, Rome, Italy.

Clough, R. and Penzien, J. (1993). *Dynamics of Structures*. McGraw-Hill, 2nd edition.

Datta, T. (2003). A state-of-the-art review on active control of structures. *ISET Journal of Earthquake Technology*, 40(1):1–17.

Den Hartog, J. (1962). *Mechanical Vibrations*. McGraw-Hill, 4 edition.

Dyke, S., Spencer, B., Sain, M. K., and Carlson, J. (1996). Modeling and control of magnetorheological dampers for seismic response reduction. *Smart Materials and Structures*, 5(5):565–575.

Dyke, S., Spencer, B., Sain, M. K., and Carlson, J. (1998). Experimental study of mr dampers for seismic protection. *Smart Materials and Structures*, 7(5):693–703.

Forum, N. L. G. H. P. (2005). Heritage and seismic upgrading, policy workshop.

Franklin, G., Powell, J., and Emami-Naeini, A. (2002). *Feedback control of dynamic systems*. Prentice Hall, London, 4th edition.

Fukuzumi, S., Sone, A., and Iba, D. (2001). Vibration control of structures considering stroke constraint constraint of auxiliary mass of tmd. *ASME, Pressure Vessels and Piping Division*, 428(2):163–169.

Hill, P. and Peterson, C. (1992). *Mechanics and thermodynamics of propulsion*. Addison-Wesley, 2nd edition.

Horwich, G. (2000). Economic lessons of the kobe earthquake. *Economic Development and Cultural Change*, 48(3):521–542.

Housner, G. (1963). Behavior of inverted pendulum structures during earthquakes. *Seismological Society of America*, 53(2):403–417.

Housner, G., Bergman, L., Caughey, T., Chassiakos, A., Claus, R., Masri, S., Skelton, R., Soong, T., Spencer, B., and Yao, J. (1997). Structural control: Past, present, and future. *Journal of Engineering Mechanics*, 123(9):897–971. Good overview.

Humar, J. (2002). *Dynamics of Structures*. A.A. Balkema Publishers, 2nd edition.

Hunt, S. (2002). *Semi-Active Smart-Dampers and Resetable Actuators for Multi-Level Seismic Hazard Mitigation of Steel Moment Resisting Frames*. Masters, University of Canterbury.

Hunt, S., Chase, J. G., and Barroso, L. R. (2002). The impact of time varying equilibrium location in the semi-active control of non-linear seismically excited structures. In *7th International Conference on Control, Automation, Robotics and Vision, ICARCV*, Singapore. Nanyang Technological University.

Jansen, L. and Dyke, S. (2000). Semiactive control strategies for mr dampers: Comparative study. *Journal of Engineering Mechanics*, 126(8):795–803.

Kao, G. C. (1998). *Design and shaking table tests of a four-storey miniature structure built with replaceable plastic hinges*. Master of civil engineering, University of Canterbury.

Kawashima, K. and Unjoh, S. (1994). Seismic response control of bridges by variable dampers. *Japan Society of Civil Engineers*, 501:143–152.

Kurino, H., Yamada, T., Matsunaga, Y., and Tagami, J. (2006). Switching oil damper with automatic valve operation system for structural control. In *4th World Conference on Structural Control and Monitoring*.

Limpert, E., Stahel, W. A., and Abbt, M. (2001). Log-normal distributions across the sciences: Keys and clues. *BioScience*, 51(5):341–352.

Mulligan, K., Chase, J. G., Elliot, R., Horn, B., Danton, G., Deam, B., and Mander, J. B. (2006a). Simple, robust hybrid test systems for non-linear structural dynamic research and development. In Moss, P. and Dhakal, R., editors, *19th Australasian Conference on the Mechanics of Structures and Materials*, pages 331–336, Christchurch, New Zealand. Taylor & Francis.

Mulligan, K., Chase, J. G., Gue, A., Alnot, T., Rodgers, G., Mander, J. B., and Elliot, R. (2005). Large scale resetable devices for multi-level seismic hazard mitigation of structures. In *9th International Conference on Structural Safety and Reliability*, Rome, Italy.

Mulligan, K., Fougere, M., Mander, J. B., Chase, J. G., Deam, B., Danton, G., and Elliot, R. (2006b). Hybrid experimental analysis of semi-active rocking wall systems. In Brabhaharan, P. and Deam, B., editors, *Remembering Napier 1931, Building on 75 Years of Earthquake Engineering in New Zealand*, Napier, New Zealand. New Zealand Society for Earthquake Engineering Incorporated.

Myrtle, R., Masri, S., Nigbor, R., and Caffrey, J. (2005). Classification and prioritization of essential systems in hospitals under extreme events. *Earthquake Spectra*, 21(3):779–802.

Nishitana, A., Nitta, Y., Ishibashi, Y., and Itoh, A. (1999). Semi-active structural control with variable friction dampers. In *American Control Conference*, volume 2, pages 1017–1021, San Diego, California, USA. Institute of Electrical and Electronics Engineers Inc.

Pan, P., Tomofuji, H., Wang, T., Nakashima, M., Ohsaki, M., and Mosalam, K. (2006). Development of peer-to-peer (p2p) internet online hybrid test system. *Earthquake Engineering and Structural Dynamics*, in press.

Pickett, M. (1995). The effects of the 17 january 1994 northridge earthquake on hospital lifelines. In M.J, O., editor, *Lifeline Earthquake Engineering*, pages 795–802, San Francisco, Calafornia, USA. ASCE.

Rodgers, G., Chase, J. G., Mander, J. B., Leach, N., and Denmead, C. (2007a). Experimental development, tradeoff analysis and design implementation of high force-to-volume damping technology. *Bulletin of the New Zealand Society for Earthquake Engineering*, (in press).

Rodgers, G., Mander, J. B., Chase, J. G., Mulligan, K., Deam, B., and Carr, A. (2007b). Re-shaping hysteretic behaviour - spectral analysis and design equations for semi-active structures. *Earthquake Engineering and Structural Dynamics*, 36(1):77–100.

Sadek, F., Mohras, B., Taylor, A., and Chung, R. (1997). Method of estimating the parameters of tuned mass dampers for seismic applications. *Earthquake Engineering and Structural Dynamics*, 26(6):617–635.

Smith, A. H. (1985). Masonary structures: The eastern earthquake hazard. *ASTM Standardization News*, 13(3):38–41.

Sommerville, P., Smith, N., Punyamurthula, S., and Sun, J. (1997). Development of ground motion time histories for phase ii of the fema/sac steel project. Technical Report SAC/BD-97/04.

Soong, T. and Spencer, B. (2000). Active, semi-active and hybrid control of structures. *Bulletin of the New Zealand Society for Earthquake Engineering*, 33(3):387–402.

Soong, T. and Spencer, B. (2002). Supplemental energy dissipation: state-of-the-art and state-of-thepractice. *Engineering Structures*, 24:243–259.

Spencer, B. and Nagarajaiah, S. (2003). State of the art of structural control. *Journal of Structural Engineering*, 129(7):845–856.

Spencer, B. and Sain, M. K. (1997). Controlling buildings: A new frontier in feedback. *IEEE Control Systems Magazine*, 17(6):19–35.

Spencer, B. and Soong, T. (1999). New applications and development of active, semi-active and hybrid control techniques for seismic and non-seismic vibration in the usa. In *International Post-SMiRT Conference Seminar on Seismic Isolation*, Cheju, Korea.

Symans, M. and Constantinous, M. C. (1999). Semi-active control systems for seismic protection of structures: a state-of-the-art review. *Engineering Structures*, 21:469–487.

Takahashi, Y. and Fenves, G. (2005). Software framework for distributed experimental-computational simulation of structural systems. *Earthquake Engineering and Structural Dynamics*, 35:267–291.

Takanashi, K., Udagawa, K., Seki, M., Okada, T., and Tanaka, H. (1975). Nonlinear earthquake response analysis of structures by a computer-actuator online system. *Bulletin of Earthquake Resistant Structure Research Center*, 8.

Teixeira, R. (2006). Modelling and experimental investigation of an active damper. *Shock and Vibration*, 13(4-5):343–354.

The New Zealand Building Act (2004). *Building Act 2004*.

Warburton, G. and Ayorinde, E. (1980). Optimum absorber parameters for simple systems. *Earthquake Engineering and Structural Dynamics*, 8:197–217.

Welham, J. (2004). *Active stabilisation of buckling in composite laminates*. Masters, University of Canterbury.

Wen, Y. (1976). Method for random vibration of hysteretic systems. *ASCE Journal Engineering Mechanics Division*, 102(2):249–263.

Yang, G., Spencer, B., Carlson, F., and Sain, M. K. (2002). Large-scale mr fluid dampers: modeling and dynamic performance considerations. *Engineering Structures*, 24(3):309–323.

Yang, J. N., E., B. J., Faryar, J., Leavitt, J., Cheng, C. P., and Lin, P. Y. (2007). Full-scale experimental verification of resetable semi-active stiffness dampers. *Earthquake Engineering and Structural Dynamics*, in press.

Yao, J. (1972). Concepts of structural control. *American society of civil engineers, Structural Division*, 98(n ST7):1567–1574.

Yi, F., Dyke, S., Caicedo, J., and Carlson, J. (2001). Experimental verification of multi-input seismic control strategies for smart dampers. *Journal of Engineering Mechanics*, 127(11):1152–1164.

Yoshida, O. and Dyke, S. J. (2004). Seismic control of a nonlinear benchmark building using smart dampers. *Journal of Engineering Mechanics*, 130(4):386–392.